Glass coating effects on Ti-6Al-4V hot forging

A Dissertation submitted in partial fulfilment
of the requirements for the degree of
doctor of philosophy

By
Ritanjali Sethy

under the supervision of

Dr. Lander Galdos Errasti
(Thesis Director)
Dr. Joseba Mendiguren Olaeta
(Co-Supervisor)

Department of Mechanical and Industrial Production Engineering
Mondragon Unibertsitatea
Arrasate, Spain

October 2017

Department of Mechanical and Industrial Production Engineering
Mondragon Goi Eskola Politeknikoa
Arrasate-20500, Gipuizkoa, Spain

Certificate

This is to certify that thesis entitled, “***Glass coating effects on Ti-6Al-4V hot forging***” submitted by **Miss. Ritanjali Sethy** in partial fulfilment of the requirements for the award of the degree of Doctor of Philosophy in the Department of Mechanical and Industrial Production Engineering. It is a bonafide record of the work carried out by her under our supervision and guidance. It is further certified that no part of this thesis is submitted for the award of any degree.

Dr. Lander Galdos
Mechanical and Industrial Production Engineering Department
Mondragon Unibertsitatea,
Arrasate (Spain)

Dr. Joseba Mendiguren Olaeta
Mechanical and Industrial Production Engineering Department,
Mondragon Unibertsitatea,
Arrasate (Spain)

“If I have the belief that I can do it,
I shall surely acquire the capacity to do it
even if I may not have it at the beginning.”
-Mahatma Gandhi

Abstract

Hot forging processes are highly influenced by the contact conditions between the work piece and the dies. An inaccurate definition of the contact conditions may lead to high deviation predictions of the final component geometry, the quantity of material necessary to fill in the cavity, the wear of the tools and the force necessary to manufacture the component. Furthermore, when dealing with high added value materials such as titanium alloys, the wrong prediction of the aforementioned variables also could lead to inaccurate microstructure predictions.

The main goal of the present dissertation was to understand the contact condition between Ti-6Al-4V work piece and heated tool steel with the purpose of calculating the coefficient of friction (COF) and the heat transfer coefficient (HTC) at the interface of the work piece and the tools. Both coefficients of Ti-6Al-4V titanium alloy under hot forging situation were determined by the combined approach of experimental tests and finite element (FE) simulations using FORGE3® finite element software. At the same time, in order to improve the flow of the material within the tools and reduce the alpha-case layer when forging titanium alloys at high temperature, three types of surfaces were analyzed in the present study: billets without coating, 40-45 μm and 80-90 μm of CONDAERO 228 glass coating.

The objectives of this dissertation were four-fold. First, a Finite element (FE) parametric study has been performed in order to obtain the sensitivity of ring and T-Shape test when addressing the issue of varying input parameters. The objective of this study was to determine and interpret the factors that affect friction behaviour. Special care must be put in some specific inputs, to obtain accurate calibration curves and avoid errors when finding the real COF based on experimental observations. It is noticed that, HTC is the most influencing factor among all and has high impact on calibration curves of the friction test, thereby affects the measurement of interfacial friction factor. Then, tribological contact conditions in both the tests were compared. It concluded that, T-shape test is best suitable to evaluate the friction condition as this test induces large contact pressure and large surface expansion similar to what is occurred during a real forming operation.

Second, columnar upsetting test was conducted for the determination of the HTC at the workpiece-die interface at two different contact pressures. An efficient numerical 3D model has been developed where, simulations have been carried out defining different values of the HTC. That gives as a result of different temperature evolutions which were used to estimate the HTC value which best fits the temperature read by the thermocouple in the real experiments. The validation of final coefficients determined by the inverse algorithm was made by comparison between the upsetting process and the FE analysis results. Variations in HTC have been obtained under different pressure with different surface condition during upsetting. Therefore, HTCs in function of pressure should be employed to generate the calibration curves for determining the interfacial COFs in friction tests.

Third, a comprehensive numerical and experimental study on the ring and T-Shape friction test were carried out to calculate the COF where, geometrical shape of specimen was chosen to simplify this methodology. The aim of this study is to analyze the same tribo-system but having different contact pressures and surface enlargement factors, which could affect the coating behavior and to estimate the friction factor taking into account the HTC as pressure dependent. Calibration curves for the tests were obtained numerically by using finite element simulations. Then, the COFs are calculated by the comparison of the experimental data and numerical simulation results using inverse analysis. The results obtained that the glass coating clearly improves the forgeability of titanium alloys reducing the COF value.

Finally, an experimentation was performed to observe the effects of alpha-case formation, cracks on the deformed T-Shape specimen and to investigate effect of coatings to reduce alpha-case formation. Using a microscope, photographs were taken and visible alpha-case region was measured and also identified the cracks on each sample. Microhardness testing was then performed to determine exact depth range of the visible alpha-case region profile of the sample. It was found that alpha-case thickness and crack depth is more in uncoated specimen than the coated specimen.

Keywords: Hot Forging; Titanium; Ti-6Al-4V; FEM simulation; Ring test; T-Shape test; COF; HTC; Inverse algorithm; Alpha-case; Cracks; Microstructure

Laburpena

Tresneria eta landu beharreko piezaren arteko kontaktu baldintzek eragin nabarmena dute beroan egindako forjaketa prozesuetan. Kontaktu baldintzak era desegokian zehazten badira, aldez aurretik zenbakizko simulazioetan iragarritako azken piezaren geometrian, tresneria betetzeko beharrezkoa den material kantitatean, tresneriaren higaduran eta pieza egiteko beharrezkoa den indarrean desbiderapen handiak eman daitezke. Gainera, titanioa bezalako balio erantsi handiko aleazioetan, aurrez aipaturiko aldagaien iragarpen ez zuzenak, materialaren mikroestrukturaren aurreikuspen okerra ekar dezake.

Tesiaren helburu nagusia, landu beharreko Ti-6Al-4V piezaren eta berotutako altzairuzko tresneriaren arteko kontaktu baldintza ulertzea da, beraien arteko marruskadura koefizientea (COF) eta bero-transferentzia koefizientea (HTC) zehazteko helburuarekin. Beroko forjaketa egoeran Ti-6Al-4V titanio-aleazioaren aipaturiko bi koefizienteak zehazteko, bi teknika ezberdinen emaitzak hartu dira kontutan: entsegu esperimentalen lorturiko emaitzak, alde batetik, eta FORGE3® simulazio softwareko emaitzak, bestetik. Aldi berean, pieza eta tresneriaren arteko fluxua hobetzeko eta titanio-aleazioen tenperatura altuko forjaketan alpha case geruza murrizteko, hiru gainazal mota aztertu dira: estaldura gabeko aleazio totxoak, 40-45 µm eta 80-90 µm CONDAERO 228 estalduradun aleazio totxoak

Lan honen helburua, lau zatitan banatzen da. Lehenik eta behin, azterketa parametriko bat burutu zen elementu finituekin (FE) hainbat parametroen sentsibilitatea Ring test eta T-Shape-n lortzeko. Ikerketa honen helburua marruskaduraren portaeran eragina duten faktoreak zehaztea eta interpretatzea. Arreta berezia jarri behar zaio sarrerako datu zehatz batzuei, kalibrazio kurba egokiak lortzeko eta akatsak saihesteko benetako COF bilatzen denean entsegu. Faktore guztien artean eragin handiena eta marruskadura entseguko kalibrazio kurbetan inpaktu handien izan duen faktorea HTC koefizientea izan da, aurpegien arteko marruskadura faktorean eragina duelako. Azkenik, entseguen arteko kontaktu tribologikoen baldintzak alderatu ziren. Marruskadura egoera ebaluatzeko T-Shape entsegua egokiena dela ondorioztatu zen proba honetan kontaktu presioak eta azalera handiko hedapenak, benetako prozesuko egoera baldintzak ondo irudikatzen direlako.

Bigarren atalean, bi presio maila desberdinetan konpresio entseguak egin ziren landu beharreko piezaren aurpegien arteko HTC koefizientea zehazteko. Zenbakizko 3D modelo eraginkor bat garatu da, eta horrekin HTC balio desberdinak erabiliz, entseguaren simulaziak egin dira. Simulazio horiekin tenperatura eboluzio ezberdinak lortu dira, eta eboluzio hauek, entsegu esperimentaletan termopareen bidez lortutako tenperaturei gehien gerturatzen zaien HTC koefizientea zehazteko balio izan dute. Alderantzizko simulazioen bitartez zehaztutako koefizienteak, konpresio entseguaren emaitzak eta FEM modeloaren emaitzen arteko konparaketaren bitartez balioztatu dira. Konpresio ematen den bitartean HTC koefizientearen aldakuntzak lortu dira, kontaktu presio eta gainazal egoera desberdinetan. Horregatik, marruskadura entseguetan aurpegien arteko COF zehazteko sortu beharreko kalibrazio kurbak lortzeko, presioaren menpekoak diren HTC koefizienteak erabili beharko lirateke.

Hirugarren, Ring test eta T-Shape entseguen zenbakizko eta esperimental ikasketak egin ziren COF kalkulatzeko, azkeneko forma geometrikoa aztertuz. Ikerketa honen helburua Tribo-system berbera aztertzea da, baina kontaktu presio eta hedapen faktore azalera desberdinetan, estalduraren jarreran eragina izan dezakelako eta COF balioa kalkulatzea presioaren menpeko HTC-a kontutan hartuz. Entsegu esperimentalentzako kalibrazio kurbak lortu ziren elementu finituen simulazioak erabiliz. Geroago, datu esperimentalak zenbakizko simulazioko emaitzekin alderatuz eta alderantzizko simulazio teknika erabiliz COF balioak kalkulatzen dira. Emaitzek, estaldurak titaniozko aleazioak forjatzeko ahalmena nabarmen hobetzen dituela erakusten dute, COF balioa murrizten delako.

Azken atalean, entsegu esperimentalak egin dira alpha case geruzaren osaketaren ondorioz sortzen diren efektuak ikusteko, deformaturiko T-Shape probetaren pitzadurak aztertzeko eta estalduren ondorioz eragindako alpha case geruzaren murrizketa efektua ikusteko. Mikroskopio baten laguntzaz, alpha case geruzaren lodiera neurtzeaz gain, probeta bakoitzean agertutako pitzaduren argazkiak atera dira. Probetetan aurki daitekeen alpha case sakonera zehazteko mikro-gogortasun entseguak egin ziren. Estaldura gabeko aleazio totxoen alpha case geruza eta pitzaduren sakonera, estalduradun totxoetan baino handiagoa dela ondorioztatu da.

Hitz Klabeak: Beroko forjaketa; Titanioa; Ti-6Al-4V; FEM simulazioa; Ring test; T-Shape test; COF; HTC; alderantzizko simulazioa; Alpha-geruza; Cracks; Mikrostruktura

Resumen

Los procesos de forja en caliente están altamente influenciados por las condiciones de contacto entre la pieza de trabajo y las herramientas del troquel. Una definición inadecuada de las condiciones de contacto puede originar errores de predicción de la geometría final del componente, cantidad de material necesaria para llenar la cavidad, desgaste de herramientas y fuerza necesaria para fabricar el componente. Además, cuando se producen componentes con materiales de alto valor añadido, una incorrecta definición de las mencionadas variables también puede conllevar errores en la predicción de la microestructura final.

El objetivo principal de este trabajo fue el de comprender las condiciones de contacto entre una pieza de trabajo de Ti-6Al-4V y una herramienta de acero caliente con el propósito de calcular el coeficiente de fricción (COF) y el coeficiente de transmisión de calor (HTC) en la intercara de la pieza de trabajo con la herramienta. Ambos coeficientes de la aleación de titanio Ti-6Al-4V en situación de forja en caliente fueron determinados mediante la combinación de ensayos experimentales y el uso de simulaciones de elementos finitos (FE) con el software de elementos finitos FORGE3®. Al mismo tiempo, con el objetivo de optimizar el flujo del material entre las herramientas y reducir la capa de “alpha-case” cuando se forjan aleaciones de titanio a altas temperaturas, en este trabajo se analizaron tres tipos de superficies: tochos sin recubrimientos y con recubrimientos de 40-45 µm y 80-90 µm de CONDAERO 228.

El objetivo de este trabajo se dividió en cuatro partes. Primero, se ha realizado un estudio paramétrico por elementos finitos (FE) con el objetivo de obtener la sensibilidad de varios parámetros en ensayos de Ring test y T-Shape. El objetivo de este estudio era determinar e interpretar los factores que afectan en el comportamiento de la fricción. Se debe prestar especial atención en algunos específicos datos de entrada, para obtener curvas de calibración adecuadas y evitar errores cuando se busca el COF real basado en observaciones experimentales. Se ha observado que, el HTC es el factor más influyente entre todos y tiene el mayor impacto en las curvas de calibración de los ensayos de fricción, afectando en la medición del factor de fricción de la intercara. Finalmente, las condiciones de contacto tribológicas de ambos ensayos fueron comparadas. Se concluyó que el ensayo T-Shape es el más adecuado para evaluar la condición de fricción ya que en este ensayo se induce a presiones de contacto y expansiones superficiales altas similares a las que se pueden observar en procesos reales de forjado.

Segundo, se realizaron ensayos de compresión para la determinación del HTC de la intercara de la pieza de trabajo a dos presiones de contacto diferentes. Se ha desarrollado un eficiente modelo numérico 3D con el cual se han realizado simulaciones del ensayo definiendo diferentes valores de HTC. Esto da como resultado diferentes evoluciones de la temperatura que han servido para estimar el valor de HTC que mejor se aproxima a las lecturas de temperatura realizadas mediante termopares en los ensayos experimentales. La validación final de los coeficientes determinados por simulación inversa fue realizada comparando los resultados del proceso del ensayo de compresión con el análisis por FE. Se han obtenido las variaciones del HTC a diferentes presiones de contacto con diferentes condiciones superficiales durante la compresión. Por ello, se debería usar coeficientes HTC en función de la presión para generar curvas de calibración para determinar los coeficientes de fricción de las intercaras en los ensayos de fricción.

Tercero, se realizaron estudios numericos y experimentales de ensayos Ring test y T-Shape para calcular el COF, analizando la forma geométrica final. El objetivo de este estudio es analizar el mismo Tribo-system, pero a diferentes presiones de contacto y factores de expansión superficial, que puedan afectar al comportamiento del recubrimiento y estimar el COF teniendo en cuenta un HTC dependiente de la presión. Se obtuvieron curvas de calibración para los ensayos experimentales usando simulaciones de elementos finitos. Posteriormente, los COF son calculados comparando los datos experimentales con los resultados de las simulaciones numéricas y usando la técnica de simulación inversa. Los resultados obtenidos muestran que el recubrimiento mejora claramente la forjabilidad de las aleaciones de titanio al reducir el valor del COF.

Finalmente, se realizaron ensayos para observar el efecto de la formación de la capa de "alpha-case", grietas en las probetas de T-Shape, e investigar el efecto de los recubrimientos en la reducción de la formación de la capa "alpha-case". Usando un microscopio, se tomaron fotografías y se midió la región de "alpha-case" y se identificaron también las grietas en cada probeta. Se realizaron ensayos de microdureza para determinar la profundidad exacta de capa "alpha-case" se podía encontrar en las probetas. Se observó que el espesor de la capa de "alpha-case" y la profundidad de las grietas era mayor en el caso de las probetas sin recubrimiento.

Palabras clave: Forja en caliente; Titanio; Ti-6Al-4V; Simulación FEM; Ring test; T-Shape test; COF; HTC; Simulación inversa; Alpha-caso; Grietas; Microestructura

Acknowledgment

> *“None of us got to where we are alone.*
> *Whether the assistance we received was obvious or subtle,*
> *acknowledging someone's help is a big part of understanding*
> *the importance of saying thank you.”*
> **-Harvey Mackay**

Successful completion of this work will never be one man task. There are many who have helped to make my experience as a student a rewarding one. I express my deep sense of gratitude and indebtedness to my thesis supervisor Dr. Lander Galdos and co-supervisor Dr. Joseba Mendiguren Olaeta and PhD adviser Dr. Eneko Saenz de Argandoña, on the helping me of my thesis work, which would be incomplete without the mention who made it possible whose precious guidance, encouragement, supervision and helpful discussions made it possible.

I am grateful to the Department of Mechanical and Industrial Production Engineering, Mondragon Unibertsitatea, for providing me the opportunity to execute this project work. I would like to give my special thanks to Mr. Xabier Chamorro and Ms. Alaitz Zabala Eguren for the invaluable support, help and motivation. I also want to thank all my PhD colleagues and all staff members especially Rafa Ortubay Ibabe and Irune Otero of this department, for creating pleasant working environment and for their inspiration and help. I express my sincere thanks to Mr. Unai Ulibarri, Mr. Imanol Gil Acedo, PhD Research Scholar for their help, advice and co-operation. Words really cannot express how grateful I am. All of you made this stay an unforgettable experience.

The financial support from the Interweave Erasmus Mundus Partnership Europe Asia program for the realization of this work is gratefully acknowledged.

I would also like to express my gratitude to my parents for providing me with support, inspiration and motivation through the years. I am very thankful to my best friend have Mr. Ranjan Kumar Hasda for his support, understanding, and motivation that guide me and give me strength to overcome all obstacles in my life. Finally, I feel pleased and privileged to fulfill my parent’s ambition and I am greatly indebted to them for bearing the inconvenience during my PhD studies.

Ritanjali Sethy

Dedicated to my Father

“God has two dwellings; one in heaven, and the other in a meek and thankful heart”
-Izaak Walton

Contents

Abstract .... **vii**

Nomenclature .... **xxiii**

List of Figures .... **xxv**

List of Tables .... **xxxi**

1. INTRODUCTION **3**

1.1. Motivation and background 3

1.2. Scope of the thesis 4

1.3. Thesis layout 5

2. LITERATURE REVIEW **11**

2.1. Overview of Titanium 11

2.1.1. Manufacturing of titanium alloys 12

2.1.2. Metallurgy of titanium alloys 14

2.1.3. Alloy classification 16

2.1.4. Ti-6Al-4V 18

2.1.5. Mechanical properties of titanium alloys 19

2.1.6. Heat treatments 21

2.2. Alpha-Case Formation 23

2.2.1. Oxidation of titanium alloys 24

2.2.2. Diffusion in titanium alloys 26

2.2.3. Mechanisms and Morphology 27

2.2.4. Prevention and removal of alpha-case in titanium alloys 32

2.3. Forging 34

2.3.1. Applications of forged parts 34

2.3.2. Forging Design Parameters 34
2.3.3. Forging Defects 35
2.3.4. Forging of titanium and its alloys 35
2.3.5. Lubrication 39
2.3.6. Coatings 42
2.4. Contact Characterization at high temperature 44
2.4.1. Heat transfer characterization test at high temperature 45
2.4.2. Tribological characterization test at high temperature 49
Critical Review: 61
Problem definition 62
3. SENSITIVITY ANALYSIS OF FRICTION TESTS 67
3.1. Introduction 67
3.1 Numerical simulations by FEM 68
3.1.1. Ring test 69
3.1.2. T-Shape test 71
3.2. Results and Discussions 72
3.2.1. Sensitivity analysis of Ring test 72
3.2.2. Sensitivity analysis of T-Shape test 74
3.2.3. Comparision of tribological contact conditions 75
3.3. Conclusions 76
3.3.1. Analysis of Ring test 76
3.3.2. Analysis of T-Shape test 77
3.3.3. Analysis of Tribology condition for both test 77
4. DETERMINATION OF THE HEAT TRANSFER COEFFICIENT BY COLUMNAR UPSETTING TEST 81

4.1. Introduction 81

4.2. Experimental Procedure 81

  4.2.1. Materials and Specimen Preparation 81

  4.2.2. Surface topography measurements 82

  4.2.3. Experimental set up 84

  4.2.4. Test procedure 85

4.3. Finite element simulation analysis 85

4.4. Results and Discussion 86

  4.4.1. Measurement of surface topography 86

  4.4.2. Temperature changes measured at specimen 88

  4.4.3. Determination of interface HTCs 89

4.5. Conclusions 91

5. INVESTIGATING FRICTION FACTOR THROUGH RING COMPRESSION TEST 95

5.1. Introduction 95

5.2. Experimental Procedure 95

  5.2.1. Materials and Specimen Preparation 95

  5.2.2. Experimental set up 96

  5.2.3. Test procedure 96

5.3. Numerical Modelling 97

5.4. Results and Discussion 99

  5.4.1. Surface topography measurements 99

  5.4.2. Determination of COF 100

5.5. Conclusions 102

6. INVESTIGATING FRICTION FACTOR THROUGH T-SHAPE COMPRESSION TEST 105

6.1. Introduction.......... 105

6.2. Experimental Procedure.......... 105

6.2.1. Materials and Tooling Preparation.......... 105

6.2.2. Experimental set up.......... 106

6.2.3. Test procedure.......... 106

6.3. Numerical Modelling.......... 107

6.4. Results and conclusions.......... 108

6.4.1. Surface topography measurements.......... 108

6.4.2. Determination of COF.......... 110

6.5. Conclusion.......... 112

7. ANALYSIS OF THE EFFECT OF GLASS COATING ON ALPHA-CASE FORMATION AND DEFECTS.......... 115

7.1. Introduction.......... 115

7.2. Methodology.......... 116

7.2.1. Sample preparation.......... 116

7.3. Experimental techniques.......... 117

7.3.1. Light Optical Microscopy (OM) Study.......... 117

7.3.2. Micro Hardness Evolution.......... 117

7.4. Results and discussion.......... 118

7.4.1. Microstructure Observation.......... 118

7.4.2. Alpha-case investigation.......... 119

7.4.3. Cracks or defect analysis.......... 121

7.5. Conclusion.......... 122

8. FINAL CONCLUSIONS AND FUTURE WORK.......... 125

8.1. Conclusions.......... 125

8.2. Future work 128

Bibliography 131

Publications 143

Nomenclature

List of Abbreviations

HTC	Heat transfer coefficient
COF	Coefficient of friction
3D	Three dimensional
2D	Two dimensional
FEM	Finite element modelling/method
FCC	Friction calibration curves
CP	Commercially pure
TMT	Thermo-mechanical treatment
ODZ	Oxygen diffusion zone
FEA	Finite element analysis
EDM	Electric discharged machined
OM	Optical microscope
SF	Spike forging

List of Symbols

Ti	Titanium
α	Alpha
β	Beta
h	Heat transfer coefficient
w	Total width
h	Flange height
T_{β}	Beta transus temperature
m	Strain rate sensitivity
η	Efficiency of power dissipation
$\xi(\dot{\varepsilon})$	Instability criterion
Q	Heat flux
$T_{w,s}$	Temperature of workpiece surface
$T_{d,s}$	Temperature of die surface
T_c	Calculated temperature
T_m	Measured temperature
μ	Friction coefficient
m	Friction factor
τ	Shear friction
p	Applied normal force
k	Shear yield limit
D_o	Outer diameter
D_i	Inner diameter
H	height
R_a	Surface roughness
Sq	Root mean square roughness
Sdq	Root mean square slope of the surface
Sdr	Developed interfacial area ratio

List of Figures

Fig. 1.1: Outline of the thesis work 6

Fig. 2.1: Crystal structure of Titanium (a) HCP α-phase and (b) BCC β-phase [LEY03] 12

Fig. 2.2: Extended Kroll process for Ti sponge production [LEY03] 13

Fig. 2.3: Processing and manufacturing cycle of Ti [PED01] 13

Fig. 2.4: The effect of alloying elements on phase diagrams of Titanium alloys [LEY03] 14

Fig. 2.5: Ti-Al phase diagram 15

Fig. 2.6: Three-dimensional phase diagram to classify Ti alloys (schematically) [BEA06] 16

Fig. 2.7: (a)Titanium Properties (b) Fatigue Titanium Properties [RMI00] 19

Fig. 2.8: Ways for modification of properties in titanium alloys 20

Fig. 2.9: Phase diagram used to predict results of forging or heat treatment practice [BEA06] 23

Fig. 2.10: Oxygen concentration profile of oxidized titanium according to Wagner's model (Schematically) [UNN86] 24

Fig. 2.11: Ti-O phase diagram [OKA11] 25

Fig. 2.12: Rate equations observed in the oxidation of titanium (Schematically) [KOF66] 25

Fig. 2.13: Microhardness-depth profiles for oxidised CP-Ti and Ti-6Al-4V (Grade 5) (36 hr at 625°C) [DEA04] 27

Fig. 2.14: SNMS results for a CP alloy (T40) treated at 720 C for 150 min. The alpha-case layer is shown as the oxide layer [SCH06] 27

Fig. 2.15: Predicted depth of alpha-case for titanium alloy IMI 834 at different exposed temperatures [GUR03] 27

Fig. 2.16: Measured microhardness profiles of titanium alloy, IMI 834, after 100 h of oxidation at various temperatures showing the depth of alpha-case [GUR03] 28

Fig. 2.17: Formation of multi-layered structure of the oxide in Ti–6Al–4V (Schematically) [DU94] 29

Fig. 2.18: Optical micrographs showing alpha-case (white layer) in (a) Ti-6242 and (b) Ti-64 heated at 593°C up to 500 hours [GAD13] 30

Fig. 2.19: Variation of hardness from the surface to the bulk of the Ti-64 sample exposed to 700°C for 500 hours. An optical micrograph showing the alpha-case of the corresponding sample (the white layer in the micrograph) [GAD13] 30

Fig. 2.20: Optical view (20x) of a Ti-6-4 at 6 hrs & 1750°F, (left) uncoated sample and (right) SJ coated sample [CHR10] 31

Fig. 2.21: Tensile testing micrographs (Damage accumulation for samples treated above the ß-transus temperature at 1050°C for 30 minutes stressed to 0.2% strain). a) and b) at magnifications of 200x. c) and d) at 500x magnification [DOB09].. 32

Fig. 2.22: Variation of (a) UTS, (b) yield strength, and (c) ductility as function of strain rate [PAT01] 33

Fig. 2.23: Typical stress strain curves for titanium alloys [MAO09] 36

Fig. 2.24: Power dissipation efficiency map and instability map obtained on Ti-6Al-4V [SES00] 37

Fig. 2.25: Use of FEM to calculate the “die chill zone” (Ti-6-2-4-2 engine disk) [LEY03] 39

Fig. 2.26: Schematic of differences between mixed and boundary lubrication [GHA15] 40

Fig. 2.27: Schematic of disadvantages of using improper lubricants [GHA15] 41

Fig. 2.28: (a) Quasi-isothermal and (b) cyclic oxidation behavior of coated and uncoated γ TiAl alloys at 750 °C [LEY02] 44

Fig. 2.29: Temperature comparison at the rest-on-die stage [CHA02] 48

Fig. 2.30: Temperature comparison at the forging stage [CHA02] 48

Fig. 2.31: Comparisons of temperature histories obtained from the closed form calculation (solid lines), FE prediction (dot lines), and experimental data (symbols) for selected locations in workpiece and die. Pressure is4 0MPa and HTC 3.5kW/m^{2}K [BAI12] 49

Fig. 2.32: Principle of the ring compression test 51

Fig. 2.33: Curves of friction calibration theory for a ring with the ratio of 6:3:2 [ALT83] 51

Fig. 2.34: Samples deformed at 30% and 50% height reduction: (a) glass lubricant and (b) dry friction [ZHU11] 53

Fig. 2.35: Calibration curves obtained from the FEM at height reduction of 0–50% and friction factors of 0–1corresponding to the different HTC, (a) 5kW$(m^2K)^{-1}$ and (b)11kW$(m^2K)^{-1}$ [ZHU11]..53

Fig. 2.36: Ring compression test with: (a) Loads over the contact area and (b) Variability of the loads [GRO13] 54

Fig. 2.37: Ring compression test with Loads over a stroke [GRO13].....................54

Fig. 2.38: Layout of T-Shape test, (a) Test set up and (b) Specimen deformation characteristics...56

Fig. 2.39: (a) Load curves with different friction factors and (b) Effects of friction factor on height of extruded part with different loads [ZHA09] 56

Fig. 2.40: Comparison between the experimental and simulated load curves [ZHA09] 57

Fig. 2.41: Tests developed for examining the friction [ZHA09]............................58

Fig. 2.42: Illustration of hybrid coulomb and constant shear friction model.........60

Fig. 3.1: Setup of compression test (left) ring test (right) T-Shape test................67

Fig. 3.2: Specimen deformation process of ring test simulation 69

Fig. 3.3: Finite element model of ring test specimen...69

Fig. 3.4: Specimen deformation process of T-Shape test simulation 71

Fig. 3.5: Friction calibration curves obtained from the FEM at height reduction of 0–50% and friction factors (m) of 0-1 with baseline or reference input conditions 72

Fig. 3.6: The influence on the calibration curves corresponding to the m of 0.1, 0.5, 0.9 for (a) Press speeds of 10, 30 and 50 strokes/min (b) HTC values of 2, 10 and 20 kW/m2K (c) Processing times of 0, 5 and 10 s (d) Mesh sizes of 0.4, 0.6 and 0.8 mm (e) Material temperature of 900, 940 and 980 ℃ and (f) Tool temperatures of 180, 200 and 220 ℃...73

Fig. 3.7: Force curves with Different HTC..75

Fig. 3.8: Force curves simulated with different friction factor (HTC=10 kW/m^2K)75

Fig. 3.9: Force curves simulated with Material changes (m=0.8 and HTC=10 kW/m^2K)...75

Fig. 3.10: Surface enlargement with m=0.8..........76

Fig. 3.11: Contact pressure with m=0.8..........76

Fig. 4.1: Geometry of HTC specimen and thermocouple locations : (left) Test-Piece, (right) Engineering Drawing; all units are in mm..........82

Fig. 4.2: Confocal profilometer SensoFar..........83

Fig. 4.3: Test set up..........84

Fig. 4.4: FE model for hot upsetting process (a) transfer (b) pre-forming and (c) forming steps..........86

Fig. 4.5: Surface topography of HTC test tool..........86

Fig. 4.6: Surface topography of HTC test sample..........86

Fig. 4.7: Temperature changes in different workpiece: (a) Experimental and (b) FE model of temperature distribution..........88

Fig. 4.8: The comparison of FE prediction and experimental results of different specimen temperature at the forging stage for 5 MPa contact pressure....89

Fig. 4.9: The comparison of FE prediction and experimental results of different specimen temperature at the forging stage for 65 MPa contact pressure..90

Fig. 4.10: Effect of glaze thickness..........90

Fig. 5.1: geometry of ring specimen: (left) Test-Piece (right) Engineering Drawing; all units are in mm..........96

Fig. 5.2: Experimental set up with the water-graphite lubricant spraying system96

Fig. 5.3: Initial and final view of ring test simulation..........98

Fig. 5.4: Surface topography of ring test tool..........99

Fig. 5.5: Surface topography of ring test sample..........99

Fig. 5.6: Samples before deformation (top) and at 50% height reduction deformation (bottom) using lubricant: (a) Uncoated, (b) 40 μm Coated and (c) 80 μm Coated 101

Fig. 5.7: Internal diameter, external diameter and height of the ring samples after the experiments..........101

Fig. 5.8: Calibration curves obtained from the FEM and experimental results at height reduction of 50% with different friction factors..........102

Fig. 6.1: (left) The sectional shape of die, (right) experimental grooved die together with deformed specimen 106

Fig. 6.2: Specimen deformation process in FEM simulation 107

Fig. 6.3: Surface topography of T-Shape test tool 108

Fig. 6.4: Surface topography of T-Shape test sample 108

Fig. 6.5: Effect of geometrical parameters with friction factor 110

Fig. 6.6: Deformed T-Shape specimen; (left) view from simulation, (right) schematic view 111

Fig. 6.7:: Calibration curves and experimental data of T-Shape tests 111

Fig. 7.1: Optical micrographs showing the microstructure of forged Ti-6Al-4V. In micrographs light or grey areas is α phase and dark areas is β 116

Fig. 7.2: Sample sectioning and mounting for metallographic analysis 117

Fig. 7.3: Optical micrographs of (left) alpha-case layer (right) crack along entire periphery of cross- sectioned samples 117

Fig. 7.4: Microhardness test marks at various places for Ti6Al4V T-Shape specimen 118

Fig. 7.5: Microstructures observed at different locations for Ti-6Al-4V T-Shape specimen 118

Fig. 7.6: Typical Optical micrographs of alpha-case measurements of Ti-6Al-4V T-Shape specimen (a) without coating, x200 (b) 45 μm coating, x500 (c) 90 μm coating, x500 120

Fig. 7.7: Micro hardness profile for Ti-6Al-4V T-Shape specimen 120

Fig. 7.8: Optical photographs of the crack area of uncoated T-Shape specimen . 121

Fig. 7.9: Optical photographs of the crack area of 45 μm coated T-Shape specimen 122

List of Tables

Table 2.1: Effects of different alloying elements on Ti [BOY92] 15

Table 2.2: Important commercial titanium alloys [LUTO7] 18

Table 2.3: Properties of α, α+β and β Ti alloys [LEY03] 21

Table 2.4: Mechanical properties of selected titanium alloys [LEY03] 21

Table 2.5: Titanium heat treatment techniques [BIE05] 22

Table 2.6: Alpha-case depth comparison of optical microscopy and microhardness at 6 hr and 1750°F [DOB09] 31

Table 2.7: Selected recommended material removal depths after thermal exposure of titanium to the atmosphere [ASM90] 33

Table 2.8: Possible forging defects [MOD05] 35

Table 2.9: Different friction regimes [MAN11] 40

Table 2.10: Typical lubricants being used for different forming processes [GHA15] 41

Table 2.11: Different methods for applying lubricants on the surface [MAN11] ... 41

Table 2.12: Overview of several coating systems and fabrication processes for titanium alloys [LEY02] 43

Table 2.13: Typical friction coefficient values using constant shear friction model [SCH83] 60

Table 4.1: Chemical composition in wt.% of Ti-6Al-4V 82

Table 4.2: Acquisition conditions used in the study 83

Table 4.3: Variables used for data processing in the study of data acquisition variables 83

Table 4.4: Conditions on which the specimens tested for HTC 84

Table 4.5: Calculated surface parameters of HTC tool 87

Table 4.6: Calculated surface parameters of HTC sample 87

Table 5.1: Testing Conditions of ring test 97

Table 5.2: Calculated surface parameters of ring test tool 100

Table 5.3: Calculated surface parameters of ring test sample 100

Table 6.1: Testing Conditions of T-Shape test 107

Table 6.2: Calculated surface parameters of T-Shape tool 109

Table 6.3: Calculated surface parameters of T-Shape sample 109

Table 7.1: Measurements performed on Ti-6Al-4V with different experimental conditions 119

CHAPTER 1

INTRODUCTION

"Begin at the beginning," and
"go on till you come to the end; then stop"
-Lewis Carroll, Alice in Wonderland

1. INTRODUCTION

1.1. Motivation and background

Titanium (Ti), named as the "wonder metal", was first obtained over two centuries ago and has been utilized in a growing list of specialized applications since then. Ti and its alloys have become very important materials. They are used extensively across the globe, owing to its unique density, corrosion resistance, relative strength and ideal for light weight design over competing materials such as aluminum, steels, and super alloys [DON00]. It withstands urban pollution, marine environments and is failure-proof in even more aggressive environments because it is one of the most noble metals, the coupling of titanium with dissimilar metals does not accelerate galvanic corrosion of the titanium.

The most commonly used Ti alloy is the two-phase alpha/beta (α+β) alloy, Ti-6Al-4V. It is known as Grade 5 Ti alloy and also known as "workhorse" of the Ti industry, accounting for more than 50% of total Ti usage. It is an alloy increasingly used due to its characteristics of high specific strength, light weight, formability, toughness and corrosion resistance that offer a wide combination of superior mechanical and physical properties which makes it attractive for applications in aerospace, automotive, chemical and biomedical industries [GUL09]. The increasing drive for lighter stronger materials is bringing Ti-6Al-4V to the forefront of high performance demanding industries and technologies.

Most of manufacturing processes of Ti alloys components are based on machining operations, which allow obtaining very accurate final shapes but, at the same time, are affected by several disadvantages like material waste and general production costs [CHO15]. During the last decade, the forging processes for Ti alloys have attracted greater attention from both industrial and scientific/academic researchers due to their potential in providing a net shaped part with minimal need for machining, reducing manufacturing costs and providing better mechanical properties [OBE09]. Because of this, components are increasingly manufactured by forging and forging is suitable for the processing of lightweight Ti components. Hot deformation in different actual industrial processes such as hot forging or rolling is extensively used for manufacturing of both semi-finished and finished products of Ti-6Al-4V alloy. This alloy is conventionally forged below the beta (β) transus temperature in order to control the microstructure evolution, to obtain a component with the desired properties. This being so, an intense field of Ti-6Al-4V forging is focused in this research.

Despite of the success in forging process, Ti and its alloys are difficult to forge and difficult to fill dies to obtain the desired shapes, since it requires the precise control of temperature and strain to create the desired microstructures and material properties. This means, on the other hand, that the material has the potential to make this forging technology stand out from others. So, it is important in dealing with Ti alloy forgings, to control the process of temperature and plastic strain in order to obtain desired microstructures and mechanical properties. Other problems that arises during the forging process are: β transus, loss of properties, tool wear and difficulty in the prediction of required force/power. In spite of these evidences, it is important from the aspect of forging technology to understand the effective factors and improve the yield through near-net shaping while securing quality.

Another important aspect to consider and often overlooked, is the alpha case formation during hot forging. Use of Ti-6Al-4V alloy in forging, can be subjected to hydrogen contamination by oxygen, nitrogen and carbon pickup during forging. This contamination could result in a deterioration in ductility which would adversely affect forming characteristics. Use of Ti-6Al-4V at elevated temperatures often experienced in applications is limited by the effects of extensive scaling due to the interaction that Ti has with the atmosphere. Recently, many studies on Ti's oxidation behaviour in air and the effects of exposure to oxygen on both the physical and mechanical properties of Ti have been published [DOB11]. A growing amount of data is becoming available; however large gaps in predictive models and the absence of extensive guidelines for the oxidation behaviour of titanium alloys remain. There is a clear need for further research and documentation into the in-air oxidation behaviour of Ti alloys at elevated temperatures.

Ti and its alloys must be protected from contamination by oxygen, nitrogen, hydrogen and carbon during heating for forging. Care should be taken to prevent the formation of excessive alpha case and to prevent contact with steel scale. This is most effectively done by coating the forging slugs in a liquid glaze or glass [IMM97]. Although, the protection offered by the glass coating, a small amount of contamination does occur and must be removed by machining, grinding or chemical etching. There is therefore a lack of knowledge regarding the glass coating effects during the Ti-6Al-4V forging processes. However, to the authors' knowledge there are currently very less studies dealing with the effect of glass coating effects on forging using Ti-6Al-4V alloy and analyzing microstructure on different parts of post-deformation specimen.

1.2. Scope of the thesis

The main goal of the present dissertation is to study the effects of glass coating on Ti-6Al-4V hot forging. In this work, the contact condition between Ti-6Al-4V specimens and heated tool steel with the purpose of calculating the heat transfer coefficient (HTC) and coefficient of friction (COF) at the interface of the specimens and the tools have been analysed. Later, the alpha case formation during hot forging was investigated by microstructural analysis.

Three types of surfaces have been analyzed for this study which are, Ti–6Al–4V specimens with no coating and two others with different layer thickness of glass coating. In order to meet this main goal, the study comprise the following specific objectives:

- Firstly, current relevant literature has been investigated concerning the broad topic of contact characterization and microstructure study of Ti-6Al-4V. Following this, an in-depth investigation has been done to identify the lacks and some relevant tests for contact characterization and alpha case formation.
- Secondly, the ring and T-Shape tests of Ti-6Al-4V alloy have been numerically analyzed using three-dimensional (3D) finite element modelling (FEM) in order to identify important influencing parameters considering different variables, which affects the frictional behaviour, force and deformed specimen geometry in the Ti-6Al-4V hot forging process.
- Next, columnar upsetting thermal test (HTC Test) has been conducted at two contact pressures to characterize HTC precisely that best fits in the contact between the Ti-6Al-4V specimens and the steel tools in forging process. The validation of final coefficients has been determined by the inverse algorithm comparing the upsetting process and the FE analysis results.
- Then, ring and T-Shape tests have been conducted to estimate the friction factor taking into account the influence of the HTC in both the tests. Numerical simulations of both Ring and T-Shape tests have been carried out for various values of friction factor using the found HTC value. Later, all the simulation results have been compared with experimental results to estimate the accurate friction factor.
- Finally, all the 3-surface specimen after forging, have been analysed in order to identify the effect of exposure to the atmosphere at elevated temperatures to study the alpha case and the defects.

1.3. Thesis layout

The current thesis has been divided into eight chapters including the introduction. All the work is sketched in Fig. 1.1, where the different chapters and associated objectives are depicted. A general description of each chapter is given below.

Chapter 2- Literature review

Chapter 2 covers an extensive literature survey of Ti and its alloys, their behaviour, properties, material and contact characterization test at high temperature and process optimization. Once the revision of literature has been done, it has been found a set of gaps in the literature which have motivated to carry out this research and also depicts some general concepts in order to understanding of the present study.

Based on these gaps, it has been found that HTC, friction and material behaviour are the important parameter in hot forging especially for FEM optimization and alpha case formation, which is a problem for crack formation during forging.

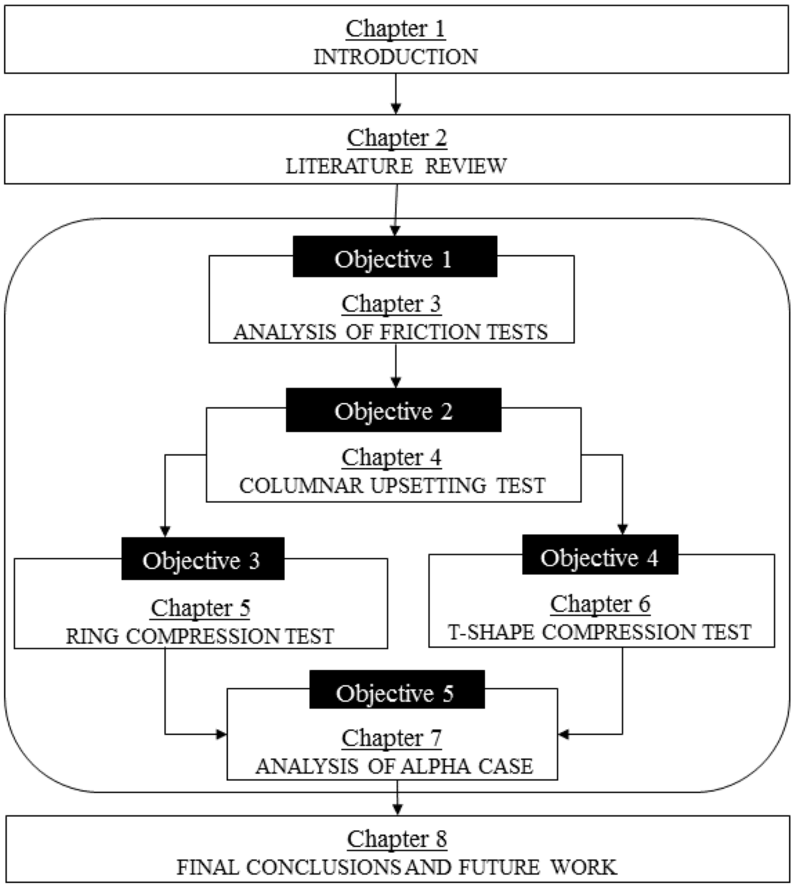
Chapter 1
INTRODUCTION
Chapter 2
LITERATURE REVIEW
Objective 1
Chapter 3
ANALYSIS OF FRICTION TESTS
Objective 2
Chapter 4
COLUMNAR UPSETTING TEST
Objective 3
Chapter 5
RING COMPRESSION TEST
Objective 4
Chapter 6
T-SHAPE COMPRESSION TEST
Objective 5
Chapter 7
ANALYSIS OF ALPHA CASE
Chapter 8
FINAL CONCLUSIONS AND FUTURE WORK

Fig. 1.1: Outline of the thesis work

Chapter 3- Sensitivity analysis of friction tests

This chapter summarizes the analysis of two friction tests, which has been carried out by a FE parametric study by means of FORGE-3D software in order to find the most important influencing parameters which affects the frictional behaviour, force and specimen geometry in Ti-6Al-4V hot forging.

The first part of this chapter deals with the numerical investigation of the high temperature ring compression test to evaluate how frictional behaviour is affected by variations of input parameters, such as; HTC, processing time, mesh size, material and tool temperature. According to the results, the HTC and the press velocity have most significant effects on frictional behavior. The final part of this chapter deals with the numerical investigation of the high temperature T-Shape test in order to obtain the sensitivity of the test. Therefore, the influence of three parameters such as HTC, material change and friction has been investigated to analyse how these variables influence the force measurement. Based on the results obtained, force is very sensitive to material properties and thus that final geometrical shape measurement could be a good way to identify this method.

Chapter 4- Determination of the heat transfer coefficient by columnar upsetting test

This chapter presents the study of a columnar upsetting thermal test to calculate the HTC accurately and efficiently at different contact pressure. This procedure is based on temperature readings inside the specimen combined with FE simulation of the process and the use of inverse analysis.

The first part of this chapter presents the experimental HTC tests at contact pressure of 5 and 65 MPa where, the temperature history of the specimen has been obtained for the HTC calculation. Then, an efficient numerical 3D model has been developed where, simulations have been carried out defining different values of the HTC for the determination of HTC at different contact conditions. That gives as a result of different temperature evolutions which were used to estimate the HTC value which best fits the temperature read by the thermocouple in the real experiments. That means, measured and predicted temperatures have been compared by using an inverse algorithm to determine the HTC. Additionally, HTC models at different temperature ranges have been analysed to study the variations in HTC but the final HTC has been considering at the stage of forging process. Variations in HTC have been obtained under different pressure with different surface condition during upsetting. Moreover, the HTCs are different for three types of surfaces conditions. Therefore, different HTCs should be employed to generate the calibration curves when all the surface conditions were applied for determining the interfacial friction coefficients in friction tests.

Chapter 5- Investigating friction factor through ring compression test

In this chapter, ring test is used with combined approach of FE simulation to determine the COF based on measuring of inner diameter. This is one of the simplest friction tests and is widely used for the evaluation of frictional conditions in forming operations. This test leads to small surface expansion and low contact pressure within the contact surfaces.

The first part of this chapter presents the experimental ring tests at different testing conditions. Based on the ring test principle, the height, the inner diameter, and the outer diameter variation for all the specimens were measured for the COF calculation. Since the inner diameter is the most important variable for the COF calculation, a mean value of this dimension has been calculated for every test condition. Then, using FEM, the friction calibration curves (FCC) have been derived by plotting the relation between the reduction in inner diameter and height. In the FCCs, both experimental and simulation results have been compared to find the best COF. It has been observed that the glass coating clearly benefits the forging of the Ti-6Al-4V alloy since a lower COF value is achieved.

Chapter 6- Frictional condition evaluation using T-shape compression test

In this chapter, a comprehensive numerical and experimental study on the T-Shape friction test has been carried out to calculate the COF where, geometrical shape of specimen has been chosen to simplify this methodology. This test is a newly introduced friction test proposed in the year of 2008, which leads to large surface expansion up to 50% and high contact pressure within the contact surfaces (It can reach four times the flow stress of the material), similar to what is occurred during a real forming operation. In this test, specific manufacturing die is required and for that reason a complex deformation path can be achieved

The first part of this chapter presents the experimental T-Shape tests at different testing conditions where a cylindrical billet is placed in the V shaped groove die and then compressed to form a T-Shape deformed specimen. The calibration curves were generated using finite element simulations for various values of friction factor and according to simulation results, the total width (w) and flange height (h) were inspected to determine the friction behavior from the finished workpiece. So, after the realization of the experiments, the shape of specimens (i.e. total height, width and flange height) have been measured and will be compared with the simulation results to estimate the friction factor under all surface conditions. These measurements with the use of adequate inverse modelling techniques enabled a precise characterization of the forging friction coefficient

Chapter 7- Analysis of alpha case formation and defects

Last but not least, the specimens after deformation have been analysed and the effect of exposure to the atmosphere at elevated temperatures has been studied (alpha case and the defects). Characterization has been achieved by micrographic analysis and micro hardness profiling from the surface into the substrate.

Overall conclusion and scope for future work have been highlighted in **Chapter 8**.

CHAPTER 2

LITERATURE REVIEW

"There are three principal means of acquiring knowledge…
observation of nature, reflection, and experimentation.
Observation collects facts; reflection combines them;
experimentation verifies the result of that combination."
– Denis Diderot

2. LITERATURE REVIEW

Literature provides a strong impression in relation to the scope as well as interest in the field of research under study. The earlier work related to the present research area by other researchers have been investigated and the progressive account of the work has been enumerated in this chapter. The following chapter will be divided in two sections. The first section presents the review of literature taking into account a full understanding of titanium (Ti) and its alloys, especially Ti-6Al-4V, alpha case formation, and the titanium forging process. The second section presents the tribological and heat transfer characterization test at high temperature with process optimization considering FEM. To conclude, a critical review of the state of the art is presented.

2.1. Overview of Titanium

Several names in the history are responsible for today's importance of titanium and its alloys in numerous disciplines. Titanium was first discovered in 1791 by William Gregor the British reverend, mineralogist and chemist. Four years later, the German chemist Martin Heinrich Klaproth isolated titanium oxide from the mineral "rutile" and he named the element titanium after the Titans from the Greek mythology. However, production of titanium in larger scales was initiated in 1932 by Wilhelm Justin Kroll, who introduced a method for production of pure titanium by combining $TiCl_4$ and magnesium. Even today this method is widely used and therefore Kroll is recognized as the father of titanium industry.

Titanium is the ninth most common element in the earth's crust which exceeded by potassium, magnesium, sodium, calcium, iron, aluminum, silicon and oxygen [DON00]. Ti is the fourth most abundant structural metal in the earth's crust and is exceeded in abundance only by magnesium, aluminum and iron [BOY94]. However, it is never found in pure state and therefore its processing is difficult and expensive. The high processing expenses, but also the impressive properties compared to other structural materials, explains the preferential use of titanium and its alloys in the aerospace industry.

Pure Ti, like many other metals, exists in a crystallised form depending on temperature and composition. Ti exists in two allotropic forms, α-titanium (α-phase) and β-titanium (β-phase). Ti is in hexagonal close packed (HCP) crystal structure at room temperature known as the α-phase and undergoes a phase transformation to the body centred cubic (BCC) β-phase at 882± 2 °C [DON00]. The crystal arrangements of α and β Ti are shown in Fig. 2.1 with their most densely packed planes shown as shaded. On one hand, In Fig. 2.1

a) one of the three most densely packed (0002) planes are shown, also known as basal plane, one of the three $\{10\bar{1}0\}$ planes, called prismatic planes and one of the six $\{10\bar{1}1\}$ pyramidal planes for the HCP crystal structure of titanium. The axes a_1, a_2 and a_3 are the close packed directions with indices $<11\bar{2}0>$. On the other hand, in Fig. 2.1 b) one of the six most densely packed {110} planes in the BCC crystal structure of titanium) is illustrated.

At 882 ± 2 °C an allotropic phase transformation from α to ß-phase occurs and this temperature is recognized as the ß-transus temperature (T_β). At room temperature and temperatures up to the ß-transus temperature the α-phase is stable, whereas at temperatures above the ß-transus the ß-phase is stable. The allotropic phase transformation temperature is strongly dependent on the alloying elements present in the metal and is therefore a factor of the purity of the metal [LUT07]. Alloying elements and interstitial elements can alter the ß transus temperature [BOY92]. The occurrence of titanium in two phases together with the corresponding allotropic phase transformation temperature is of particular importance for the processing metallurgy of titanium and its alloys, since that is the basis for achieving good mechanical properties [LEY03].

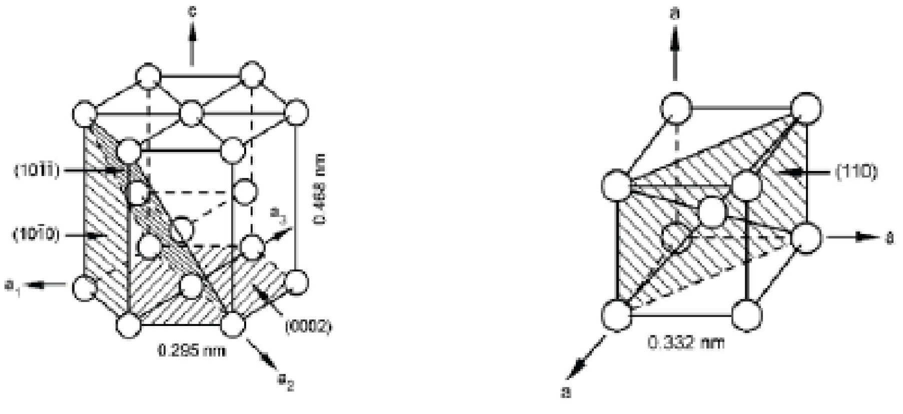

(a) (b)

Fig. 2.1: Crystal structure of Titanium (a) HCP α-phase and (b) BCC β-phase [LEY03]

2.1.1. Manufacturing of titanium alloys

Ti is not present in metallic form in the earth's crust and hence needs to be processed to extract from its ore. Across the globe, Australia, Canada, China, Norway, South Africa and Ukraine are the countries which are the major producers of Ti. Important Ti ores are Ilmenite (FeTiO3), Rutile (TiO2) and Leucoxene [LEY03]. Kroll process made the extraction of this material from ores a commercial possibility in 1932 [IMA96], which involves subjecting the ore by a reduction process in the presence of coke and then chlorinating to obtain TiCl4. The TiCl4 is then reduced using Mg to obtain Ti sponge [LEY03]. The complete conversion from Rutile/Ilmenite to titanium sponge follows the following process flow Diagram shown in Fig. 2.2.

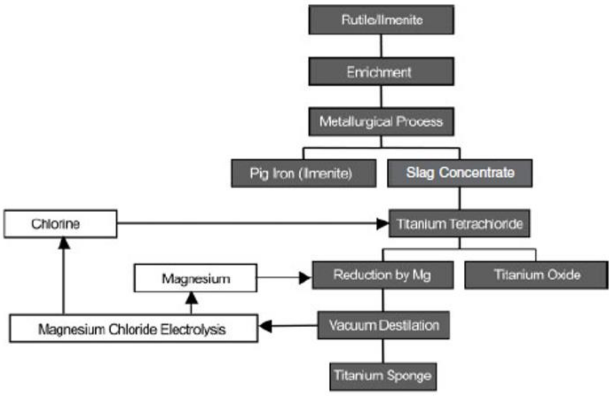
Rutile/Ilmenite
Enrichment
Metallurgical Process
Pig Iron (Ilmenite)
Slag Concentrate
Chlorine
Titanium Tetrachloride
Magnesium
Reduction by Mg
Titanium Oxide
Magnesium Chloride Electrolysis
Vacuum Destilation
Titanium Sponge

Fig. 2.2: Extended Kroll process for Ti sponge production [LEY03]

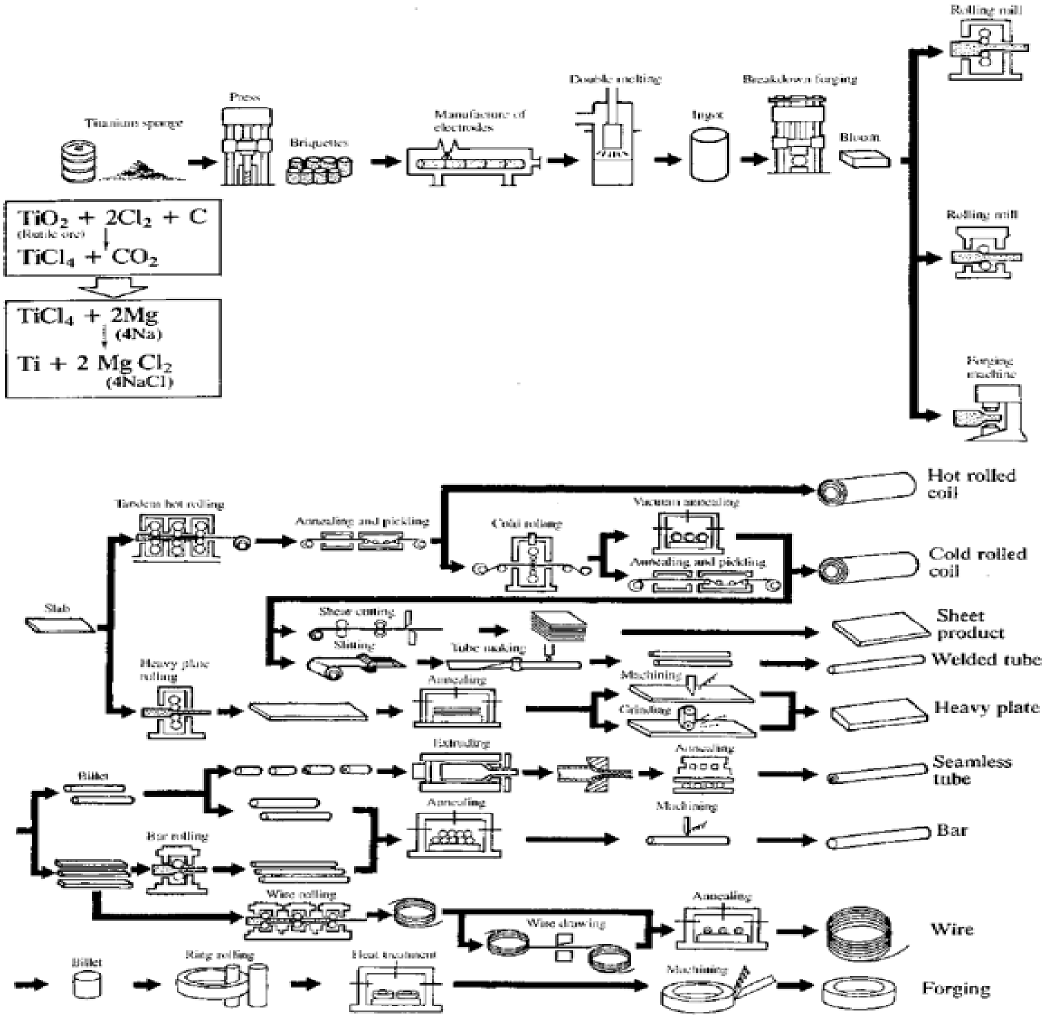
Titanium sponge
Press
Briquettes
Manufacture of electrodes
Double melting
Ingot
Breakdown forging
Bloom
Rolling mill
Rolling mill
Forging machine
TiO2 + 2Cl2 + C
(Rutile ore)
TiCl4 + CO2
TiCl4 + 2Mg
(4Na)
Ti + 2 Mg Cl2
(4NaCl)
Tandem hot rolling
Annealing and pickling
Cold rolling
Vacuum annealing
Annealing and pickling
Hot rolled coil
Cold rolled coil
Slab
Shear cutting
Slitting
Tube making
Sheet product
Welded tube
Heavy plate rolling
Annealing
Machining
Grinding
Heavy plate
Billet
Extruding
Annealing
Seamless tube
Annealing
Machining
Bar
Bar rolling
Wire rolling
Wire drawing
Annealing
Wire
Billet
Ring rolling
Heat treatment
Machining
Forging

Fig. 2.3: Processing and manufacturing cycle of Ti [PED01]

Once the Ti sponge is obtained, ingots are produced by mixing the sponge with alloying elements and Ti scrap is re-melted in vacuum arc furnaces under inert atmospheres. Multiple melting operations are carried out in the same furnace to enhance the homogeneity of the ingot. Once the ingot is produced and a primary operation or fabrication such as forging is done to obtain a mill product, secondary fabrication such as extrusion is carried out on the mill products into the final product. Fig. 2.3 shows a schematic sketch of the processing and manufacturing cycle of Ti.

Due to the difficulty in processing Ti, at approximately $50/kg, is more expensive than steel and aluminium which are $1/kg and $4/kg respectively. However due to its good combination of mechanical and physical properties, it is still used in niche markets where functionality outweighs cost. Ti has a high melting point of 1725 ºC which is about 200 ºC higher than that of melting point of steel and is considered to be a refractory material. Ti has a density of 4.51 g/cm^3 which puts it between aluminium and steel [BIE05]. This gives Ti a high specific strength which is ideal for aerospace and automotive applications where minimization of weight is essential for peak functionality and performance.

2.1.2. Metallurgy of titanium alloys

As mentioned before pure titanium exists in two phases with respect to the temperature. The stability of the phases and their amount at room temperature can be changed by adding different alloying elements. Moreover, adding alloying elements to titanium also changes the ß-transus temperature. Fig. 2.4 shows the effect of some alloying elements on the ß-transus temperature.

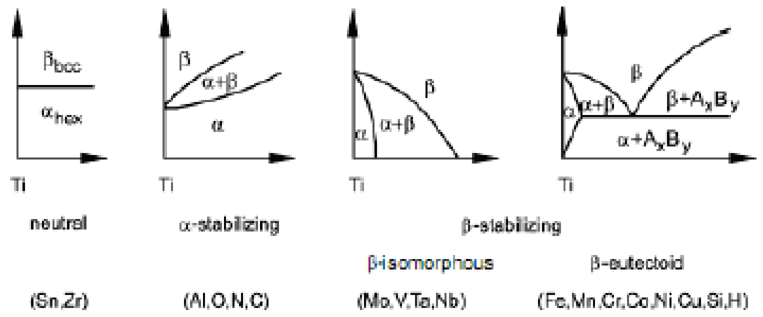

Fig. 2.4: The effect of alloying elements on phase diagrams of Titanium alloys [LEY03]

As seen from Fig. 2.4 there are elements that added to titanium increase the ß-transus temperature through stabilizing the α-phase and those elements are called α-stabilizers. In contrast, there are elements known as ß stabilizers that are stabilizing ß-phase thereby decreasing the ß-transus temperature. The ß-stabilizing elements are divided into ß-isomorphous and ß-eutectoid elements. Those elements have high solubility in titanium are ß-isomorphous, whereas the ß-eutectoid elements have limited solubility and tend to form intermetallics. On the other hand, there are also elements that do not affect the ß-transus temperature and they are called neutral elements.

Aluminum is the most common used α-stabilizing alloying element because it is the only element that raises the ß-transus temperature and has large solubility in both α and ß-phase (see Fig. 2.5). However, its content in most titanium alloys is limited to about 6 wt. % in order to avoid formation of Ti_3Al precipitates in the α-phase. From the Ti-Al phase diagram shown in Fig. 2.5, it can be seen that for about 6 wt. % aluminium the β-transus temperature is elevated from 882 to about 1000 °C. Moreover, the Ti-Al phase diagram is also the basis for the development of titanium-aluminum intermetallics that are characterized with high strength at high temperatures, but also with very low ductility and fracture toughness compared to the conventional titanium alloys. Other α-stabilizing elements include B, Ga, Ge and some rare-earth elements but because of their low solubility they are not commonly used as alloying elements.

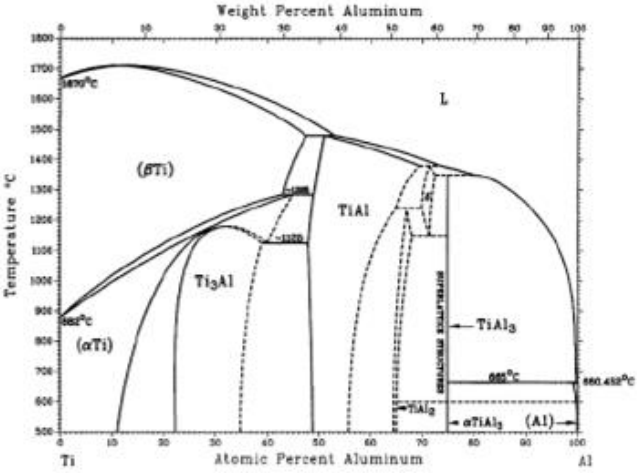

Fig. 2.5: Ti-Al phase diagram

Most frequently used β-isomorphous stabilizing elements include V, Mo and Nb that in sufficient amounts stabilize the β-phase at room temperature. In the group of β-eutectoid stabilizing elements that are used in many titanium alloys belong Cr, Fe and Si, whereas Zr, Hf and Sn behave neutral i.e. do not have strong impact on the β-transus temperature. Some of the most common alloying elements and their stabilizing effect are shown in Table 2.1. Oxygen is also an important alloying element that has significant impact by increasing the strength of titanium alloys and is used to obtain the desired strength levels.

Table 2.1: Effects of different alloying elements on Ti [BOY92]

Alloying elements	Range (appx. wt%)	Effect on structure
Aluminium	2-7	α stabilizer
Tin	2-6	α stabilizer
Vanadium	2-20	β stabilizer
Molybdenum	2-20	β stabilizer
Chromium	2-12	β stabilizer
Copper	2-6	β stabilizer
Zirconium	2-8	α and β strengthener
Silicon	0.2-1	Improves creep resistance

2.1.3. Alloy classification

Today more than 100 titanium alloys are known, of which, only 20 to 30 have reached commercial status. Of these, the classic alloy Ti-6Al-4V covers more than 50% of usage where, another 20 to 30% are unalloyed titanium.

Usually titanium alloys are classified as α, α+β, and β alloys, with further subdivision into near-α and metastable β alloys. The classification is based on the type and amount of alloying elements which determines the dominate phase at room temperature. This is schematically outlined in a three-dimensional phase diagram, which is composed of two phase diagrams with an α and a β-stabilizing element respectively (see Fig. 2.6).

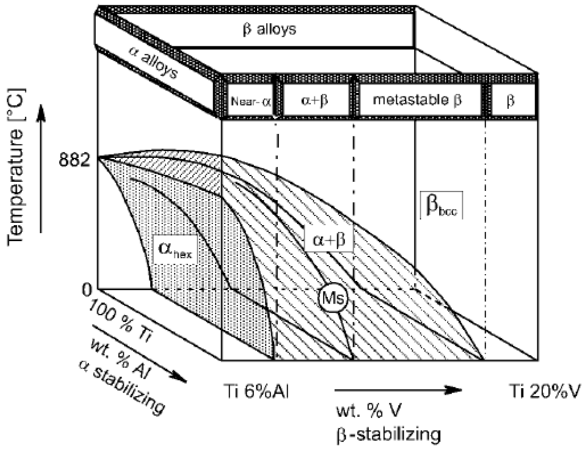

Fig. 2.6: Three-dimensional phase diagram to classify Ti alloys (schematically) [BEA06]

α and Near α alloys

This class of alloys comprise commercially pure (CP) titanium and alloys that contain α-stabilizing and/or neutral elements such as aluminum, oxygen, gallium and tin are known as α alloys [BOY94, DON00]. The CP titanium grades differ only in the oxygen content that drastically increases the strength, but also reduces the ductility. Elements like iron and carbon are considered as impurities obtained mainly from the manufacturing process. These alloys exhibit a HCP crystal structure at room temperature. Some of the alloys belonging to α-phase are Ti-5Al-2.5 Sn and Ti-Al-Ga alloys.

When α alloys are mixed with small amounts of β stabilizers (maximum of 2% [WEI99]) then such group of alloys are classified to be “super α” or “near α” alloys [LEY03]. These alloys are used in high temperature applications (500-550 °C) since they have excellent creep behaviour and high strength. The excellent creep properties at elevated temperatures are due to the small additions of Si. This tends to segregate on dislocations and form TiSi precipitates in the grain boundaries, thus preventing dislocation climb and deformation. Some of the alloys belonging to near α group are: Ti-8Al-1Mo-1V and Ti-6Al-2Nb-1Ta-0.8Mo.

α alloys are known for their strength, creep resistance, toughness and weldability [WAL05]. As of these properties α alloys have found their usages in the field of cryogenic applications. Near α /super α alloys can be heat treatable only to a certain extent. Thermo-mechanical operations such as forgings can be done using small reduction steps to control their microstructural properties.

α+β alloys

α+β alloys are the class of titanium alloys which contain one or more α stabilizers in addition to one or more β stabilizers. Since these alloys contain both the α and β stabilizers, their microstructure is a combination of α-phase (HCP) and the β-phase (BCC). This class of alloys is recognized by the combination of high strength and ductility in comparison with the other two main classes of titanium alloys.

Among the α+β alloys, Ti-6Al-4V is by far the most popular titanium alloy. It is the most popular and most used alloy because of the good balance of properties such as good castability, plastic workability, heat treatability and weldability. Some of the other α+β alloys are Ti-6Al-6V-2Sn, Ti-7Al-4Mo, Ti-5Al-2Sn-2Zr-4Mo-4Cr.

β Alloys

β alloys are the class of titanium alloys which contain one or more β stabilizers and very small amounts of α stabilizers [BOY92]. β alloys are characteristic for their high hardenability and have excellent forgeability.

β-phase is generally a metastable phase and hence has a tendency to transform into equilibrium α+β structure. β alloys are considered for their good castability, deep hardenability and good corrosion resistance. The disadvantage of β alloy in comparison to α+β alloys are high density, low creep resistance and low ductility [DIE88]. β alloys have found their usage in military, aerospace and bio medical applications. Some of the β alloys are Ti-13V-11Cr-3Al, Ti-10V-2Fe-3Al and Ti-3Al-8V-6Cr-4Mo-4Zr.

Metastable β Alloys

In the last few decades the importance of metastable β alloys has steadily increased and these alloys can be hardened to extremely high strength levels of more than 1400 MPa. In the case of β alloys like TIMETAL 10-2-3 and β C, the complex microstructure enables the designer to optimize for both high strength and high toughness. Other β alloys like TIMETAL 15-3 can be deformed at room temperature down to thin foils. TIMETAL 21S was specially developed as an oxidation resistant foil alloy to be used as the matrix for long fiber reinforced titanium alloys. TIMETAL low cost ß (LCB) is a price-sensitive ß alloy particularly aimed at applications beyond the aerospace sector, e.g. for the automotive industry. ß-CEZ was developed in France for application at moderate temperatures in gas turbine engines. Due to its very fine grained bimodal microstructure, the Japanese alloy SP 700 features excellent superplastic behavior even at temperatures as low as 700 ºC. Wide spread application of ß alloys is, however, limited by its relatively high specific weight, modest weldability, poor oxidation behavior, and complex microstructure. A list of the most important commercial alloys belonging to each of these different groups is shown in Table 2.2.

Table 2.2: Important commercial titanium alloys [LUTO7]

Commercial name	**Composition (wt. %)**	**T_β (ºC)**
α alloys		
High purity Ti	99-98 Ti	882
Grade 1	CP-Ti (0.2Fe, 0.18O)	890
Grade 2	CP-Ti (0.3Fe, 0.25O)	915
Grade 3	CP-Ti (0.2Fe, 0.35O)	920
Grade 4	CP-Ti (0.5Fe, 0.4O)	950
Grade 7	Ti-0.2Pd	915
Grade 12	Ti-0.3Mo-0.8Ni	880
Ti-8-2.5	Ti-5Al-2.5Sn	1040
Ti-3-2.5	Ti-3Al-2.5V	935
α+β alloys		
Ti-811	Ti-8Al-1V-1Mo	1040
TIMET 685	Ti-6Al-5Zr-0.5Mo-0.25Si	1020
TIMET 834	Ti-5.8Al-4Sn-3.5 Zr-0.5Mo-0.7Nb-0.35Si-0.06C	1045
Ti-6242	Ti-6Al-2Sn-4Zr-2Mo-0.1Si	995
Ti-64	Ti-6Al-4V (0.20O)	995
Ti-64 ELI	Ti-6Al-4V (0.13O)	975
Ti-662	Ti-6Al-6V-2Sn	945
Ti-550	Ti-4Al-2Sn-4Mo-0.5Si	975
β alloys		
Ti-6246	Ti-6Al-2Sn-4Zr-6Mo	940
Ti-17	Ti-5Al-2Sn-2Zr-4Mo-4Cr	890
SP-700	Ti-4.5Al-3V-2Mo-2Fe	900
Beta-CEZ	Ti-5Al-2Sn-2Cr-4Mo-4Zr-1Fe	890
Ti-10-2-3	Ti-10V-2Fe-3Al	800
Beta 21S	Ti-15Mo-2.7Nb-3Al-0.2Si	810
Ti-LCB	Ti-4.5Fe-6.8Mo-1.5Al	810
Ti-15-3	Ti-15V-3Cr-3Al-3Sn	760
Beta C	Ti-3Al-8V-6Cr-4Mo-4Zr	730
B120VCA	Ti-13V-11Cr-3Al	700

2.1.4. Ti-6Al-4V

The work presented in this thesis is with Ti-6Al-4V an α+ß alloy which has a chemical composition of 6% aluminium, 4% vanadium, max. 0.25% iron, max. 0.2% oxygen and the rest is titanium. It is remarkably stronger than commercially pure titanium while having the same stiffness and thermal properties. Among its many advantages, it is fully heat treatable in section sizes up to 15 mm and is used up to approximately 400 °C (750 °F).

This grade has an excellent combination of strength, corrosion resistance, weld and workability which makes it attractive for applications in aerospace, pressure vessels, surgical implants among others [BOY94, BOY92]. This alloy is unique in that it combines attractive properties with inherent workability and it will continue to be the most-used titanium alloy for many years in the future.

Components for these applications have precise requirements on mechanical and physical properties [JAM03]. In fact, about two thirds of all titanium metal produced is used in aircraft engines and frames. Fig. 2.7a discloses the superior structural efficiency of high strength titanium alloys with comparing to structural steels and aluminum alloys. Titanium alloys also exhibit excellent S-N fatigue strength and life in air, which remains relatively unaffected by seawater in Fig. 2.7b and other environments [RMI00].

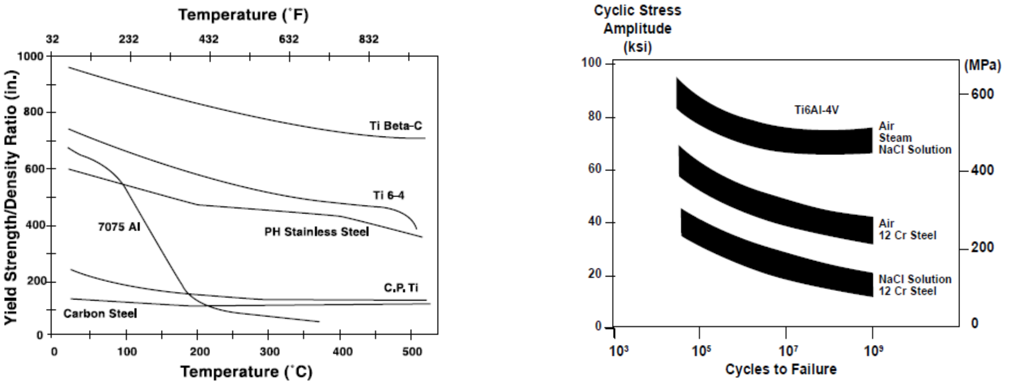

(a) (b)

Fig. 2.7: (a)Titanium Properties (b) Fatigue Titanium Properties [RMI00]

Ti-6Al-4V can be produced in a various formulation. Depending on the field of application the amounts of the oxygen and nitrogen in the alloy can be controlled. The amount of oxygen in the alloy is between 0.08 to 0.2% and the maximum concentration of nitrogen is 0.05%. The higher the concentrations of nitrogen and oxygen result in greater strength of the alloy; conversely lower concentrations of nitrogen and oxygen increase the ductility, fracture toughness, stress corrosion resistance and resistance to crack growth [DON00, BOY92].

2.1.5. Mechanical properties of titanium alloys

The mechanical properties of titanium alloys can be adjusted through alloying and processing. Fig. 2.8 shows schematically these relationships.

Alloying is the method used to adjust the properties through balancing the chemical composition of the alloy. Different elements are used to modify the strength via precipitation and/or solid solution hardening mechanisms. This type of modification also determines the physical properties such as density, Young's modulus and thermal expansion coefficient. Moreover, the alloying also determines the chemical resistance of the alloy, such as oxidation and corrosion. Processing is another important way to balance the mechanical properties of titanium alloys. This allows obtaining the desired type of microstructure that fulfils the specific properties required for the final application.

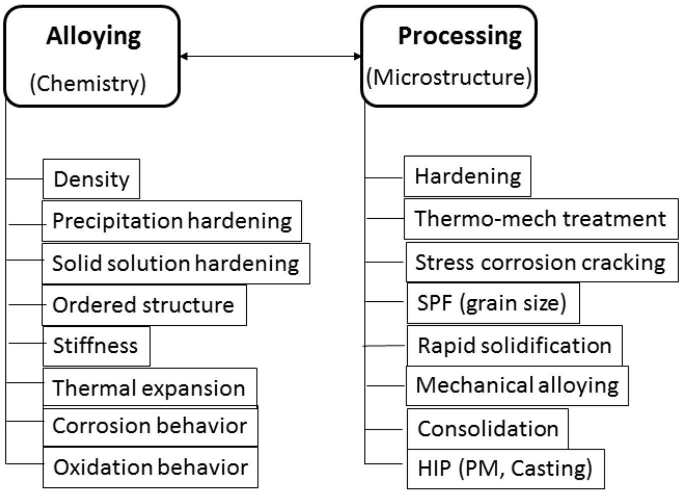
Alloying
(Chemistry)
Processing
(Microstructure)
Density
Precipitation hardening
Solid solution hardening
Ordered structure
Stiffness
Thermal expansion
Corrosion behavior
Oxidation behavior
Hardening
Thermo-mech treatment
Stress corrosion cracking
SPF (grain size)
Rapid solidification
Mechanical alloying
Consolidation
HIP (PM, Casting)

Fig. 2.8: Ways for modification of properties in titanium alloys

The properties of titanium alloys are primarily decided by an arrangement, volume fraction, and individual properties of the two phases α and ß. Compared with the body-cantered cubic ß, the hexagonal α is more densely packed and has an anisotropic crystal structure. Compared with ß, α is characterized by the following properties:

- higher resistance to plastic deformation
- reduced ductility
- anisotropic mechanical and physical properties
- a diffusion rate which is at least two orders of magnitude lower
- higher creep resistance

In Tables 2.3 and 2.4, the essential differences between the three alloy classes – α, α+ß and ß- are outlined on the basis of physical, mechanical, and technological properties. The chemical composition, frequently used short or trade names, the ß-transus temperature, the developing company and the year of introduction of the individual alloys are also noted. Not listed are alloys of the CIS states since their usage in western countries is still limited.

Table 2.3: Properties of α, α+β and β Ti alloys [LEY03]

	α	**α+β**	**β**
Density	+	+	–
Strength	–	+	++
Ductility	–/+	+	+/–
Fracture toughness	+	–/+	+/–
Creep strength	+	+/–	–
Corrosion behavior	++	+	+/–
Oxidation behavior	++	+/–	–
Weldability	+	+/–	–
Cold formability	– –	–	–/+

Table 2.4: Mechanical properties of selected titanium alloys [LEY03]

Alloys	**Developer**	**Year**	**Hardness (HV)**	**E (GPa)**	**YS (MPa)**	**TS (MPa)**	**% El**	**K_{Ic} (MPa $m^{1/2}$)**
α alloys								
High purity Ti			100	100-145	140	235	50	
Grade 1	Miscellaneous		120		170-310	>240	24	
Grade 4	Miscellaneous		260	100-120	480-655	>550	15	
Grade 6	Miscellaneous	1953	300	109	827	861	15	70
Near-α alloys								
Ti-6242	RMI, USA	1970	340	114	990	1010	13	70
TIMET 1100	Timet, USA	1988		112	900-950	1010-1050	10-16	60-75
TIMET 685	IMI, UK	1969		120	850-910	990-1020	6-11	68
TIMET 834	IMI, UK	1984	350	120	910	1030	6-12	45
α+β alloys								
Ti-64	Miscellaneous	1954	300-400 300-400	110-140	800-1100	900-1200	13-16	33-110
Ti-662	Miscellaneous			110-117	950-1050	1000-1100	10-19	30-70
Ti-62222				110-120	1000-1300	1100-1300	8-15	65-110
Ti-6246	Pratt & Whitney, USA		330-400	114	1000-1100	1100-1200	13-16	30-60
Ti-17	GE, USA	1968	400	112	1050	1100-1250	8-15	30-80
Metastable β alloys								
SP 700	NKK, J	1989	300-500	110	900	960	8-20	60-90
Beta III	Colt/Crucible, USA	1960	250-450	83-103	800-1200	900-1300	8-20	50-100
Beta C	RMI, USA	1969	300-450	86-115	800-1200	900-1300	6-16	50-90
Ti-10-2-3	Timet, USA	1976	300-470	110	1000-1200	1000-1400	6-16	30-100
Ti-15-3	Timet, USA	1981	300-450	80-100	800-1000	800-1100	10-20	40-100

2.1.6. Heat treatments

Titanium, like many other metals and alloys, is often subjected to heat treatments to alter the physical and mechanical properties to better suit particular applications. Heat treatments for titanium are performed for the following reason;

- To reduce residual stresses of fabrication
- To obtain optimum combinations of ductility, machinability and dimensional stability

- To increase strength
- To optimize fracture toughness, fatigue strength and high temperature creep resistance

The type of heat treatments and their resultant effects are dependent on the processing history and alloying elements present in the particular titanium alloy. Unalloyed titanium is often stress relieved and annealed; however, it is not possible to solution heat treat. Comparatively, alloys with large amounts of alloying elements such as Ti-6Al-4V are often able to be solution heat treated to increase strength. Table 2.5 displays some typical heat treatments performed on titanium along with recommended treatment conditions [BIE05].

Table 2.5: Titanium heat treatment techniques [BIE05]

Technique	**Applicable alloys**	**Effect**	**Treatment description**
Stress Relieving	α, β and α+β	Removal of residual stresses from prior fabrication steps and heat treatments	2-4 hrs, 500 °C-600 °C, air cool
Annealing	α, β and α+β	Primarily increase fracture toughness, room temperature ductility and high temperature creep resistance	2 hr, 700-800 °C, air cool
Solution Treating	β and α+β	Used to tailor ratios of α to β by methods of strategic heat in cooling to provide a foundation for ageing heat treatments	10 min, 940 °C, water quench
Quenching	α, β and α+β	Cooling technique used for control of α+β morphology and production of thermodynamic driving force for further low temperature heat treatments	Rapid cool achieved by water quench
Ageing	β and α+β	Final heat treatment step for large increase via the decomposition of the super saturated β-phase	4 hr, 500 °C-550 °C, air cool

Heat treatment of titanium must be carefully performed in controlled environments so as to avoid unwanted contamination due to the interstitial diffusion of oxygen and nitrogen present in the atmosphere. Extended exposure to atmospheric conditions at elevated temperature results in the formation of an oxygen rich surface layer which can often cause unwanted changes in morphology of the grain structure and physical surface of the component as well as the mechanical properties of the component. Alternatively, to treatment in a controlled environment, treatment may be carried out in atmospheric conditions and the affected layer be removed by mechanical or chemical methods.

Fig. 2.9 shows the possible locations for die forging temperature and/or heat treatment temperatures of a typical α+β alloy such as Ti-6Al-4V schematically. The higher the processing temperature in the α+β region, the more β will be available to transform on cooling.

On quenching from above the ß-transus, a completely transformed, acicular structure arises. The exact form of the globular α and the transformed ß structures produced by processing depends on the exact location of the ß-transus, which varies from heat to heat of a given alloy and also on the degree and nature of deformation produced, as well as the cooling rate from forging.

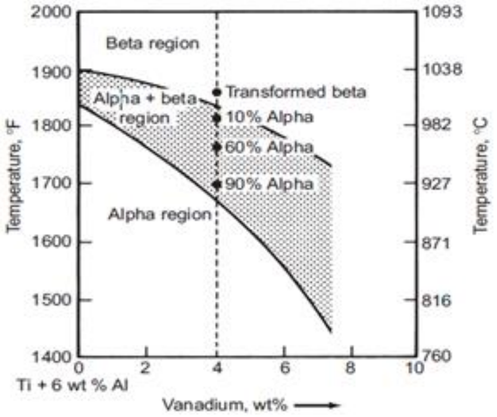

Fig. 2.9: Phase diagram used to predict results of forging or heat treatment practice [BEA06]

2.2. Alpha-Case Formation

Titanium alloys have an affinity to form a hardened surface layer termed as alpha-case, when subject to unsuitable heat treatments or harsh operating conditions involving elevated temperatures. A “thin, continuous, hard, brittle surface layer” that is created during the forging process as titanium interacts with oxygen is called alpha-case which significantly reduces several important mechanical properties of titanium alloys [KEA07]. There is limited data available to characterising the alpha-casing at high temperatures and also to study relationships between the alloy composition and the rate of alpha-case formation are poorly understood. There are two principle processes which occur in the oxidation of titanium alloys:

1. Formation of an oxide scale termed alpha-case (not to be confused with the naturally occurring α phase of pure titanium)
2. Dissolution of non-metals into the sub surface zone

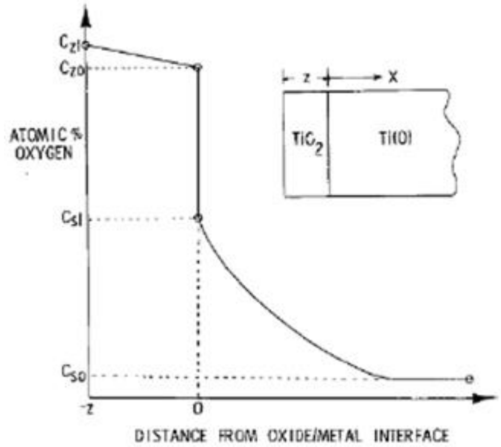

Fig. 2.10: Oxygen concentration profile of oxidized titanium according to Wagner's model (Schematically) [UNN86]

The simultaneous oxide scale and alpha-case formation can be described by the Wagner's model [JOS52] which shows schematically in Fig. 2.10. As shown in Fig. 2.10 the oxygen concentration profile is composed of two individual concentration profiles, one for the oxide (TiO_2) and the other one for the oxygen diffusion layer i.e. alpha-case layer. Both profiles have specific thicknesses, TiO_2 has thickness (*z*), whereas the alpha-case layer has thickness (*x*). The alpha-case layer has large oxygen solubility range starting with the highest oxygen concentration at the point C_{sl}, i.e. the oxide/metal interface and ending at distance C_{so} where the oxygen content reaches the oxygen bulk concentration present in the base metal. In contrast, the solubility of oxygen in the oxide scale is limited and it can be considered to be linear. It can be seen that the oxygen concentration present in the metal gradually decreases. The oxygen concentration at the oxide/metal interface (C_{sl}) is dependent on the exposure temperature and time and it can reach a maximum value of 14.3 wt. %, which is the maximum solid solubility of oxygen in α-titanium.

2.2.1. Oxidation of titanium alloys

Oxygen, time, and temperature are the most dominating factors in alpha-case formation [GUR03]. Since oxygen readily diffuses into titanium at high temperatures, as the amount of atmospheric oxygen is increased, the alpha-case layer becomes more delineated. Similarly, at greater time intervals and temperatures the alpha-case layer becomes more pronounced.

Titanium has high tendency to react with oxygen when exposed to oxidizing environments. The reaction between titanium and oxygen at room temperature results in the formation of a thin and passive TiO_2 layer which provides protection of the metal surface from oxidation and corrosion in different corrosive environments. However, at elevated temperatures the TiO_2 layer loses its protectiveness and allows oxygen to be dissolved into the titanium bulk metal. In case of α-titanium, the solubility of oxygen is about 30 at. %

showing very small variations with temperature, whereas the solubility in ß-titanium increases with temperature and at 1700 °C reaches maximum solubility about 8 at. %. Fig. 2.11 shows the Ti-O phase diagram, from where it can be seen that many stable titanium oxides such as Ti_2O, TiO, Ti_2O_3 and Ti_3O_5, Ti_nO_{2n-1} (4 < n < 38) and TiO_2 can be formed. However, for oxidation at temperatures below 1000 °C and at near-atmospheric pressures only the Ti_2O rutile type modification has been detected in the oxide scales [KOF88].

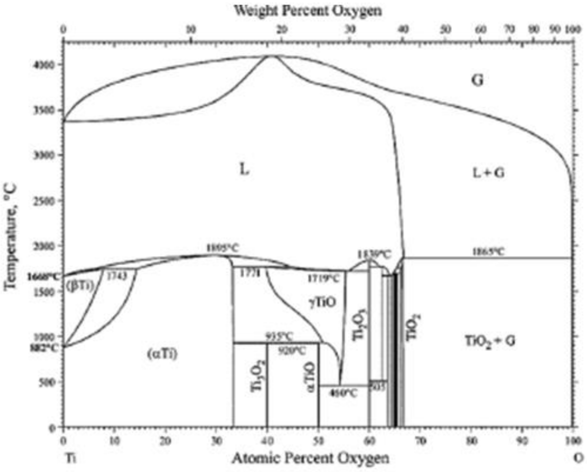

Fig. 2.11: Ti-O phase diagram [OKA11]

The oxidation of Commercially pure titanium in different types of domains at wide temperature ranges have been broadly investigated by many authors. The most remarkable studies of oxidation on titanium in oxygen at atmospheric pressures and broad temperature range have been performed [KOF58,66,88, STR60]. In these researches, different oxidation behaviour of titanium has been reported mainly dependent on the oxidation temperature and time, shown in Fig. 2.12. From Fig. 2.12, it was observed that temperatures below 400 °C the oxidation rate of titanium follows logarithmic law, in the temperature range 400-600 °C cubic law and in the temperature range 600-700 °C parabolic behaviour. However, after prolonged oxidation times they have observed a change of the parabolic rate to approximately a linear rate. Moreover, at temperatures higher than 900 °C, the observed oxidation rate was linear, followed with slower rates after longer times.

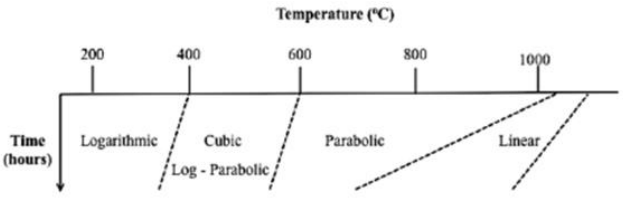

Fig. 2.12: Rate equations observed in the oxidation of titanium (Schematically) [KOF66]

The oxidation of Ti-6Al-4V alloy has been investigated in different oxidizing conditions at different temperatures and times by many scientists [DU96, PIT04, POQ13, ZEN14]. The oxidation behavior of Ti-6Al-4V alloy in the temperature range of 600-700 °C in air up to 300 hours have studied [FRA94, GUL09]. It has reported that the oxidation kinetics in this temperature range follows mainly parabolic behavior, but changing to linear behaviour at 700 °C after 50 hours exposure time. The reason for the change in oxidation behaviour from parabolic to linear is considered to be due to the changes in the morphology of the formed oxide scale. At lower temperatures, the formed oxide scale is dense and compact, whereas at higher temperatures it becomes porous and spalls off which leads to an increase of the oxidation rate.

2.2.2. Diffusion in titanium alloys

Diffusivity of various elements in titanium is of metallurgical and technological importance and many of the production processes, such as heat treatments are diffusion dependent. As mentioned previously titanium oxidizes easily when exposed to elevated temperature and oxygen containing environments. The overall oxidation reaction includes oxide formation and inward oxygen diffusion in the titanium. The diffusion of oxygen is possible due to the high solubility of oxygen in α-titanium and the stabilizing effect by the oxygen of the HCP crystal structure of α-titanium. The oxygen diffusion rate into the bulk can be determined using different methods. One of the simplest and most conventional methods to measure the oxygen diffusive layer thickness is the microhardness method, since the increase of oxygen concentration in the metal corresponds to an increase of the hardness [AER07]. Several models of oxygen diffusion and oxidation of titanium have been presented in the literature and are discussed in this following section.

Oxygen diffuses into titanium via interstitial diffusion and causes the formation of a brittle oxide layer (alpha-case) on the surface. The two most common forms of the TiO_2 oxide layer are Rutile and Anatase [GUL09]. The further inward diffusion of oxygen into the exposed component results in an oxygen diffusion zone (ODZ) in which the mechanical and physical properties are affected [VEN09]. This can be seen by the increase in hardness toward the surface in Grade 5 and CP titanium after 36 hours of heat treatment at 625°C as shown in Fig. 2.13. Fig. 2.14 shows the results of secondary neutral mass spectrometry (SNMS) performed from the sample surface to the centre cross section on an affected component of commercially pure titanium. It can be seen that the surface is oxygen rich and forms the oxide layer, above a critical oxygen concentration.

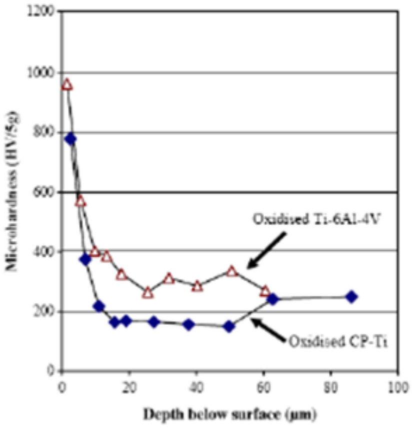

Fig. 2.13: Microhardness-depth profiles for oxidised CP-Ti and Ti-6Al-4V (Grade 5) (36 hr at 625°C) [DEA04]

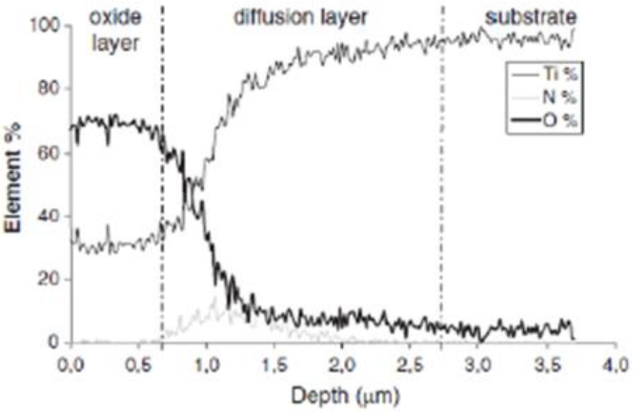

Fig. 2.14: SNMS results for a CP alloy (T40) treated at 720 C for 150 min. The alpha-case layer is shown as the oxide layer [SCH06]

2.2.3. Mechanisms and Morphology

I. Gurappa at the Metallurgical Research Laboratory of India, conducted a study to determine the depth of alpha-casing in regard to time and temperature. Fig. 2.15 [GUR03] shows the predicted depth of alpha-casing with respect to increasing time and temperature. As shown over a set period of time, temperature has a significant effect on the alpha-case layer.

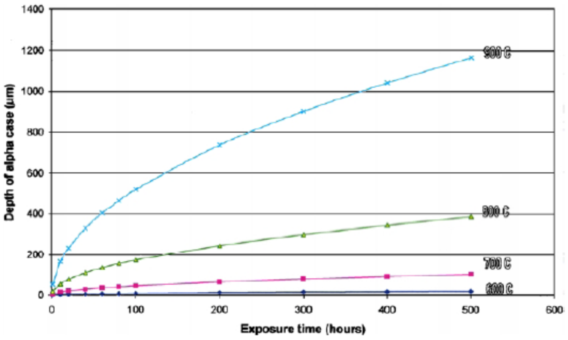

Fig. 2.15: Predicted depth of alpha-case for titanium alloy IMI 834 at different exposed temperatures [GUR03]

Fig. 2.16 [GUR03] shows a similar graph of measured microhardness profiles, however the alpha-case depth is reported as a function of microhardness. The depth is a minimum at 25 µm at 600 °C and a slight increase is seen with a minimum of 50 µm at 700°C. Then, finally at 900 °C, a drastic increase to 140 µm is observed.

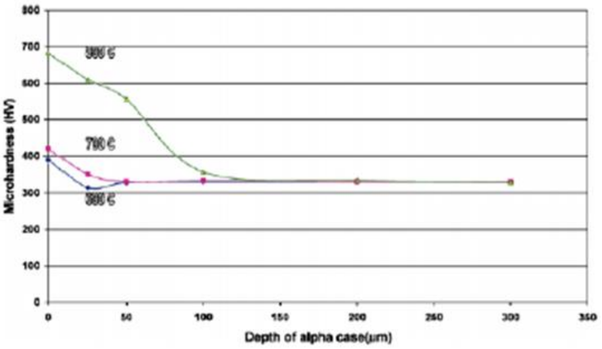

Fig. 2.16: Measured microhardness profiles of titanium alloy, IMI 834, after 100 h of oxidation at various temperatures showing the depth of alpha-case [GUR03]

Du et al. [DU94] presented a mechanism of formation of the multi–layered oxide scale structure that involves the activity of titanium and aluminum regarding oxygen and the oxygen partial pressure present in the oxide scale. Once the TiO_2 is formed the alloy is separated from its environment by the oxide scale and the partial oxygen pressure in the oxide moving from the gas/oxide interface towards the oxide/metal interface is decreasing to a value close to that of the dissociation pressure of TiO_2. At such low oxygen, partial pressures the minimum activities required to form Al_2O_3 at different elevated temperatures are high and therefore unlikely to form Al_2O_3 at the oxide/metal interface. In contrast, the oxygen partial pressure at the gas/oxide interface is relatively high which allows formation of Al_2O_3 layer on top of the already formed TiO_2 oxide scale. This indicates that oxygen is diffusing inward to the oxide/metal interface, reacting to form TiO_2 increasing the thickness of the TiO_2, whereas aluminum diffuses outward towards the gas/oxide interface where it reacts with oxygen and forms an outer layer of Al_2O_3. Once the double oxide layer of TiO_2 and Al_2O_3 is formed the consequent grow of the oxide scale causes cracks at the oxide/metal interface when some critical thickness of the oxide scale is reached. Additionally, the cracking is a result of the different thermal expansion coefficients of the oxide scale and the metal substrate that initially would start at the edges and expand progressively through the entire surface of the oxide. The detachment of the oxide scale from the metal substrate would increase the oxygen partial pressure close to the oxide/metal interface that would produce conditions favorable for formation of the second TiO_2 layer. As the oxidation continues, these processes will repeat resulting in formation of multi-layered structure of TiO_2 and Al_2O_3 layers of the oxide scale in Ti-6Al-4V. The oxidation mechanism of formation of multi-layered oxide scale in Ti-6Al-4V is schematically shown in Fig. 2.17.

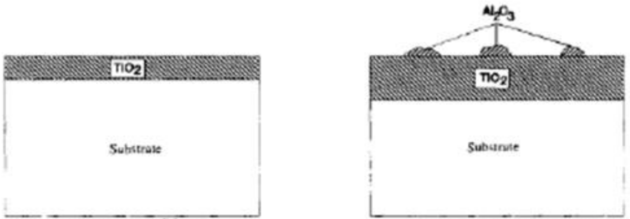

(a) Formation of TiO_2 layer

(b) Nucleation of Al_2O_3 and thickening of TiO_2 layer

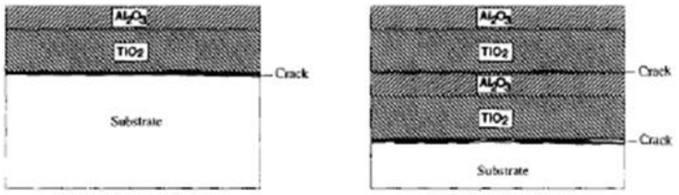

(c) Formation of Al_2O_3 layer and occurrence of crack

(d) Subsequent Al_2O_3 and TiO_2 layering

Fig. 2.17: Formation of multi-layered structure of the oxide in Ti–6Al–4V (Schematically) [DU94]

Gaddam et al. [GAD13] evaluated the alpha-case depth formed in Ti-6Al-2Sn-4Zr-2Mo (Ti-6242) and Ti-6Al-4V alloys after isothermal heat treatment in ambient air and times up to 500 hours. The selected temperatures were 500 and 593 °C for Ti-6242 and 593 and 700 °C for Ti-6Al-4V, respectively. Moreover, the isothermal oxidation behaviour was studied for both alloys using thermal gravimetric analysis (TGA) in dry air at 593 °C for times up to 200 hours. The analysis of the TGA curves for Ti–6242 and Ti-6Al-4V showed consequent increase of the weight gain per surface area with respect to the exposure time which approximately followed parabolic behaviour in both alloys. From the TGA curves a higher weight gain per surface area for Ti-6Al-4V than for Ti–6242 was observed. It is believed that the higher weight gain is due to the formation of thicker oxide scale in Ti-6Al-4V (~ 5 µm) in comparison with Ti–6242 (< 1 µm).

In addition, the alpha-case depth was measured and compared for the two alloys. The alpha-case depths of all the samples and for both alloys were measured optically after using a two-step etching procedure, where the alpha-case appeared as bright continuous layer next to the edge of the samples (see Fig. 2.18). An approximately parabolic behaviour of the alpha-case growth with respect to the exposure time at all tested temperatures in the two alloys was found. Similar maximum values for the depth of the alpha-case layers (~ 30 µm) formed after the heat treatment performed at 593 °C for 500 hours were observed in both alloys. This indicated that there is not any significant influence of the differences in the chemical composition and the microstructure of the two alloys on the alpha-case depth at 593 °C. Additionally, the heat treatment at 500 °C for Ti–6242 and at 700 °C for Ti-6Al-4V resulted in formation of 10 µm and 200 µm alpha-case depths after 500 hours exposure time.

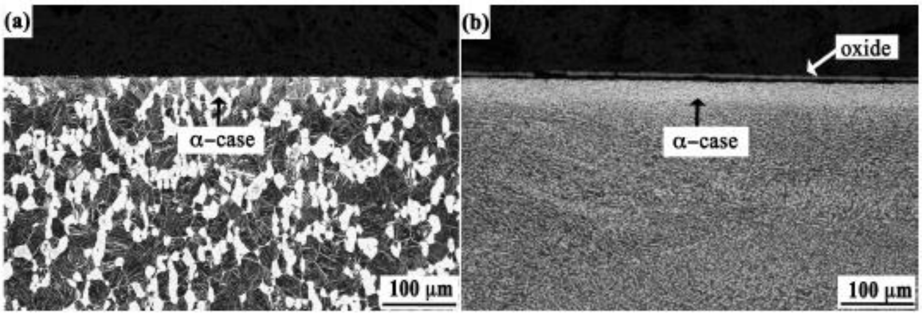

Fig. 2.18: Optical micrographs showing alpha-case (white layer) in (a) Ti-6242 and (b) Ti-64 heated at 593°C up to 500 hours [GAD13]

Moreover, in this paper the hardness of the alpha-case layer was measured and compared with the bulk hardness. It was found that the hardness in the alpha-case layer for both alloys is higher compared with the bulk hardness of the alloys. Additionally, the hardness profile of the Ti-6Al-4V sample heat treated at 700 °C for 500 hours showed that the hardness is gradually decreasing from the surface into the bulk of the alloy to a depth of ~ 250 µm (shown in Fig. 2.19).

To predict accurately diffusion kinetics of oxygen into titanium during heat-treatment, Chretien et al. [CHR10] in cooperation with Wyman-Gordon Company commissioned this study to obtain an accurate rate of alpha-case formation within titanium and investigated reduce alpha-case formation by the use of coatings. This project consisted of heat-treating Ti-6Al-4V and Ti-6Al-4V ELI samples that were uncoated, coated with an SJ, and SJ advanced coating over a condition for a maximum of 6 hours and at 1750°F. These samples were analyzed through optical microscopy and microhardness to determine alpha-case depth (shown in Fig. 2.20 and Table 2.6). The project aimed to find the most economic and optimal solution to reducing alpha-case formation which concluded with a cost analysis.

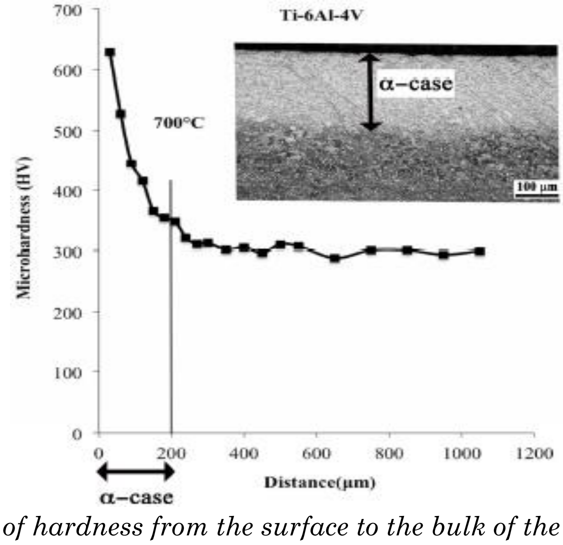

Fig. 2.19: Variation of hardness from the surface to the bulk of the Ti-64 sample exposed to 700°C for 500 hours. An optical micrograph showing the alpha-case of the corresponding sample (the white layer in the micrograph) [GAD13]

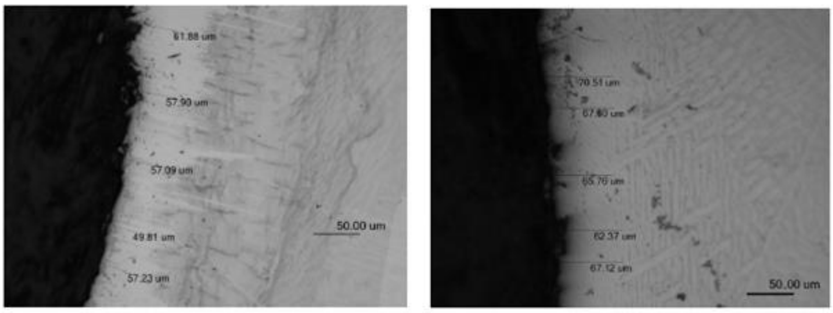

Fig. 2.20: Optical view (20x) of a Ti-6-4 at 6 hrs & 1750°F, (left) uncoated sample and (right) SJ coated sample [CHR10]

Dobeson et al. [DOB09] analysed and document alpha-case formation and its effects on the tensile properties and prevention on Grade 2 and Grade 5 titanium alloys. The investigation looked at the effects of exposure to the atmosphere at elevated temperatures with respect to depth and morphology of the surface layer and grain structure. Microstructural and microhardness analysis have been performed from the surface into the substrate and models of alpha-case development have been created using Fick's Second Law of Diffusion and an Arrhenius law. These models aid in both the prediction of oxygen diffusion and its effects on the surface and bulk mechanical properties of heat affected components. Further, the effects on the bulk mechanical properties have been analysed by tensile testing of selected samples. It has been found that the alpha-case held no structural integrity, even at early stages of tensile deformation. The alpha-casing also caused premature crack initiation in affected samples (shown in Fig. 2.21).

Table 2.6: Alpha-case depth comparison of optical microscopy and microhardness at 6 hr and 1750°F [DOB09]

Titanium Grade	**Coating Condition**	**Optical Depth (µm)**	**Microhardness Depth (µm)**	**Microhardness to Optical Increase (%)**
Ti-6Al-4V	Uncoated	57	90	60
Ti-6Al-4V	SJ	67	110	60
Ti-6Al-4V	SJ advanced	42	50	20
ELI	Uncoated	43	80	90
ELI	SJ	45	100	120
ELI	SJ advanced	21	30	40

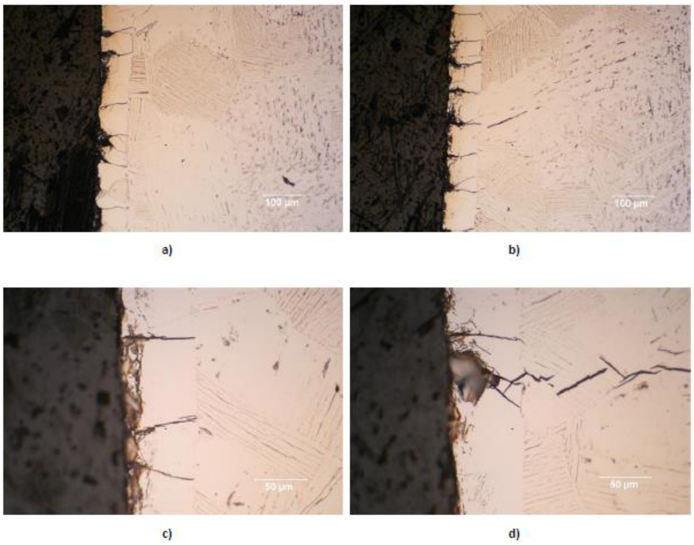

a) b) c) d)

Fig. 2.21: Tensile testing micrographs (Damage accumulation for samples treated above the β-transus temperature at 1050°C for 30 minutes stressed to 0.2% strain). a) and b) at magnifications of 200x. c) and d) at 500x magnification [DOB09]

2.2.4. Prevention and removal of alpha-case in titanium alloys

High temperature coatings like ceramics [LUT07, LEY03, GUR01] are used to prevent oxygen to enter into the base material. When exposed to temperatures greater than 500°C oxygen readily diffuses into titanium. It is necessary to reduce that absorption of oxygen in order to more efficiently forge at higher temperatures. Ceramic coatings cannot be utilized as they have too low malleability and are not stable at the high temperatures necessary to forge. Metallic coatings are more stable at higher temperatures but have the tendency to diffuse metallic particles to the titanium and therefore produce a contaminated alpha-case layer [GUR01]. As an alternative, sodium silicate (Na_2SiO_3) is frequently applied to titanium as an oxygen barrier coating to prevent alpha-case formation. Patankar et al., have been applied Na_2SiO_3 on Ti-6Al-4V and the result shows an ultimate tensile strength (UTS) and yield strength relatively uninfluenced by application of the Na_2SiO_3 coating, as shown in Fig. 2.22 [PATO1]. The only negative effect from the coating was that was an increased ductility. Because this coating was able to prevent alpha-casing, retained its original finishing and most physical properties, this coating seems feasible to be applied to Ti before forging provided ductility is not of major concern.

However, this detrimental alpha-case layer may be removed by machining with tungsten carbide (WC) tools and chemical milling or pickling in nitric or hydrofluoric acid solutions [BIE05]. The chemical milling process includes treatment of the component in chemical baths i.e. removal of the alpha-case by using chemical agents. Mixture of HF and HNO_3 acids in aqueous solution are used. The acid concentration and the bath temperature are controlling the rate of removal. HF dissolves the oxide scale and the titanium metal, whereas HNO_3 serves as oxidizing agent and repassivate the surface of the titanium. The metal dissolution is exothermic and therefore continuous cooling of the bath is required. If the removal rate is very high then gas is forming on the metal surface, which can cause uneven removal. Moreover, good control of the acids ratio in the chemical bath is required, because of the possibility of formation of high quantity of hydrogen that can be absorbed by titanium. Hydrogen uptake during the chemical milling process can be harmful and therefore must be avoided. ASM International [ASM90] provides recommendations for minimal metal removal after thermal exposure of titanium to the atmosphere. Selected treatment temperatures and times taken from the recommendations are displayed in Table 2.7.

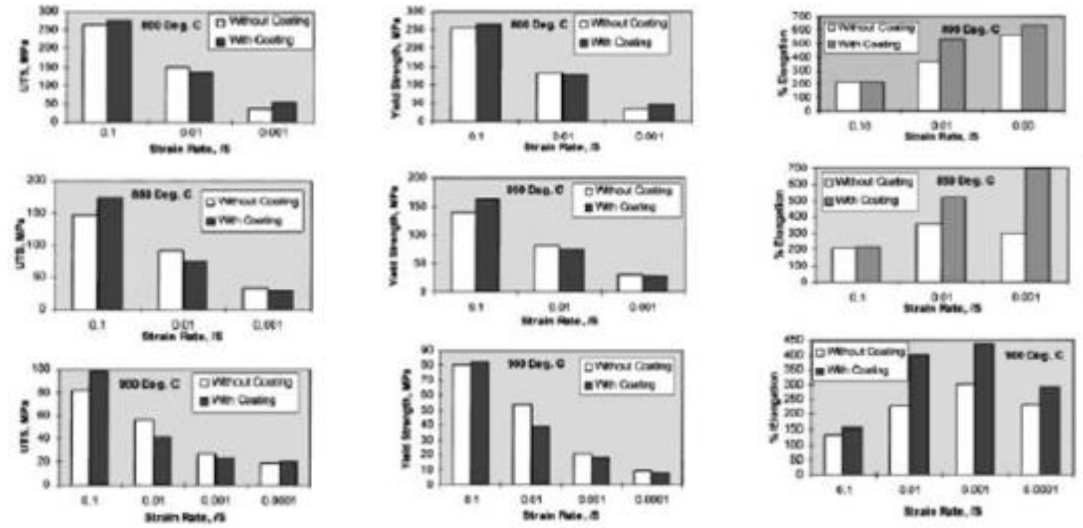

(a) (b) (c)

Fig. 2.22: Variation of (a) UTS, (b) yield strength, and (c) ductility as function of strain rate [PAT01]

Table 2.7: Selected recommended material removal depths after thermal exposure of titanium to the atmosphere [ASM90]

Treatment Temperature (°C)	Treatment Time (h)	Minimum Removal Depth (µm)
480-593	≤ 12	5
705-760	≤ 1	25
955-982	≤ 0.5	114
983-1010	≤ 0.5	145

Also, the alpha-case may be prevented by replacing the atmosphere of the furnace with a neutral gas such as argon or by treating the part under vacuum [SCH06]. In both cases, the use of oxygen getters such as ground titanium dust provides the necessary extra precaution to alpha-case prevention. These procedures do however call for heavy and/or expensive equipment. These techniques of removal and prevention are inapplicable to the formation of alpha-casing on parts in service.

2.3. Forging

As one of the earliest metal working processes, forging has had a long history of development. Forging is usually described as plastic deformation of a bulk metal to a predetermined shape by compressive forces using a hammer or press. Forging technology has a special place between all manufacturing processes because it offers to produce parts of superior mechanical properties with minimum waste of material, the ability to precisely tailor microstructures through deformation and heat treatment resulting in significant material and energy savings. Compared to casting, forging is stronger and has a better response to heat treating and enables production of larger cross sections. Compared to machining, forging has a wider size range of desired material grades and a preferable grain orientation along surface; besides, forging makes material savings as great as 75% compared to machining [SCH98]. By appropriate processing and strict process control, highly reproducible properties are possible. Thus, process is efficiently attractive when a large number of parts must be manufactured and/or when the mechanical properties needed in the finished product can be obtained only by a forging process. Thus, forging is preferred in applications where reliability, strength, fatigue resistance and economy are critical.

2.3.1. Applications of forged parts

Most of the forged parts are in the aerospace and automotive industries. More than 250 forgings can be found in a typical car or truck; most of these parts experience large stress and shock, such as connecting rods, crankshafts, transmission shafts and differential gears. Some aircrafts contain more than 450 structural forgings as well as hundreds of forged engine parts. Considering the required material properties, high specific strength materials like titanium alloys can increase the payloads as well as range and performance. Other industrial applications of forged parts are also found in agricultural machinery, off-highway equipment, industrial equipment, ordnance and oil field equipment.

2.3.2. Forging Design Parameters

Forging process has several design parameters which are specific to itself in terms of the selection of presses, forging and die materials, temperature, forging sequence, preforms. Those are help the final component to have the desired material properties and geometrical shape, the parting plane, dimensions of dies such as gutter and flash and the location of impressions. As it is bulk forming operations, cost is also a very important factor that influences the selection of the above parameters. The control of the above parameters helps the manufacturer to predict the characteristics of the final product. In a general bulk forming process, the key areas of interest should include [ALT97],

- workpiece material: shape and size, chemical composition and microstructure, flow properties under processing conditions, thermal and physical properties
- dies or tools: geometry, surface conditions, material and hardness, surface coating, temperature, stiffness and accuracy
- interface conditions: surface finish, lubrication, friction, heat transfer.
- work zone: mechanics of plastic deformation, material flow, stresses, velocities, temperatures.
- equipment used: speed, production rate, force and energy capabilities, rigidity and accuracy.

2.3.3. Forging Defects

A defect is a flaw in a component that is typical of a process, but not inevitable. Good forging practice can eliminate most of them. They can be summarized in a table as below.

Table 2.8: Possible forging defects [MOD05]

Defects	Description	Problem
Segregation	Non-uniform distribution of elements in metal	Non-uniform hardness
High-hydrogen content	Forms of hydrogen fissures (flakes)	Embrittlement
Inclusions	Non-metallic particles in metal	Act as stress-raisers; make machining difficult (tool breakage)
Bursts	Internal tears (effect of forging operations on inclusions, etc.)	Cracking
Poor grain structure	Overheating, improper billet size, poor die design, etc.	Poor properties in crucial directions; fatigue failure
Laps (folds)	Hot metal folded over and forged into surface, creating discontinuity	Stress-raisers; may cause machining or heat treat cracking problems
Cold shuts	Defective metal flow	Low strength
Cracks, tears	Internal discontinuity (poor design; poor practice- metal)	Cracking

2.3.4. Forging of titanium and its alloys

In order to accurately predict the forging process of titanium alloys, it is of great interest to make deformation behavior well understood. The flow behavior of titanium alloys is characterized by an initial hardening followed by flow softening as shown in Fig. 2.23. Depending on materials, forming temperature and strain rate, the strain associated with peak stress may vary a lot.

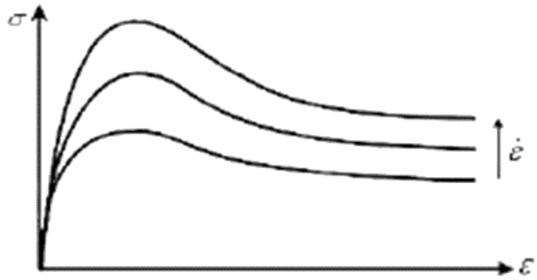

Fig. 2.23: Typical stress strain curves for titanium alloys [MAO09]

With the consideration of dynamic recrystallization, viscoplastic constitutive equations have been employed by [ZHO98] to model the flow stress of titanium alloy IMI834. The dynamic recrystallization, which causes the flow softening, was modelled as internal variables. Material constants were determined by procedure developed by the author. Experiments carried out at different temperatures and strain rates indicated that the model can predict the flow stress successfully in isothermal forging conditions.

For many materials, the flow stress alone is not sufficient to design the processing route since it provides no information on deformation capability and microstructural development. Besides the use of stress-strain curves, another approach to model constitutive behavior is processing maps. It is based on principles of dynamic materials model, in which, the metal being hot worked is assumed to be a nonlinear dissipater of power [PRA98]. The energy is dissipated through temperature rise and microstructural change. How the input power is partitioned between the two is decided by strain rate sensitivity of flow stress m. The efficiency of power dissipation through microstructual process η is defined as:

$$\eta = \frac{2m}{m+1} \tag{2.1}$$

The efficiency of power dissipation represents the constitutive response of the metal under various microstructural mechanisms. The power dissipation map, which is constituted by variation of η with temperature and strain rate, can be directly correlated with specific microstructural mechanisms such as dynamic recrystallization, dynamic recovery, and wedge cracking. A continuum instability criterion is used to identify the regimes of flow instabilities. The instability parameter is defined as:

$$\xi(\dot{\varepsilon}) = \frac{\partial \ln(m/m+1)}{\partial \ln(\dot{\varepsilon})} + m \tag{2.2}$$

Flow instability is predicted when $\xi(\dot{\varepsilon})$ becomes negative. Thus, the instability map can be superimposed on the power dissipation map to give a flow instability zone. This map is called processing map because it can guide process design to optimize workability.

Using power dissipation map and processing map, influences of oxygen content and starting microstructure on hot deformation of commercial pure titanium, ELI Ti-6Al-4V and IMI 685 has been studied [PRA98]. The authors have been concluded that wide instability regimes existed due to adiabatic shear bands formation at higher strain rates; the processing of titanium materials is very sensitive to oxygen content and starting microstructure. The same method was taken by Seshacharyulu and to investigate high oxygen grade Ti-6Al-4V with equiaxed α + β microstructure [SES00]. Material was tested by compression tests at strain rates of 0.0003, 0.001, 0.01, 0.1, 1, 10 and 100 s^{-1} and temperature range of 750-1100 °C at an interval of 50 °C. The flow stress values were given in great detail and power dissipation efficiency map and instability map were developed based on these values (Fig. 2.24). The microstructures of compressed samples were examined and the correlations between the microstructure and maps were explained.

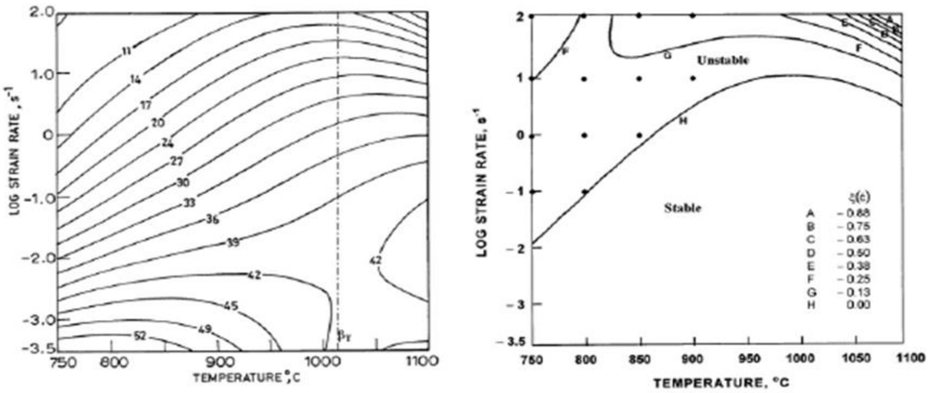

Fig. 2.24: Power dissipation efficiency map and instability map obtained on Ti-6Al-4V [SES00]

Deformation behavior of β alloy Ti-10V-4.5Fe-1.5Al in hot forging has been studied by Balasubrahmanyam et al. [BAL02]. Stress strain curves were recorded at temperature range from 650 °C to 900 °C and strain rate of 0.001, 0.01, 0.1, 1, 10 and 100 s^{-1}. Power dissipation efficiency maps and instability maps were plotted for strain of 0.2 and 0.4, respectively. It was found that the power dissipation efficiency map did not change significantly with increase of strain; and the instability map at strain of 0.4 was almost the same as that at strain of 0.2. By studying phase transformation and microstructure, it was found that forging temperature, degree of deformation and annealing temperature have pronounced effect on fatigue strength of α + β titanium alloys [KUB98].

The mechanical behavior of Ti-6Al-4V at high and moderate temperatures has been studied [MAJ02]. In addition to the test conducted in hot processing temperature range, more tests have been done at temperature between 380-680 °C to investigate the influence of strain rate on the sharp drop in flow stress usually observed in low strain rate experiments. The test results were correlated with the evolution of the microstructure. The authors also proposed a physical-based model and the various deformation mechanisms over the tested range. On the contrary, Bruchi et al. [BRU04] investigated workability of Ti-6Al-4V at high temperature and strain rate. Correlations between the microstructure of deformed specimen and deformation parameters were established. At the tested conditions, increasing temperature or decreasing strain rate can result in a more homogeneous microstructure. The research also identified a stable flow zone at a temperature between 940 and 950 °C and strain rate less than 15 s^{-1}.

2.3.4.1. Finite Element Simulation

The increasing costs of material, energy, and, especially, power require that forging processes and tooling be designed and developed with minimum amount of trial and error with shortest possible lead times. Therefore, to remain competitive, the cost-effective application especially, finite element analysis (FEA)-based computer simulation is an absolute necessity. The practical use of this technique requires a thorough knowledge of the principal variables of the forging process and their interactions. These variables are the flow behavior of the forged material under processing conditions, die geometry and materials, friction and lubrication, the tool and workpiece temperatures, the heat transfer during deformation, the mechanics of deformation, i.e., strains and stresses, the characteristics of the forging equipment, the geometry, tolerances, surface finish and mechanical properties of the forging, and the effects of the process on the environment.

Finite element (FE) programs have been used for quite some time to simulate deformation. Increased computer capacity and improved simulation programs now allow complex 3D component calculations. 3D finite element method (FEM) simulations has been used to evaluate material deformation, geometric changes, and load-displacement results. Apart from mere calculation and optimization of loads, material flow and tooling loads, there is the chance to calculate the microstructural development and so indirectly the component properties [KAR95]. Currently, predictions of microstructures for titanium alloys are restricted to some. Nevertheless, FE simulations can be used to design and optimize processes with respect to modeling of component properties.

This is shown in Fig. 2.25 for a β-forged gas turbine engine compressor disk made of Ti-6-2-4-2. To avoid a continuous precipitation of the α-phase at grain boundaries during processing, rapid cooling of the forged component after die forging is essential. As the temperature distribution in the left figure shows, immediately after deformation large portions of the parts are still above the β-transus temperature (1000 °C). 30 s after deformation the temperature near the surface has already dropped 50 °C below the β-transus. Knowing the time-dependent α+β transformation behavior (e.g. from TTT diagrams) the thickness of the "die chill zone", which shows an undesirable microstructure, can be estimated. If included in the forging allowance, this zone can be removed during subsequent machining without leaving a negative influence on the final component.

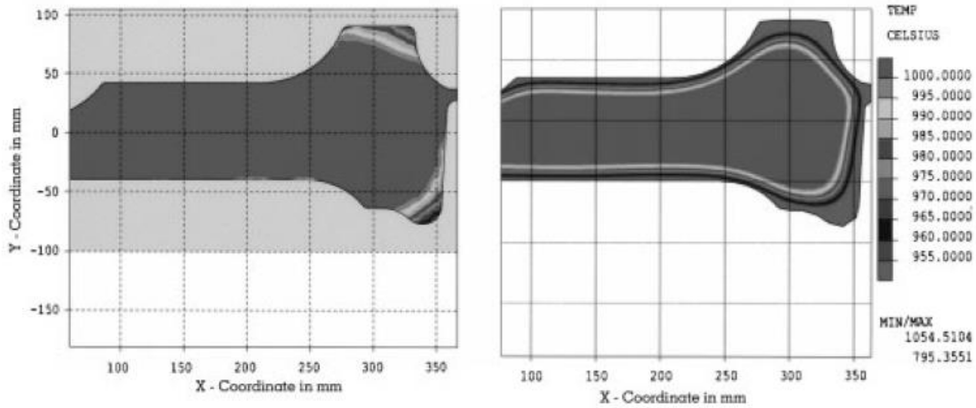

Fig. 2.25: Use of FEM to calculate the "die chill zone" (Ti-6-2-4-2 engine disk) [LEY03]

A lot of research on manufacturing of titanium components, specifically turbine blades, has been done. Finite element modeling of titanium aluminide aerofoil forging conducted by Brooks et al. [BRO98] incorporates flow stress model into finite element codes to simulate isothermal forging. The predictions of press load and microstructure were in good agreement with the experiments. The use of re-meshing in simulations also proved to improve the quality of the calculation. Hu et al. [HU99] determined the evolution of microstructure in blade hot forging by internal state variables. This was extended to intermetallic alloys later [HU01]. Based on their extensive research on blade forging, Zhan et al. [ZHA04] studied the precision forming of a complex blade with damper platform. In order to inspect and analyze the deformation process, 4 cross sections and one longitudinal vertical-section were selected. By analyzing the metal flow and field variable distribution of these 2D cuttings, the complicated 3D deformation nature can be understood better.

2.3.5. Lubrication

In order to avoid direct metal-to-metal contact, a lubricant have introduced at the interface. It is preferred to reduce the friction in bulk metal deformation by using proper types of lubricants to lower the frictional resistance between the die and the workpiece and to present wear as well as galling on the tools [GHA15]. Based on the form of the contact between the tool and the workpiece, the various friction and lubrication conditions can be summarized as in Table 2.9. Various types of friction regimes at the interface have been shown schematically in Fig. 2.26.

Table 2.9: Different friction regimes [MAN11]

Friction regime	**Definition**	**Remarks**	**Relative friction level**
Solid friction (dry)	When there is no separating layer (except oxide layers) between two solids in direct contact in metal forming	Desirable in only rare situations such as hot rolling of plates and slabs	High
Boundary friction	There is a molecular layer of chemical substances covering the contacting surfaces. The lubricant layer is created from surface- active substances and their chemical reaction products	Practical when thick long-lasting lubricant films are technically impossible to achieve in a variety of geometrical and thermal conditions	Medium
Fluid film friction	When a thick layer of a hydrodynamically formed lubricant is present between contacting partners	Only works when the interfacial normal pressure, temperature and relative speed of die and the workpiece are low	Medium
Mixed friction	Combination of the fluid and boundary frictions	Using the appropriate lubricants containing special organics, the machine elements experience mixed friction when starting and stopping their operation	Low

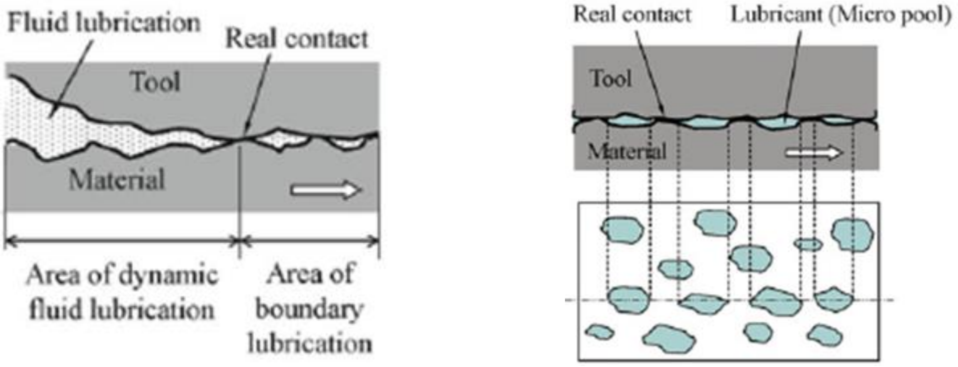

(a) Mixed lubrication (b) Boundary lubrication

Fig. 2.26: Schematic of differences between mixed and boundary lubrication [GHA15]

The selection of the lubricant depends on many factors, hence is verifiable, with a little analysis-based information. Poor selection or poor application of the lubricant type may cause partial direct contact with high pressure between tool and workpiece (Fig. 2.27). This leads to microscale adhesion which leads to galling or seizure or scratch on the final part's surface. The most familiar types of lubricants use in the industry may be categorized as listed in Table 2.10. The most commonly used lubricant application methods can be summarized in Table 2.11.

Table 2.10: Typical lubricants being used for different forming processes [GHA15]

Type of lubricant	Typical lubricant
Liquid lubricant for cold working	Mineral, synthetic, and vegetable oil, wax
Solid lubricant for cold/hot working	Graphite, MoS_2, BN, metallic soap, glass
Chemical conversion coating for cold working	Zinc phosphate+metallic soap, Aluminum fluoride+metallic soap

Table 2.11: Different methods for applying lubricants on the surface [MAN11]

Application method	Definition	Remarks
Dripping	Dripping the liquid lubrication on the blank during the process	Cheap and simple, but difficult to control the proper amount of desired lubricant
Roll coating	Lubricant is applied on the blank moving between two rollers with a certain pressure	Precise control of the amount of lubricant but applicable only for rolling processes
Physical/chemical coating	Physical/chemical or electrical deposition of a layer of solid lubricant on the blank	No lubricant wastage, but relatively more expensive
Spraying	Spraying a controlled amount of liquid lubricant on the blank during the process	Minimal lubricant wastage, but it does not work for high viscous lubricants

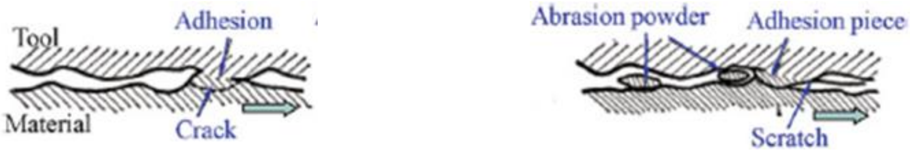

(a) Adhesion (b) Scratch

Fig. 2.27: Schematic of disadvantages of using improper lubricants [GHA15]

Solid lubricants such as graphite, molybdenum di sulfide form shear layers, which can provide the lamellae aligned parallel to the surfaces. Molten glass is the lubricant used for hot forming such as hot extrusion, where other lubricants include boron nitride, Teflon, calcium fluoride, cerium fluoride and polyethylene. Lubricant absorption on surface could be improved by phosphate treatment of steel surfaces. In cold extrusion of ferrous materials, phosphate coating is used a carrier of lubricant. For some alloy steels oxalate coating is preferred. For hot extrusion of non-ferrous alloys, graphite or lube oil are used as lubricant.

Hydrodynamic lubrication includes the separation of the two surfaces with the help of a thick film of lubricant which is more usual in rolling, drawing, extrusion, deep drawing, Lubricant forms a thick film with sufficient pressure to separate the die and work piece surfaces, when the lubricant is drawn into the wedge-shaped gap between the die and workpiece and when the die or work piece move fast. High forming velocity is necessitating for hydrodynamic or thick film lubrication. Thick film lubrication is occasionally reducing the surface finish-surface that arrives rough and matt finish like where as thin boundary lubrication is preferred for good surface finish with shiny surface. Hydrodynamic lubrication is used during wet drawing of wires, in which the wire is dipped in a liquid lubricant container before drawing. The lubricating oil sticks to the surface of the wire and also the oil is hydro-dynamically drawn into the die and forms a film due to high speed.

Boundary lubrication involves the formation of a thin film of lubricant which separates the surfaces. In this type of lubrication, the load is uniformly transferred from die to work surface. Moreover, higher loads can be transferred across the film. The net result is good surface finish and uniform surface deformation. Therefore, for metal forming thin film lubrication is most desirable. Lubricants such as stearates, contain polar molecules which react with the surface oxides and establish strong bonding. This increases the shear strength of the film, thereby preventing metal to metal contact. Fatty acids, compounds of phosphorous and sulfur are also used as lubricants for boundary lubrication.

2.3.6. Coatings

Titanium and its alloys in forging must be protected from contamination by oxygen, nitrogen, hydrogen and carbon during heating for forging. This is most effectively done by glass liquid or glaze which is allowed to dry before heating for forging. The coating binds at between 500 ºC and 600 °C forming a viscous surface which protects the material from contamination. The proprietary liquid glass coatings have lubricating properties which assist metal flow during forging.

A large variety of different coating systems have been applied to titanium alloys and titanium aluminides for more than 30 years now. Table 2.12 summarizes the major coating systems and fabrication techniques published in the open literature. Magnetron-sputtered Ti-Al based coatings were started in order to increase the maximum service temperature of conventional titanium alloys from the present 520-600 ºC, the temperature limit set by the mechanical capabilities of most advanced alloys. The coatings not only demonstrated magnificent oxidation resistance but also indicated beneficial effects on mechanical properties. Initial results on Cr-containing Ti-Al based coatings indicated significant potential for application on titanium aluminides [LEY00]

Thin coatings (ca. 1 µm) improved the creep behavior [FUJ80] and the fatigue resistance of conventional titanium alloys [FUJ80]. However, overlay coatings were often shown to degrade the mechanical properties, particularly the fatigue behavior of the substrate material [DAE92, COC96]. This fact is considered to be a major hurdle for oxidation resistant coating to make their way into service on titanium-based alloys. Novel coating concepts are based on metallic overlay coatings from the Ti-Al-Ag system [NIE01] or on nitride coatings [LEY02]. In addition to good oxidation resistance, nitride coatings offer the advantage of wear resistance at high temperatures, an important property for applications in the compressor of gas turbine engines. In order to fully use the high temperature potential of titanium alloys, protective coatings are required.

Table 2.12: Overview of several coating systems and fabrication processes for titanium alloys [LEY02]

Coating	Substrate	Deposition process
Ni, NiTi	Ti-64, Ti-6242	Electroplating
Pt, Pt/C, Au, Ni/Au	Ti-11, Ti-6242	ion plating
Pt	Ti-6242	ion plating
Pt	Cp-Ti, Ti-5Al-2.5Sn	ion plating
Pt	Ti-6242	ion plating
Pt, Pt/Rh, Au	Ti-6242	ion plating
Pt	Ti-6242S	ion plating
Pt	Ti-6242	ion plating
Ti-Si	Cp-Ti	CVD
Si	Cp-Ti	ion plating
Al	Cp-Ti, Ti-6242	EB-PVD
Pt	Ti-6242	ion plating
TiAl, $TiAl_3$	Cp-Ti	CVD
Al, Silicates, Al-Silicates, SiO_2, Al-SiO_2		EB-PVD, CVD, sputtering
Al_2O_3, Al_2O_3/Ni, Al_2O_3/ Ni-Cr, Al_2O_3/TiO_2	KS 50	plasma spraying
$TiAl_3$	Ti-14Al-24Nb	CVD
Ti-Si	Ti	CVD
Cr, Pt, TiAl, Ni, Ti_3Al+Nb, NiCr, FeCrAlY	IMI 829	sputtering
Ti-Si	IMI 829	sputtering
Ni-Cr	Cp-Ti, Ti-64	electroplating, sputtering
Ni-Cr, SiC, Si_3N4, Al	Cp-Ti	sputtering
MgO, Y_2O_3, ZrO_2, HfO_2, SiO_2, B_2O_3, Al_2O_3, Na_2O, CaO, CaF_2, YF_3	Ti-14Al-21Nb	sputtering, sol-gel
$TiAl_3$	TiAl	CVD
$Cr2O_3$	Ti 685	EB-ion implantation
$TiAl_3$	Ti-14Al-21Nb	CVD
$TiAl_3$	Ti-25Al-10Nb-3V-1Mo	CVD
SiO_2/Al, Ni-Al, NiCoCrAlY	Ti-6242	plasma spraying, EB-PVD
Al, Al-O	Ti-64, Ti-14Al-21Nb, TiAl	sputtering
SiO_2, B_2O_3, P_2O_5, MgO, Al_2O_3, ZrO_2, dúplex and triplex systems	Cp-Ti, Ti-14Al-21Nb	sol-gel
Si_3N_4/Cr	IMI 829	IBAD
Al, Al-Si	Ti-15-3-3-3, Ti-21Al-14Nb-3V-Mo	slurry technique
CrN, Cr	Ti-64	sputtering

Fig. 2.28 gives an overview of some of today's most advanced coating systems for conventional titanium alloys and titanium aluminides. At 750 °C in air, TiAlCrYN coatings improve the oxidation resistance of already reasonably oxidation resistant γ TiAl alloy Ti-45Al-8Nb by one order of magnitude. After 3000 h exposure, the coatings were fully intact

and lacking any sign of degradation. Ti-Al-Ag coatings tested at 800 °C also demonstrated excellent oxidation resistance. Under cyclic thermal conditions, TiAlCrYN coatings provide excellent protection for more than 1000 h of exposure. Even at temperatures up to 900 °C the coating systems appear to provide reasonable protection. However, mechanical tests yet have to prove the potential of these coatings for use at high temperatures in demanding applications.

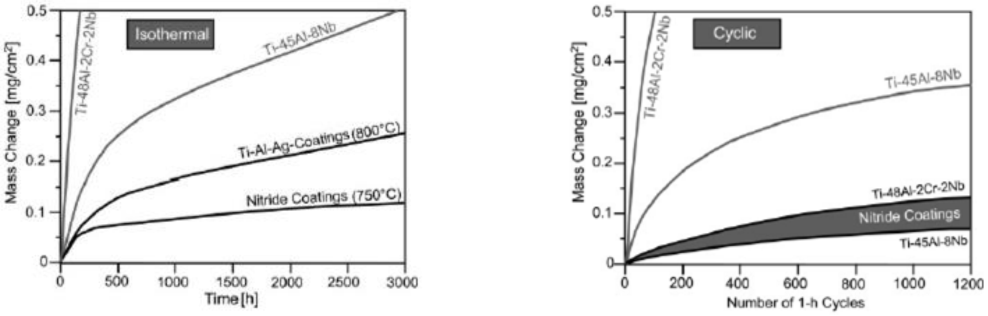

(a) (b)

Fig. 2.28: (a) Quasi-isothermal and (b) cyclic oxidation behavior of coated and uncoated γ TiAl alloys at 750 °C [LEY02]

2.4. Contact Characterization at high temperature

The accuracy of finite element simulations of metal forming processes largely depends on the accuracy of material and contact models. The implementation of accurate material and contact models and microstructure stability models into FEM will enable to get more accurate results resulting in a better forging process definition. Therefore, to develop advanced FE numerical Models for the simulation of high value forging components through which to be able to design robust Ti forging processes, it is necessary to develop new contact tests for high temperature and high contact pressure of selected alloy.

The heat transfer and frictional conditions between work-piece and tools, are two difficult factors to analyse during forming. For the heat transfer conditions in the hot forging process, die temperatures are much lower than those of the work-piece, which leads to the chilling of work-piece near the die surface. Thus, the flow stress of the work-piece increases as does the contact pressure at the die/work-piece interface. This could result in a breakdown of the lubricant layer, increasing both flow of heat to the die and die temperature. Consequently, die strength is reduced and wear is increased. Also, heat transfer can influence work-piece attributes such as; microstructure, mechanical and physical properties. The frictional conditions prevailing at the tool/work-piece material interface, in general, increase the redundant work in all metal forming operations by increasing the load and energy requirements. Friction also plays a significant role in determining the life of the tools and the formability of the work-piece material. In order to obtain a scientific understanding of thermo-mechanical processes, the nature of interfacial heat transfer and frictional conditions, arising during hot forming, has to be quantified and understood.

In this chapter, following the review of previous research, the methods employed for investigating interfacial heat transfer and frictional conditions will be presented. These include experimental work and FE modelling and discussion of results.

2.4.1. Heat transfer characterization test at high temperature

Heat transfer has significant effects on the forging process, especially in hot forging. It causes non-uniform temperature distributions in the workpiece that can affect the quality of forged components. Heat loss from the workpiece causes its temperature to fall and thus increases the resistance to plastic flow. This effect increases the power required to perform the operation and can also affect the metal flow and thus die filling. The temperature increase in the dies softens the surface layers, making them more susceptible to wear. Thermal fatigue cracking on the die surface is also related to the temperature gradients occurring in the surface layers. Heat transfer at the workpiece-die interface is complicated [CHA02]. The influencing factors include the surface finish of the die and workpiece, the pressure, microstructures, the film thickness of lubricant and consequently on the quality of hot formed parts [MAL94]. The mechanism of heat loss to the die is complex in nature and is mainly dependent on the physical properties of the work-piece, the die material and the characteristics of the interface [JAI90]. It is crucial to be able to estimate and perhaps control temperature fields arising during hot metal forming processes [JEO01]. Numerical simulation of forging process is able to predict temperature change and other information such as forging load and stress and strain distribution load history in the die and in the work-piece [WIL04]. However, to ensure that the simulation is viable for improving the forging quality or reducing the cost and lead time, there is a need to obtain accurately the interfacial heat transfer coefficient (IHTC, HTC, h) for the simulation.

The heat transfer coefficient (HTC) is defined as the ratio between the heat flux and the temperature difference between the surface of the die and the surface of the work-piece [MEN16].

$$h = Q/\left(T_{w,s} - T_{d,s}\right) \tag{2.3}$$

where, h represents the heat transfer coefficient and Q is the heat flux through the interface. The temperature on the work-piece surface at the exchange interface is defined as $T_{w,s}$ and the temperature on the die surface at the exchange interface as $T_{d,s}$. The higher value of h causes more heat loss in the work-piece and therefore work-pieces cools down faster.

The measurement of temperature is needed to determine the HTC for modelling heat transfer during forging processes and a number of experimental methods have been used to measure interfacial temperature and thus get heat flux in order to calculate the HTC. Determination of the interface HTC has been investigated by Vigor and Hornaday [VIG63]. In their research, they studied the effects of process parameters such as lubrication, speed and reduction on die heating but did not attempt to estimate heat transfer coefficient from their data, since the influences of deformation heating, heat distribution within work-pieces and interfacial friction heating are difficult to quantify.

Kellow et al. [KEL69] applied the concept of thermal conductance to the study of distribution of temperature in forging dies and, based on their analysis, calibration curves were generated to determine HTC. They developed a robust and responsive surface thermocouple to measure the temperature on the surface of die during simple upsetting forging operations at high and low forging speeds. They suggested that the internal heat generation within the workpiece, the high-speed frictional heating in the outer regions of operations and the oxidation of the workpiece have significant effects on the die temperature.

Earlier, Beck et al. [BEC58] gave extensive consideration to heat transfer and thermodynamics in simple upsetting and die forging operations. Steel and an aluminium alloy were used as work-piece materials with operations being carried out on a hydraulic press, crank press and drop hammer. Die temperatures beneath the surface of the die were measured with thermocouples from which the die surface temperatures were predicted. This semi-empirical analysis resulted in an intercept chart which can be used for calculating the temperature drop in forgings during and before deformation. From his research, he concluded that the heat transfer coefficient under nominally zero load was an order of magnitude less than that under high pressure. In addition, above a certain threshold pressure, its value was relatively constant.

There are essentially two methods for determining the HTC for the forging process. The first method is to use the time-temperature profiles fixed by experiments to evaluated the temperatures of the two contacting surfaces and to apply the definition of HTC as the ratio of the heat flux to the temperature difference of the surfaces. The method forms a set of curves for different HTC during the process. The method may suppose the heat transfer at the contact interface to be a one-dimensional problem in which an analytical solution has been obtained. Though, this approach does not take account of plastic deformation which may have remarkable effects on heat generation during the forging process. The second method seeks to choose the HTC such that measured and calculated temperature distributions will agree closely. A numerical simulation of the forging process and numerical method can be used to minimize the difference between the measured and calculated temperatures.

Nshama et al. [NSH94] directly measured temperature at the work-piece/die interface and the subsurface of the die during upsetting operations and subsequently the least-square method was employed to determine the HTC and to minimize the difference between the measured and the predicted temperatures. This approach with the FE simulation was used by Hu [HU98] and it was found that the thermocouples located at the die surface were insufficiently robust to withstand the high forging pressure during the tests. Also, this approach was used by Wilson [WILO4] to determine the IHTC in hot die forging of titanium alloy where HTC model incorporates the influence of contact area, lubricant film thickness and the thermal properties of the lubricant.

Malinowski et al. [MAL94] used temperature measurement within two dies in contact and an FE technique to develop an empirical relation which gives the IHTCs as a function of time, temperature and pressure. Jeong et al. [JEO01] examined die surface treatments and various lubricants in warm forging.

Semiatin et al. [SEM87] conducted two-die experiments for measuring temperature, in which two instrumented dies were heated to different temperatures and brought together under various pressure levels. The experimental data obtained by Semiatin et al. were interpreted using closed-form analytical solutions based on one dimensional heat transfer models. A set of 'calibration' curves was then established as a function of the heat transfer coefficients. Moreover, two dies heated to the same temperature were used for ring upsetting and the heat transfer coefficients were also estimated. A very similar experimental construction was employed for a further study of the effects of forging pressure, deformation rate and lubrication [BUR90]. Bariani et al. [BAR02] determined the heat transfer conditions in warm and hot forging based on temperature readings inside the die combined with FE simulation of the process and the use of inverse analysis.

Chang and Bramley [CHA02] determined the HTC at the work-piece/die interface for forging process by conducting an upsetting test where the surface temperature of the die was recorded and the process was simulated using FE software. A surface thermocouple has been constructed to measure the temperature at the die surface, where a high pressure occurs, for the simple upsetting forging process. The measured and predicted temperatures were then used in an inverse algorithm with an iterative approach to determine the IHTC. The results show that the predicted temperatures modelled by a constant IHTC at the rest-on-die stage were in good deal with the experimental measurement (Fig. 2.29). However, for the forging stage, the IHTC values vary significantly during the process (Fig. 2.30). This has important consequences in the implementation of simulation software.

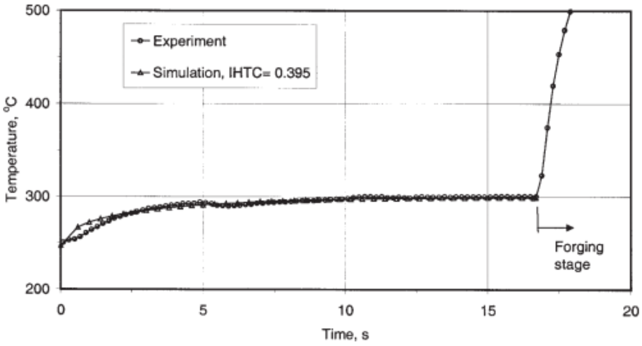

Fig. 2.29: Temperature comparison at the rest-on-die stage [CHA02]

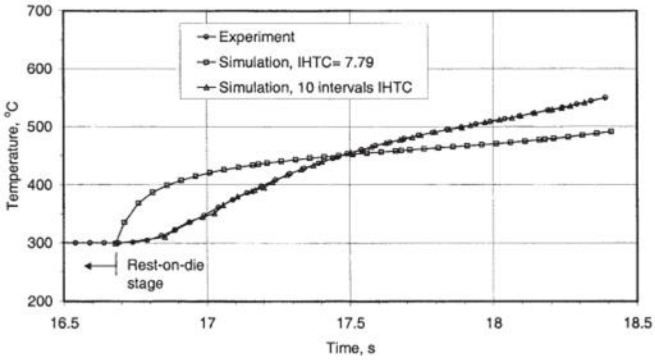

Fig. 2.30: Temperature comparison at the forging stage [CHA02]

The inverse algorithm [YEO11] is an optimization technique for obtaining the h by minimizing the temperature difference between measured and calculated temperatures. Temperature change of the die or workpiece is usually calculated by FE simulation. The formation of the objective function for minimizing the temperature difference between FE calculated and measured temperatures can be expressed by the following equation.

$$\emptyset(h) = \sum_{time} \sum_{position} (T_c - T_m)^2 \tag{2.4}$$

where, *Tc* and *Tm* are FE calculated and measured temperatures at corresponding positions and time over that period. In other words, *Tm* is a constant obtained from the test and *Tc* is the constant depending on the interface heat transfer coefficient (h). Therefore, in order to find the h value, an optimization scheme can be used for minimizing the objective function ($\emptyset(h)$).

Bai et al. [BAI12] introduced an efficient closed-form technique for the determination of HTC at different forming and contact conditions based on FE heat transfer analysis using FE software DEFORM. The development of a new simple one-dimensional model to determine the IHTC as a boundary condition for eventual employ in the FEM of gas turbine blade forging processes. An upsetting test was used to generate the initial conditions and boundary conditions for the numerical model. A numerical procedure has been developed and applied for determining the surface temperatures of work-piece and die, the contact heat flux, and the IHTC. The numerical model was validated by the comparison of experimental, numerical and FE results (shown in Fig. 2.31). Here, the work-piece is coated with borate-based glass before being preheated where, graphite lubricant is usually sprayed onto the die surfaces. The temperature at the interface depends on thickness of the glaze, surface roughness and pressure at the interface, so experiments were performed to study the effects of pressure, glaze thickness and surface roughness on the IHTC between a Ti-6Al-4V work-piece and H13 steel die.

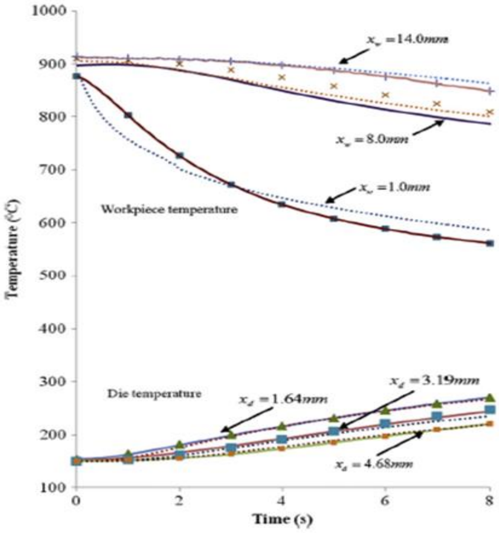

Fig. 2.31: Comparisons of temperature histories obtained from the closed form calculation (solid lines), FE prediction (dot lines), and experimental data (symbols) for selected locations in workpiece and die. Pressure is4 0MPa and HTC 3.5kW/m²K [BAI12]

In published research, values of heat transfer coefficient vary substantially, perhaps due to different experimental methods, material properties, lubricant and forming conditions. Therefore, it is essential to derive the values according to a specific forming condition. The HTC value that governs the heat interchange between the work-piece and the tool will be calculated by an inverse analysis approach in this dissertation.

2.4.2. Tribological characterization test at high temperature

Friction plays a very considerable role in metal forming operations and its role must be taken into account during the design process. It affects metal flow, workpiece integrity and surface finish, cost considerations, and energy conservation [MEN09]. Excessive friction leads to heat generation, wear, pick-up and galling of the tool surface. Friction can increase the inhomogeneity of the deformation, leading to defects in the finished product. The aim of accurate metal forming is to produce parts close to final dimensions without any defect, with the minimum waste of material and at lowest tool costs. To reach this aim, it is necessary to have a correct understanding of material properties, the process parameters and the behaviour between the workpiece and the die, i.e. friction [ROB04]. Application of a suitable lubricant may reduce friction, but will never eliminate it completely [DUT99]. Furthermore, when dealing with titanium alloys, the alpha-case formation due to oxidation is critical. Especially hot forming process of titanium alloy is sensitive to the friction. Thus, is necessary to evaluate correct friction coefficient and choosing a proper test method to understand the friction phenomenon in the contact area of the workpiece and the die under different deformation processes in order to optimize the forming process of titanium alloy [ZEN00].

Recently, several methods have been developed for quantitative evaluation of interface friction to determining friction coefficient (μ) or factor (m) during forging obtain and prominent among them are ring compression, T-Shape, double cup extrusion, upsetting-sliding and spike tests which has been described here. In these tests, friction condition is basically determined by observing the geometric change of the test-pieces. These tests rely on a comparison of geometric changes or flow patterns of the work-pieces. The test methods for these tests are simple. With the aid of theories, the results can be quantified, but with uncertainties [SCH83]. The measurements are usually made subsequent to the tests; thus, the results relate to the final stage of the deformation while possible different intermediate values of friction are not accounted for. This type of test is also suitable for ranking or comparing various frictional conditions and lubricants. By contrast, the FEM is thought to be one of the most popular and widespread numerical methods and particularly suitable for resolving the complex plasticity equations and analyzing the deformation mechanics of processes with complicated geometries and boundary conditions. Contrarily, it is immensely difficult and time-consuming to acquire the calculated result from plasticity equations using analytical methods [IM03].

2.4.2.1. Ring-compression test

Ring-compression test is a widely-accepted way to measure the interface friction friction coefficient μ or friction factor m in bulk forming process due to its simplicity [ALT83] between the workpiece and dies. This method was first used by Kunogi [KUN56] and was later developed and presented by Male and Cockcroft [MAL64]. A flat ring-shaped specimen is compressed in the ring compression test, to known as height reduction. The change in internal and external diameters of the compressed ring is significantly sensitive to friction condition at the die-ring interface, as shown in Fig. 2.32. Generally, it can be said that if the internal diameter of the specimen increases during deformation, friction is low and if the internal diameter decreases during deformation, friction is high. Thus, the change in the internal diameter is used as a friction indicator. The friction condition is expressed as the shear friction factor (m), which can be quantified by analogizing the internal diameter of the compressed ring to the values predicted by using various constant shear friction factors in a theoretical analysis [ALT83]. Today, these values are most often predicted by the FEM [ALT05]. Using this relation, the curves demonstrating the relationship between the percentage decrease of the internal diameter and their height of specimens are shown for different values of friction as shown in Fig. 2.33.

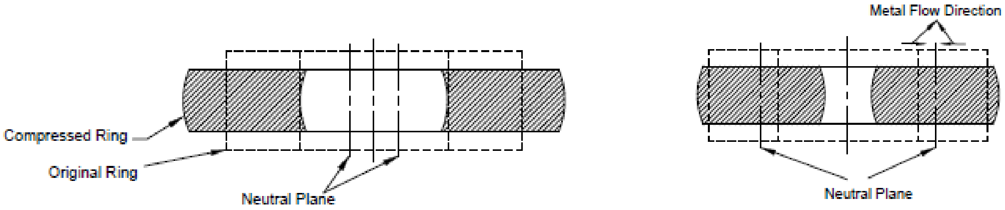

(a) Low friction *(b) High friction*

Fig. 2.32: Principle of the ring compression test

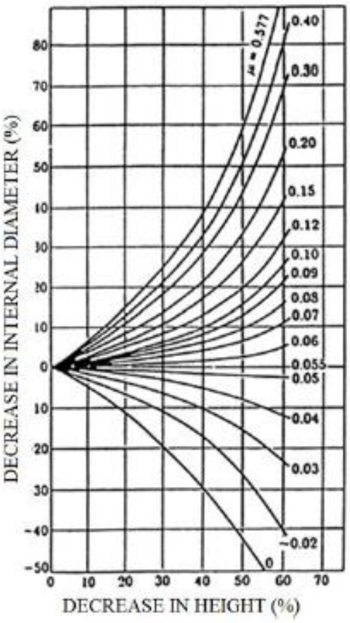

Fig. 2.33: Curves of friction calibration theory for a ring with the ratio of 6:3:2 [ALT83]

The most accepted and widely used ring geometry is 6:3:2 because of correctness and dependability of the results. However, 4:2:1 has been widely applied in recent years and corresponding determined results is the same correctness and dependability as 6:3:2. Luo and Guo [LUO86] investigated the rules of specimen size when the ring-compression method was used for determining the friction coefficient, found that the sensitiveness of the change ratio of inner diameter to the inter-facial lubricant condition is concerned with the size proportion of sample and that the thinner samples is suitable for improving the sensitivity in test, and thus suggested three size proportions of 6:3:2, 4:2:1 and 6:3:1.

There are few previous studies of friction in hot metal forming by using the ring compression test. Felder and Montagut [FED80] carried out ring compression tests at 1250 °C. They discovered that the tool velocity had a significant effect on friction and it was shown that if the velocity increases, the friction reduces. Jain and Bramely [JAI67] have made a detailed investigation of the relations between the coefficient of friction and the forging speed using the ring test at the constant temperature using various lubricants it was concluded that in all cases, as the impact speed increased the frictional coefficient would be reduced. Sadeghi and Dean [SAD90] investigated the effect of temperature on friction using the ring compression test. The tests were carried out using steel specimens with a graphite based lubricant. It was shown that in the temperature range of 700°C-1150°C, the magnitude of the shear factor m increased with increasing temperature. According to address the dependency of the calibration curves on the parameters such as barreling, material properties, relative velocity, and the numerical method such as the FEM is used to elaborate the friction calibration curves (FCC) [JOU09]. Lin [LIN95] applied a thermo-elastic-plastic coupling model to generate the friction calibration curves and considered that a combination of ring-compression test and FEM is a simple and useful method for estimating the performance of a lubricant.

Few studies have been undertaken to understand friction in hot metal forming, especially when addressing an issue of whether changing magnitudes of strain rate and temperature at the interface influence the level of friction. Rudkins et al. [RUD96] investigated friction experimentally using the ring compression test under hot forming conditions. The experiments show how variations in temperature at the interface affected the frictional behaviour and FE simulations were also completed under similar temperatures as in the experiments. The correlation between the experimental measurements and the results of the process modelling is presented in the paper. By using the ring compression test, Li et al. [LI01] studied the lubricities of glass and graphite in deformation process of Ti-6Al-4V titanium alloy under high temperatures and strain rates and presented that increasing the strain rate leads the friction to reduce.

However, the calibration curves can be affected by several factors including the type of materials [SOF02] and HTC, which is particularly important to study the friction behavior of high temperature deformation for materials. Zhu et al. [ZHU11] had presented detailed investigation on the friction factor of Ti-6Al-4V titanium alloy at the die/work-piece interface in forming process involving large deformations under hot forging situation by the combined approach of ring-compression tests and FE simulations. Ring-compression tests of Ti-6Al-4V alloy with glass lubricant and dry friction are conducted in this research at the temperature of 940^{0}C and height reductions of 30% and 50% shown in Fig. 2.34. The effects of variations in HTC on material flow and friction calibration curves are investigated as the emphasis of this paper. It is noticed that the HTC has remarkable effects on the calibration curves and metal flow, thereby affects the measurement of interfacial friction factor. This is because that the increase in HTC significantly effects on the interface temperature, sequentially influences the velocity of metal flow, which is similar to the increase in friction. Therefore, different HTC should be employed to generate the calibration curves when both of the lubricant conditions were used for determining the interfacial friction coefficients (shows in Fig. 2.35).

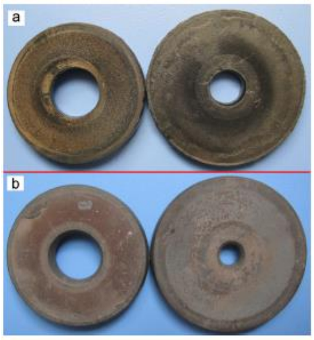

Fig. 2.34: Samples deformed at 30% and 50% height reduction: (a) glass lubricant and (b) dry friction [ZHU11]

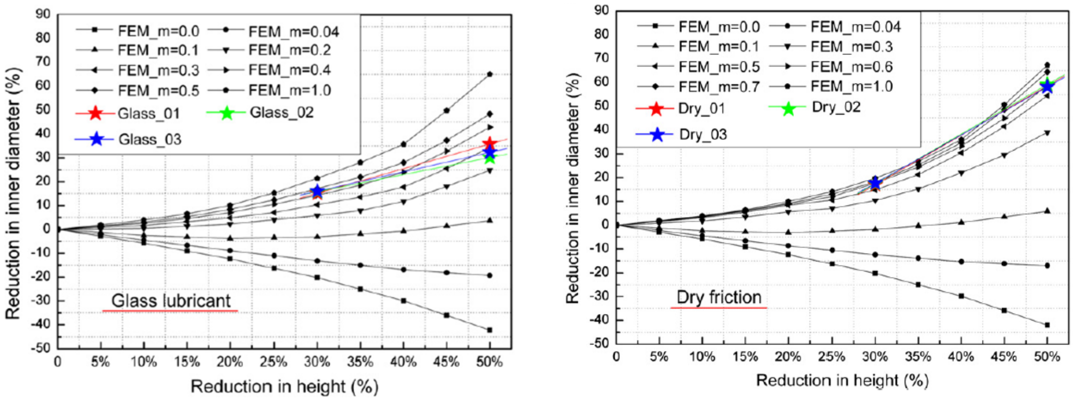

(a) (b)

Fig. 2.35: Calibration curves obtained from the FEM at height reduction of 0–50% and friction factors of 0–1corresponding to the different HTC, (a) 5kW(m^2K)$^{-1}$ and (b)11kW(m^2K)$^{-1}$ [ZHU11]

Bonab et al. [BON15] has studied, the heat transfer coefficient of lubricants is considered as a parameter in plotting FCC. Furthermore, the process of experimental and FEM is presented to find the calibration curves of the 6082 aluminium alloy using Graphite, Teflon and Mica sheets as lubricants. The results of the ring compression test are analyzed by using experimental and FEMs for considering the effect of different lubricants on the calibration curves. The results demonstrate that the best lubrication case of the hot working of 6082 aluminium alloy is achieved when the shear friction coefficient of m=0.32 is used whereas the value of m=0.69 is obtained in the case when no lubricant is used. Burte et al.

[BUR93] evaluated heat transfer and friction during hot forging in upsetting 304 stainless steel, and Ti-6Al-4V rings. The rings were deformed under lubricated or dry and both isothermal as well as non-isothermal conditions. The values of the h and m or μ are needed as inputs to advanced analyses, so that the results of process simulations are realistic, reliable, and useful. As expected, the h, increases with pressure and when lubrication is used. The h, can be generally evaluated without regard to *m*. Conversely, the *m* cannot be estimated in the ring test without regard to *h*.

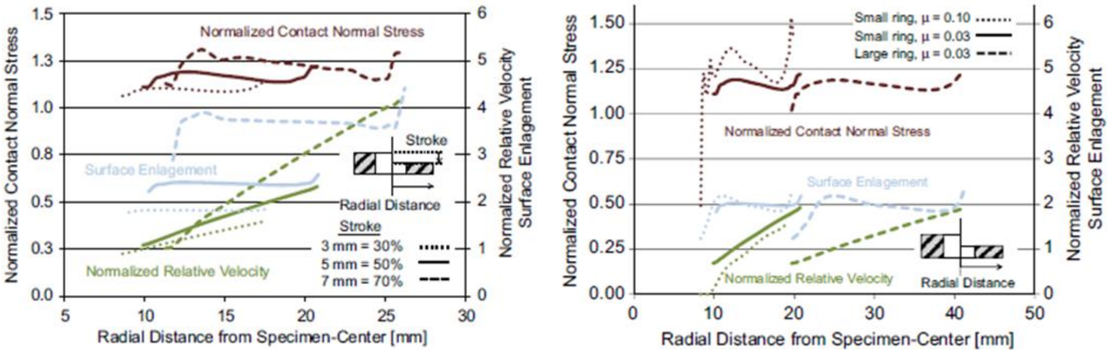

(a) (b)

Fig. 2.36: Ring compression test with: (a) Loads over the contact area and (b) Variability of the loads [GRO13]

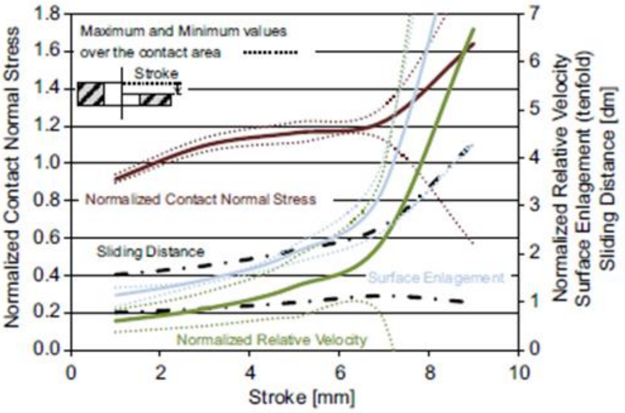

Fig. 2.37: Ring compression test with Loads over a stroke [GRO13]

Fig. 2.36a displays the surface enlargement, the normalized contact normal stress and the normalized relative velocity among them the tool and the workpiece at three Different strokes with the friction coefficient of μ=0.03 [GRO13]. The ring was made of 16MnCr$_5$ material and has an inner diameter of 15mm, an outer diameter of 30 mm and a height of 10mm. The results were gained by an axially symmetric FEM simulation with simufact forming GP 10 and it reveals that the contact normal stress is approximately constant over time and place until a stroke of 7 mm. The small occurring rise can be explained with the strain hardening effect. On the other hand, the surface enlargement has a similar value on the contact area, but rises with the proceeding process stroke. The normalized relative velocity even has a very high scatter over the position and time. Accordingly, the sliding distances of the inner and outer radius of the specimen are not uniform, either, as shown in Fig. 2.37. analyzing the normalized relative velocity and sliding distance at about 70% punch travel, it displays that the movement of the inner part of the ring flips to a negative amount. This is unfortunate since a second contact between points of the tool and workpiece comes. Therefore, the stroke of the ring compression test should be limited to approximately 70% of height reduction. No significant influence of the ring geometry is recognizable, because of the fact that the large ring, having doubled geometric values, displays results in the same range. Different friction coefficients lead only to small variations in the contact normal stress and surface enlargement (shown in Fig. 2.36b).

Overall, the ring compression test is an indirect, easy, cheap and fast opportunity to measure friction. Although, the reachable loads are not sufficient and hard to vary. Also, the result is influenced by calibration curve, which depends on several parameters as strain rate, strain hardening and the material properties. Additionally, the barreling and the heat transfer involve the accuracy of the ring compression test [ROB04]. A suitable friction experiment should provide conditions as similar as possible to those usually noticeable in most the practical forming operations. Recently a T-Shape test has been developed by Zhang et al. [ZHA09] to avoid the difference of friction conditions as shown schematically in Fig. 2.38.

2.4.2.2. T-shape compression test

T-shape compression, a new testing method to determine friction coefficient by combined compression and extrusion. A cylindrical specimen is located in a V-shaped groove die as is shown in the Fig. 2.38a. The punch, specimen and die are three parts of this test. While the punch moves downwards, the specimen is compressed between the punch and die. Some metal is extruded into the groove and some is upset and moves sideways between the flat surfaces. The deformed specimen is similar to `T´ letter which is shown in Fig. 2.38b and that’s why it’s named as T-Shape test. Since the round billet is placed horizontally, only the cylinder surface has direct contact with the dies during deformation.

The geometry of the deformed sample and the forming load are sensitive to frictional conditions. Therefore, these two factors could be used for evaluating the friction factor. Meanwhile, this test induces a complex deformation path, large contact pressure and rather large surface expansion. The surface expansion ratio may be up to 50% and the contact pressure can reach four times the flow stress of the material [FER11]. Samples with various diameters can be tested with the same set of dies. In addition, the cost and time of die manufacture are smaller than the ones of other friction tests, such as forward extrusion and double cup extrusion.

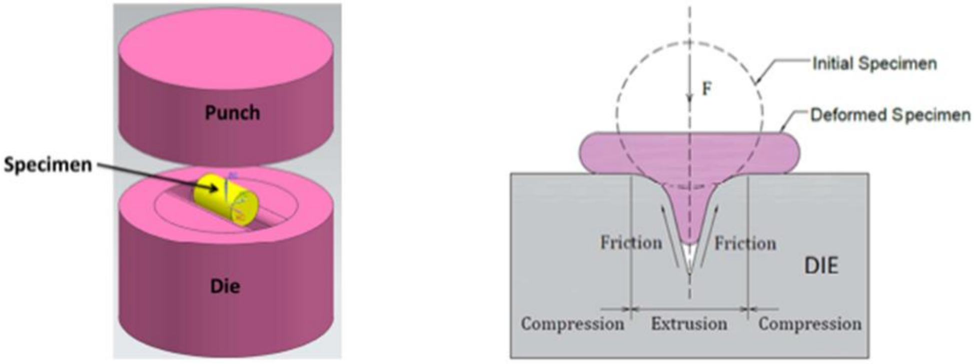

(a) *(b)*

Fig. 2.38: Layout of T-Shape test, (a) Test set up and (b) Specimen deformation characteristics

Zhang et al. [ZHA09] described the T-shape friction tests with different lubrication conditions i.e; solid coating (phosphate + soap), oil and mixed condition, have been carried out on low carbon steel sample. Then m and μ were determined of these various lubrication conditions by using experimental results and the calibration by numerical simulation. The results of experiments and simulations displays that the stroke-load curve and the height of the extruded part are both sensitive to friction (shown in Fig. 2.39). To maximize the sensitivity of the T-shape compression test, the influence of two geometrical parameters was investigated and that were corner radius and V-groove angle. Two commercial FE codes, FORGE 3D and ABAQUS, were used and provided very similar results for a given friction condition. Based on the results obtained, the solid lubricant produces lower friction than oil lubricant, because the oil can be easily squeezed away from the high-pressure contact zone where as the lubrication performances of solid lubricant and mixed lubricant are similar. The experimental values of the slope of the load curve and the height of the formed specimen shape were compared to the results of the numerical simulations (shown in Fig. 2.40).

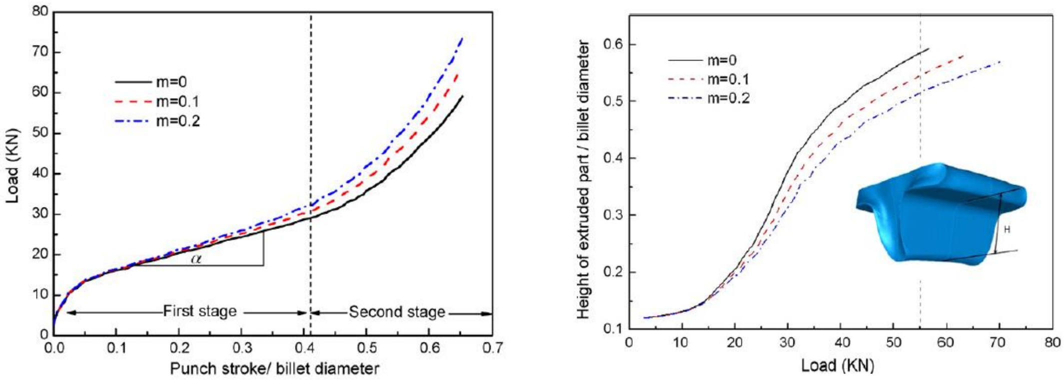

(a) (b)

Fig. 2.39: (a) Load curves with different friction factors and (b) Effects of friction factor on height of extruded part with different loads [ZHA09]

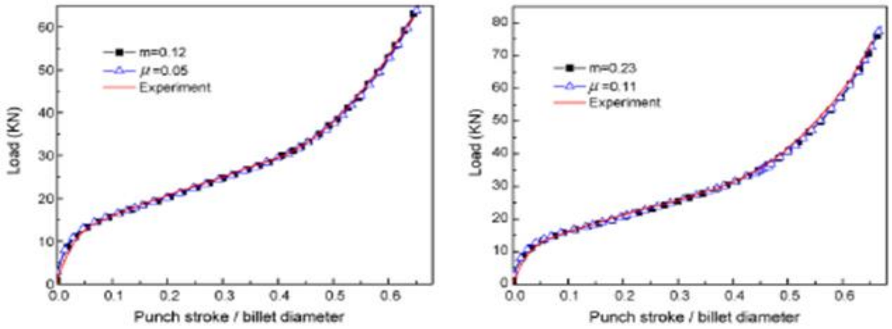

(a) Solid lubricant (b) Oil lubricant

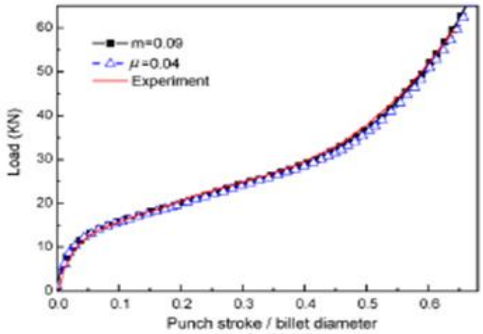

(c) Mixed lubricant

Fig. 2.40: Comparison between the experimental and simulated load curves [ZHA09]

Fereshteh et al. [FER11] evaluated the friction factor of a magnesium alloy such as AZ31 and AZ80 at elevated temperature which is concerned with both experimental and numerical studies. Based on the experimental results it was found that, when the die edge radius decreased or the test temperature or ram velocity increased, the friction sensitivity of T-shape experiment increased. Good repeatability of this test was also observed during experimental part of this research work. Lastly, using the flow curves gained from the compression tests and friction factors obtained from the T-shape experiments for the FE simulations of this test, resulted in a very good agreement between the numerical and experimental load curves. T-Shape friction test was redesigned to make it more suitable for application to micro-forming processes [TAU12]. Workpiece with aspect ratio (length/diameter) of 5 was preferred in order to ease workpiece handling. The die geometry was also modified from the original test to improve friction sensitivity mainly within the range of friction factors often observed in metal forming. Geometric deviation of the die was simulated using Deform-2D to establish the acceptable tolerance for the fabrication. The effect of variation in workpiece mechanical properties on the test behavior was also investigated through Deform-2D simulation and it was shown that variations in workpiece mechanical properties of up to 10% do not crucially influence the friction test results. Eventually, T-Shape experiment was conducted using copper workpieces to examine how the test complied with the friction behavior observed in the experiment.

2.4.2.3. Other friction tests

Double cup extrusion, was initially explored by Geiger [GEI76] and then developed by Buschhausen et al. [BUS92] as shown in Fig. 2.41a. In this test, a cylindrical specimen was located in a die with the same nominal diameter. Then it was deformed between two punches with the same diameter which smaller than that of specimen. Two cups with a single base were produced when the upper punch moves downwards. Therefore, the ratio of top cup height to bottom cup height (H1/H2), depends on the friction along the container. Cup height ratio will increase with large friction along the container/ specimen interface. The minimum cup height ratio is equal to one, if no friction force is generated along the container inner surface. However, Schrader et al. [SCH07] found that the maximum contact pressure between specimen and container is rather small (for example <700MPa for low carbon steel).

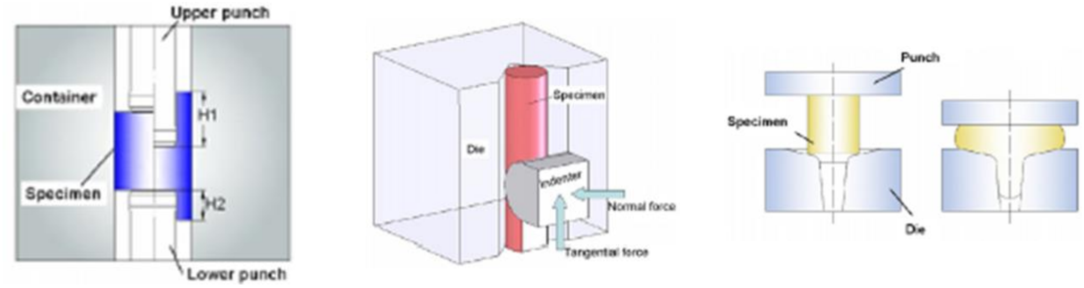

(a) Double-cup extrusion *(b) Upsetting-sliding test* *(c) Spike test*

Fig. 2.41: Tests developed for examining the friction [ZHA09]

The upsetting-sliding test, proposed by Lazzarotto et al. [LAZ98], where the test includes three main components: indenter, die and specimen. The indenter plays the role of a drawing or extrusion die, whose surface roughness should be the same as that of the tool to be used in the cold forging process. The specimen with lubricant layer is fixed in the die (see Fig. 2.41b). Before the test, the position of indenter is adjusted to give the required penetration depth between the extremity of indenter and surface of specimen. Then the indenter moves along the specimen with a constant speed and deforms its surface. The normal and tangential forces are measured to evaluate the friction condition between indenter and specimen. The advantage of this test is that some process conditions, such as sliding speed and temperature, can be readily adjusted. However, this method is not like a real forging process as only a local region of the specimen deforms significantly and the surface expansion ratio is small.

Spike forging (SF) is an axisymmetric forging process combining extrusion and upsetting. A cylindrical billet squeezed between the dies flows both sideways and into the orifice. The spike test requires a bottom die with a sharp-corned tapered orifice of circular cross-section and a flat-top die. Higher friction restricts sideways flow and therefore a longer spike is extruded (see Fig. 2.41c). It can be used to determine friction, because the load and spike height increases with friction. This test geometry was introduced in a FE analysis by Oh [OH82] and the SF geometry was proposed as a suitable friction test for forging application by Isogawa et al. [IS092] and was claimed to be more suitable for forging applications than ring test as it produces higher contact pressure and higher new surface generation.

2.4.2.4. Friction Models for the simulation of ring tests

To date, several friction models have been developed for evaluation of friction in metal forming, and normally are applied in FE analysis as follows [TZO00] and theoretical approaches for determining the calibration curves of friction test are numerous [WAN01]. It should be noted that there are various theoretical models to study friction, some of them are here explained briefly.

Coulomb Friction Model

The Coulomb friction model is a friction model which is usually used in computer software based on the Amonton law and this law is valid for the elastic mode as well as in the case of a shaping process with low pressure [KOB89]. It is expressed as follows:

$$\tau = \mu . p \tag{2.5}$$

where τ is the shear friction, μ is the friction coefficient and p is the applied normal force.

Shear or Constant Friction Model

This is used on condition of high pressure existing at the common surface of the workpiece and the die and is as follows [SCH83]:

$$\tau = m . k \tag{2.6}$$

where m is the shear friction factor which ranges from m=0 to 1. m=0 for zero friction surface and m=1 for adhesive friction. k is the shear yield limit. The mean Coulomb friction coefficient, μ, can be calculated which is used to measure m as in Eq. 2.7 [AVI64]:

$$k = \frac{\sigma_0}{\sqrt{3}} \tag{2.7}$$

$$\mu = \frac{m}{\sqrt{3}} \left(\frac{\sigma_0}{P_{ave}}\right) \tag{2.8}$$

where σ_0 is the yield limit, P_{ave} is the mean pressure at the surface, k is the shear yield limit and m is the shear friction. A general standard of friction coefficients for different bulk metal forming processes are listed in Table 2.13.

Table 2.13: Typical friction coefficient values using constant shear friction model [SCH83]

Bulk forming process	Shear friction coefficient
Cold forming (carbide dies)	0.08
Cold forming (steel dies)	0.12
Warm forming	0.25
Hot forging (lubricated)	0.3
Hot forging (dry)	0.7

Hybrid Friction Model

A hybrid friction model is the combination of the coulomb and constant shear models which is often used when rolling or elastoplastic deformation is considered. The general function is as Eq. 2.9.

$$\begin{cases} \tau = \mu p \; (\mu p < mk) \\ \tau = mk \; (\mu p \geq mk) \end{cases} \tag{2.9}$$

This model describes that at low normal pressure, the friction is proportional to the normal pressure whereas at high normal pressure, the friction is proportional to the workpiece shear stress. The frictional behavior is illustrated in Fig. 2.42.

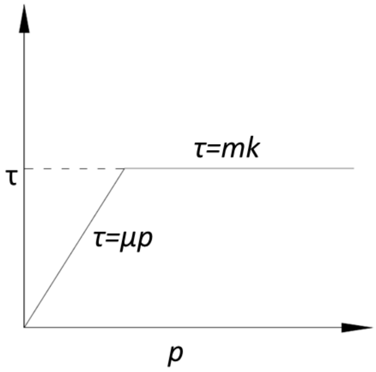

Fig. 2.42: Illustration of hybrid coulomb and constant shear friction model

General Friction Model

This model is a combination of the previous models which also takes into consideration the different friction behaviors under low/high normal pressure and is presented as follows:

$$\tau = f\alpha\, k \tag{2.10}$$

where τ and k represent the friction stress and shear yield stress of the material, respectively. f is the friction factor and α is the real contact area ratio.

Tan [TAN02] examined the above friction models and their variations and found that it was very hard to identify which friction model in FE simulations is of higher accuracy because of the agreement of shape of calibration curves and experimental data can always be obtained by adjusting the value of friction coefficient, or friction factor. It is meaningless if the validity of a friction model is judged only according to FE analysis. Nevertheless, the use of calibration curves and friction models can provide indications of relative difference in friction values under various forming circumstances. The constant shear friction model is used in most research on hot forming, and widely used in simulations of bulk metal forming because of its theoretical simplicity and numerical rigidity [JOU09].

In the present study, the law of constant friction is used to model the friction interface for the hot forging of Ti-6Al-4V alloy.

Critical Review:

The following are the critical conclusions of the literature survey:

(1) The increasing drive for lighter stronger materials is bringing titanium to the forefront of high performance demanding industries and technologies. Although there is more work has been done on Ti and its alloys especially Ti-6Al-4V in titanium forging; few works have been done about ceramic coatings and lubricant influence on tribological and contact behavior regarding Ti-6Al-4V.

(2) The determination of heat transfer and friction coefficient is desired since interface friction and heat transfer plays an important role in the hot forging process. Very few studies regarding contact analysis has been done for improvement of Ti-6Al-4V forging process. For that it is necessary to develop new contact tests for high temperature and high contact pressure of Ti-6Al-4V alloy.

(3) The implementation of accurate contact models into FEM will enable to get more accurate results resulting in a better forging process because of Contact, material characterization and also many other parameters are the very important (crucial) parameter for FEM optimization.

(4) HTC is very influent to estimate the COF whereas very few studies have been performed where first the HTC has been precisely characterized.

(5) Few studies have been undertaken to understand the friction in hot forming, especially when addressing the issue of varying input parameters. Better understanding of their role hence needed in order to obtain accurate results in numerical simulations.

(6) Several friction tests are available for calculating friction coefficient but considering the same coating surface of specimen have not been tested under different conditions like contact pressure and surface enlargement.

(7) Ring test, the simplest friction test, only gives μ or m values for low contact pressure. The development of new tests, similar to the T-shape test can cover all the contact pressure range for Ti-6Al-4V forging application and therefore increase the accuracy of numerical model's trough a proper identification of the friction coefficient.

(8) Alpha structure is may be a problem during forging process, so that we have to study microstructure. In spite, an in depth practical investigation was performed to gather data to form an analysis and summary of alpha-case formation, however large gaps in predictive models and the absence of extensive guidelines for the oxidation behaviour of titanium alloys remain. Alpha-case is a problem for crack during forging. The prediction of alpha-case formation at a range of temperatures and times is still difficult as it is an area which has not been comprehensively addressed. There is a clear need for further research and documentation into the in-air oxidation behaviour of titanium alloys at elevated temperatures.

Problem definition

The outcome of the present literature survey stimulates the following problems:

(1) This project has been analyzed taking the Ti-6Al-4V specimens where Three types of surfaces that are, Ti-6Al-4V specimens with no coating, 40-45 and 80-90 μm of glass coating with the lubricant based on graphite diluted in water.

(2) The columnar tests with die and billet surface temperature estimation will allow a precise characterization of the heat transfer coefficient with different contact pressures and is simple to perform. The process was also simulated by a commercial FE package. The predicted and measured temperatures were then used in an inverse algorithm with an iterative approach to determine the HTC.

(3) Using FEM, the numerical simulations of Ring and T-Shape test are carried out for various values of friction factor using the estimated HTC value which will be comparing with experimental results to estimate the friction. compression tests have been carried out by using of adequate inverse modelling techniques enabled a precise characterization of the forging friction coefficient.

(4) To evaluate how frictional behaviour is affected by variations of input parameters using the parameters like press velocity, Heat Transfer Coefficient (HTC), processing time, mesh size, material and tool temperature for ring test, FE parametric study has been performed. In order to obtain the sensitivity of the test of the T-Shape test

has been performed. Therefore, the influence of three parameters such as HTC, material change and friction has been investigated to see how these variables influence the force measurement by using also FE parametric study.

(5) This project has been looked at the effects of exposure to the atmosphere at elevated temperatures for studying the alpha-case and the defects under all the surface conditions. Characterization has been achieved by micrographically analysis and micro hardness profiling from the surface into the substrate.

CHAPTER 3

SENSITIVITY ANALYSIS OF FRICTION TESTS

"The only simple truth is that
there is nothing simple in this complex universe.
Everything relates. Everything connects"
-Johnny Rich

3. SENSITIVITY ANALYSIS OF FRICTION TESTS

3.1. Introduction

An obvious understanding of process parameters, material behavior, forming tools and interfacial frictional conditions are required to produce defect-free components. Frictional conditions can affect surface finish of the produced components, die wear and forming load. Therefore, a precise estimation of frictional condition is essential. Various friction tests have been proposed for evaluating frictional conditions of forming processes such as: the ring compression test, double cup and forward extrusion test, upsetting-sliding test, spike test and T-shape compression test [PEZ11]. Many works have been done by employing ring and T-Shape compression method to investigate friction behavior of metal forming experimentally and numerically [ZHU11, GRO13, TAU12, FER11].

On the one hand, ring compression test is a simple way, cheap and fast opportunity to determine the friction factor, which was developed by Male and Cockcroft in 1964 [MAL64]. This test is very simple and one of the widely used friction tests for evaluation of frictional conditions in forming operations, using the geometry of finished workpiece. The geometry of tools and samples are also very simple resulting a very simple deformation path and relative small surface expansion ratio which nearly equals to 20% in the test as shown in Fig. 3.1.

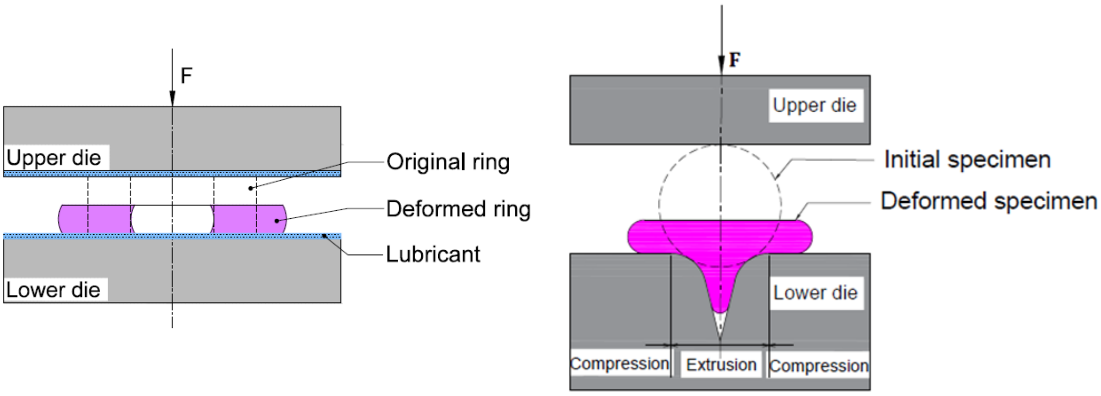

Fig. 3.1: Setup of compression test (left) ring test (right) T-Shape test

On the other hand, T-shape compression test is a newly introduced friction test for evaluation of frictional condition using extruded height and load curves throughout the normalized stroke, which was proposed by Zhang et al. in the year of 2008 [ZHA08]. Severe deformations, including both extrusion and compression are involved in this test, which require a specific manufacturing die as shown in Fig. 3.1. This test includes large surface expansion may reach to 50% and high contact pressure can attain 4 times the initial flow stress of the material, similar to what is occurred during a real forging operation [ZHA09]. Therefore, results of this test have not been compared with other friction tests yet.

In addition, FE simulation of forging processes requires precise value of friction factor. The use of the finite-element method (FEM) in metal-forming modelling has increased in recent years, one reason for which may be that the numerical routines in the FEM today can be considered relatively reliable and well known. The finite element method not only provides overall quantities but it also reveals the details of the deformation characteristics. However, the mechanism of friction is still not yet known in detail and friction remains one of the most elusive input variables in metal forming technology [THO69]. FE simulations are used to derive different sets of friction calibration curves and to evaluate material deformation, geometric changes and load-displacement results. With FEM, it is therefore possible to investigate the factors which have effects on calibration curves in the compression test. In the present research, the frictional conditions of hot Ti-6Al-4V alloy forging have been studied numerically using the ring and T-shape compression tests.

Few studies have been undertaken to understand the friction in hot forming, especially when addressing the issue of varying input parameters. Better understanding of their role is therefore needed in order to obtain accurate results in numerical simulations. In the present study, a FE parametric study has been performed in order to obtain the sensitivity and main characteristics of ring and T-Shape test. The ring and T-Shape test of Ti-6Al-4V alloy have been numerically analyzed using FEM simulation and the main objective has been to determine and interpret the factors that affect friction behaviour. Based on the FEM, friction calibration curves have been calculated in order to investigate influencing factors by varying the parameters namely press velocity, HTC, processing time, mesh size, material temperature and tool temperature during ring test simulation in hot forging. Then, the influence of three parameters such as HTC, material change and friction has been investigated in T-Shape test, to analyse how these variables influence the force measurement and final shape of specimen. Finally, tribological contact conditions in both the tests have been compared.

3.1 Numerical simulations by FEM

In this study, the constant friction law is used to model the interface friction related to test conditions in ring test and T-Shape tests, since it has been widely proved to be an appropriate law for representing high temperature forging processes [SCH83].

3.1.1. Ring test

In order to study the influencing factors of friction in the ring tests, calibration curves were developed. These curves were obtained using numerical simulation and the analysis was done by using the FORGE3® 3D finite element software. Finite element code was used in the simulation of simple compression of a ring made of Ti-6Al-4V material having 30 mm in outer diameter (Do), 15 mm in internal diameter (Di) and 10 mm in height (H). The ratio of the initial dimensions Do: Di: H was 6:3:2, which is known as the standard ring geometry recommended by Male and Cockcroft [MAL64] as shown in Fig. 3.1.

Fig. 3.2. illustrates the stages of deformation during the ring compression test simulation. The top die was modeled as a rigid body being the specimen deformable with the material properties of the Ti-6Al-4V, characterized using hot compression tests. In this simulation, symmetry has been applied to the specimens in order to reduce the computational time needed to run the simulations. This way, only one eighth of the cross section of the ring specimen is required to be modelled using tetrahedron elements as shown in Fig. 3.3.

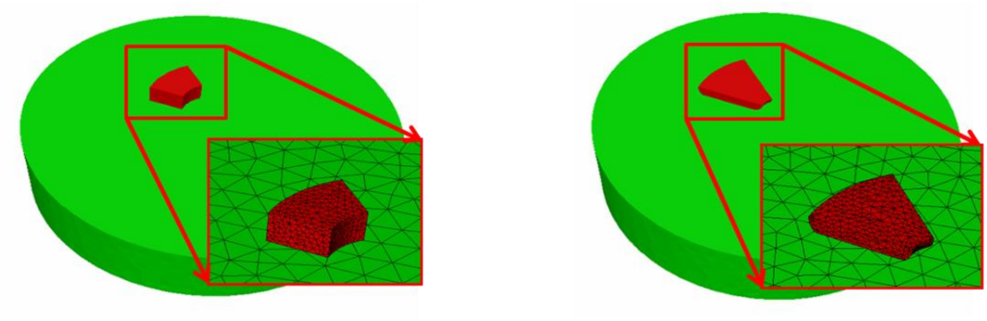

Fig. 3.2: Specimen deformation process of ring test simulation

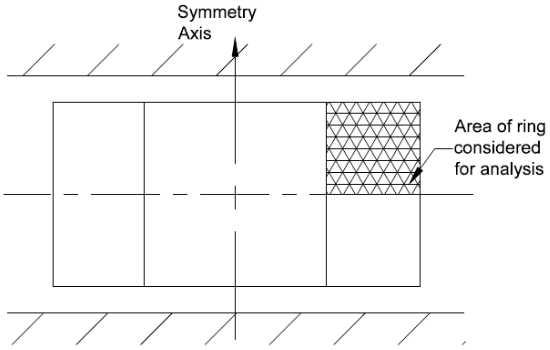

Fig. 3.3: Finite element model of ring test specimen

In the finite element discretization, the specimen was divided into 14207 tetrahedron elements with 3223 nodes and die was divided into a total of 2352 tetrahedron elements with 1178 nodes. Finer mesh was employed in the inside and outside layers of the ring, where severe deformation usually occurs and the average mesh size was 0.6 mm. During the entire simulation, the evolution of the height and the internal diameter of the ring were monitored.

This way, the relation between the internal diameter and the height was continuously plotted and the calibration curves were obtained for different coefficients of friction.

In this simulation, an air cooling was previously applied to the specimens in order to emulate the transfer time between the furnace and the tool. After this initial cooling step, with transfer duration of 5 s, a dwell time of 3 s was applied to simulate the test. After this, the ring was deformed until a deformation of 50% in height and several simulations were carried out over the whole range of friction coefficient from 0.0 to 1.0 (i.e from frictionless to sticking condition) as shown in Fig. 3.5. The simulation was performed using a mechanical press where the rotation speed of the press was 30 strokes per minute and the total ram stroke was 100 mm. For the baseline or reference simulations, the temperatures of the ring and dies were set to 940 ºC and 200 ºC respectively and the temperature of surroundings was assumed 20 ºC. The heat transfer coefficient (HTC) between workpiece and surroundings was chosen as 10 kW/m^{2}K (medium value in the software).

From this calculated curve, the calibration curves of 0.1, 0.5, and 0.9 friction coefficients were randomly chosen as reference curves (indicated with a Ref. in the graphs) for determining the influencing factors by comparison with curves produced by varying the input parameters. In order to investigate the influencing factors on friction, simulations were done varying the inputs indicated below, using the same procedure. Input variation ranges were established taking into account the experimental representative values, simulation typical mesh sizes and possible temperature errors.

Influencing Factors

- Press speed: 10, 30 and 50 strokes/min
- Heat Transfer Coefficient (HTC): 2, 10 and 20 kW/m^{2}K
- Processing time: 4, 8, and 12 seconds of cooling time before deformation
- Mesh size: 0.4, 0.6 and 0.8 mm
- Material temperature: 900 ºC, 940 ºC and 980 ºC
- Tool temperature: 180 ºC, 200 ºC and 220 ºC

These are the most common design parameters used in a forging process that help the final product to have the desired material properties and geometrical shape and also from the literature survey it has been found that these parameters are the key areas of interest to study. The control of these parameters helps the manufacturer to predict the characteristics of the final product.

3.1.2. T-Shape test

Fig. 3.4. illustrates the stages of deformation during the T-Shape simulation (also see Fig. 3.1). In the T-Shape test simulation, two symmetry planes have been applied to the specimens in order to reduce the computational time needed to run the simulations. This way, only one quarter of specimen has been simulated. The model used rigid tools being the specimen deformable with the material properties of the Ti-6Al-4V. The shape of specimens and the dies used in the simulation are shown in Fig. 3.4.

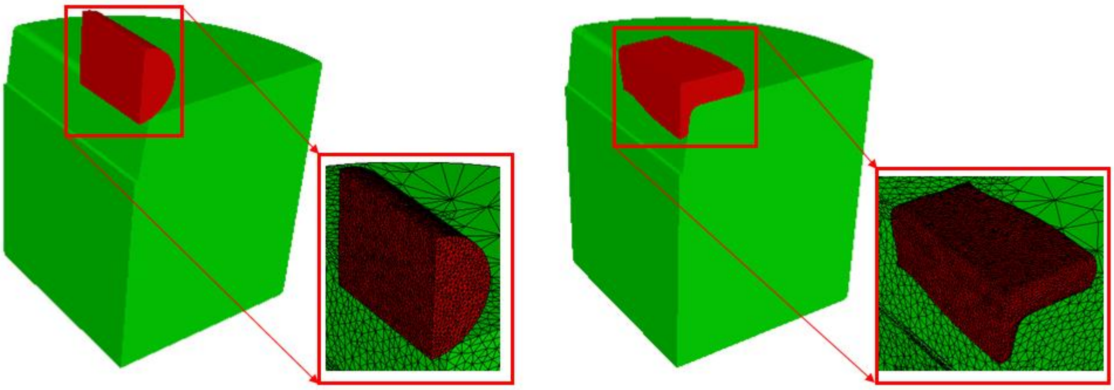

Fig. 3.4: Specimen deformation process of T-Shape test simulation

In the finite element discretization, the specimen has been divided into 47261 tetrahedron elements with 10309 nodes. Lower die has been divided into a total of 2178 tetrahedron elements with 1156 nodes. In order to investigate the friction factor, simulations have been done using the inputs indicated below. The simulation was done using a mechanical press where the rotation speed of the press was 30 strokes per minute and the total ram stroke was 100 mm. For the baseline or reference simulations, the temperatures of the samples and dies were set to 940 °C and 200 °C respectively, and the temperature of surroundings was 20 °C. The HTC between workpiece and surroundings was chosen as 10 kW/m^{2}K. Finer mesh was employed in the inside and outside layers of the specimen, where severe deformation usually occurs, and the average mesh size was 0.78 mm. The simulation was conducted over friction coefficient from 0.0 to 1.0.

Like ring test simulation, after the initial cooling step, with transfer duration of 10 s and a dwell time of 2 s was applied to simulate the test to get the final deformation shape. In order to investigate the influencing factors, the influence of three parameters such as HTC, material change and friction have been investigated to see how these variables influence the force measurement and simulations were done varying the inputs with the same described procedure.

The influencing parameters for T-shape test has been chosen after examining the results of ring-test. From the ring test, it has been found that HTC is the most influencing factor where other factors does not affect so much. So, for T-shape test, HTC was chosen as an influencing parameter along two new parameters i.e friction factor and material changes.

Influencing Factors

- Heat transfer Coefficient (HTC): 1, 10 and 100 kW/m²K
- Friction factor: 0.2, 0.4, 0.6, 0.8, 0.9, 1.0
- Material changes: The value of coefficient **A** (parameter from Hansel Spittel law) has been increased and decreased of 20 %, which compared with real value of **A**

3.2. Results and Discussions

3.2.1. Sensitivity analysis of Ring test

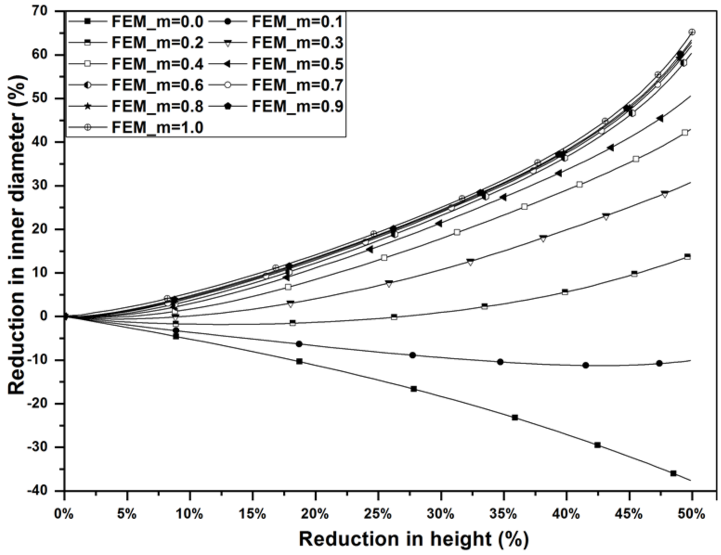

Fig. 3.5: Friction calibration curves obtained from the FEM at height reduction of 0–50% and friction factors (m) of 0-1 with baseline or reference input conditions

Influencing Factors

Fig. 3.6(a) shows the calculated calibration curves for different press speeds (10, 30 and 50 strokes/min) when the other variables are the same. The figure shows that press strokes slightly changes the calibration curves when stroke is 10 strokes/min, where as it does have a large effect on the curves when the applied stroke is 50 strokes/min (reference is 30 strokes per minute). Similarly, it can be concluded from Fig. 3.6(b) that having different HTC values (2, 10 and 20 kW/m²K) gives different calibration curves, indicating that this input is very influencing in the high temperature ring test.

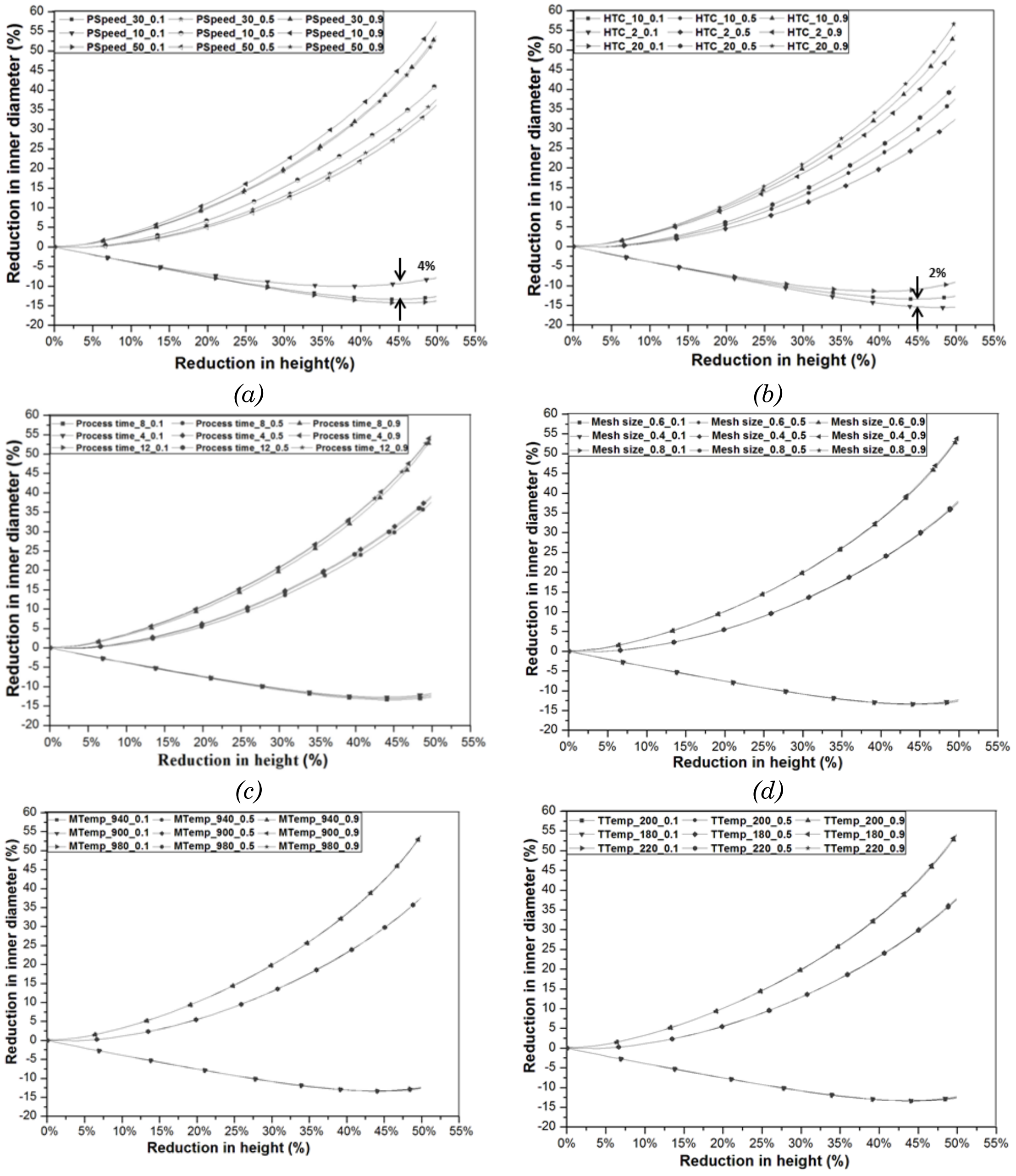

(a) *(b)*

(c) *(d)*

(e) *(f)*

Fig. 3.6: The influence on the calibration curves corresponding to the m of 0.1, 0.5, 0.9 for (a) Press speeds of 10, 30 and 50 strokes/min (b) HTC values of 2, 10 and 20 kW/m2K (c) Processing times of 0, 5 and 10 s (d) Mesh sizes of 0.4, 0.6 and 0.8 mm (e) Material temperature of 900, 940 and 980 °C and (f) Tool temperatures of 180, 200 and 220 °C

In Fig. 3.6(c) calibration curves were obtained where ring had different processing times (4 s, 8 s, and 12 s of cooling time). Simulations were split in two different steps. Firstly, heated ring was cooled down in air for a certain time of 8s (cooling time of 5s and waiting time of 3s) and secondly the ring was forged of 4s numerically like in previous studies. Very slight influence of the processing time was observed in the calibration curves.

Fig. 3.6(d) curves were obtained by considering mesh sizes of 0.4 and 0.8 mm and were compared to the reference one, where 0.6 mm mesh size was used. In Fig. 3.6(e) curves were obtained by considering material temperatures of 900 °C, 940 °C and 980 °C. Finally, in Fig. 3.6(f), the curves were calculated by considering tool temperatures of 180 °C, 200 °C and 220 °C. As it can be observed, very slight influence is observed for all of them.

3.2.2. Sensitivity analysis of T-Shape test

Fig. 3.7 shows the effects of the HTC on the slope of force curve and its sensitivity. Three different HTC values have been taken i.e. 1 kW/m^{2}K, 10 kW/m^{2}K and 100 kW/m^{2}K and the friction factor has been considered as 0.8. Similarly, Force curves with different friction factors are shown in Fig. 3.8. Results illustrate that both the HTC and friction factor has the biggest influence on the force measurement with very short forging time.

Meanwhile, the material influence on this test is shown in Fig. 3.9. After conducting a compression test on a given material, the test efforts can be obtained based on displacement tools curve. Depending on the test curves, one wishes to identify the rheological law that characterizes the material in question. The problem occurs because rheological law may have many parameters, which are unknown as to identify. An example of such law is Hansel Spittel law with many rheological parameters has been selected in order to see the influence of the material changes because it is the material law typically used in FORGE3.

The Hansel Spittel law is:

$$\sigma_f = Ae^{m_1 T} T^{m_9} \varepsilon^{m_2} e^{m_4/\varepsilon} (1+\varepsilon)^{m_5 T} e^{m_7 \varepsilon} \dot{\varepsilon}^{m_3} \dot{\varepsilon}^{m_8 T} \tag{3.1}$$

Where, σ_f is the Yield strength, T is the Temperature, ε is Strain and $\dot{\varepsilon}$ is the Strain rate and A, $m_1 - m_9$ are the coefficients of the Hansel Spittel equation and are potential optimization unknown parameters.

To analyse the material influences, the value of coefficient A has been increased and decreased of 20 %, which compared with real value of A. It has been observed that the influence of material on force measurement is very high as compared with the influence of HTC and Friction results.

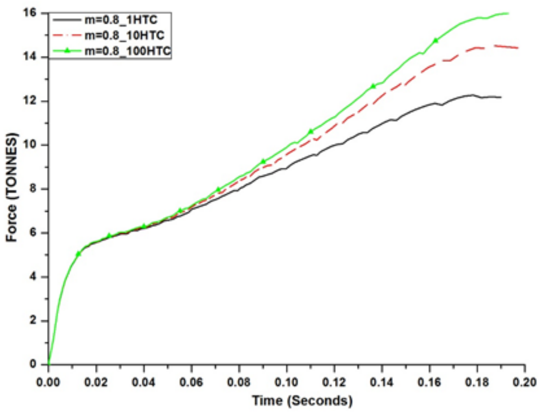

Fig. 3.7: Force curves with Different HTC

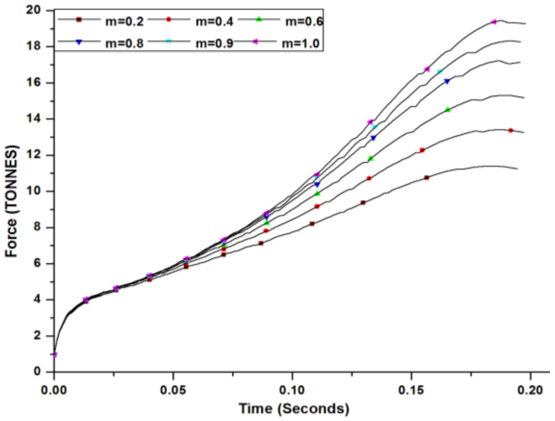

Fig. 3.8: Force curves simulated with different friction factor (HTC=10 kW/m²K)

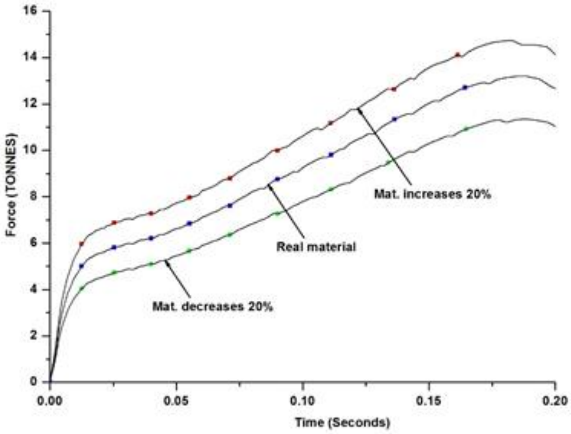

Fig. 3.9: Force curves simulated with Material changes (m=0.8 and HTC=10 kW/m²K)

It has been found that the force has changed a lot with all the three cases, such as the influence of HTC, friction factor and material changes. However, force is very sensitive to material properties and thus to identify the correct *m* value we must do a complete characterization of the material at high temperatures and different strain rates using either hot compression or torsion tests, which is very expensive. So, it has been needed an independent variable to show the material changes correctly. Although measuring the force and extruded height is the most common way to identify *m* in T-Shape test but our hypothesis is that geometrical shape of specimen could be a good way to simplify the methodology for a big range of materials.

3.2.3. Comparision of tribological contact conditions

However, friction depends on many varying parameters, the most important influencing parameters are the surface enlargement, contact pressure. Zhang et al. [ZHA08] proposed that to obtain a representative value of friction coefficient (μ) for a real forging operation, the contact condition of friction test should be similar to those in forging operation, because experiments show that different μ can be deduced from friction tests due to the different contact conditions. These conditions are often related to the mean contact pressure as well as the surface enlargement.

Fig. 3.10 shows the surface enlargement (surface area expansion/initial surface area in percentage) between the tool and the work piece at different strokes of both ring and T-Shape test gained from simulation. The friction factor has been considered as 0.8. The surface enlargement of the T-Shape test reaches a value at about 35% whereas for the ring test the value at about 5%. For the T-Shape tests, the surface enlargement continuously rises with the proceeding process stroke whereas surface enlargement of the ring test decreases initially and then increases.

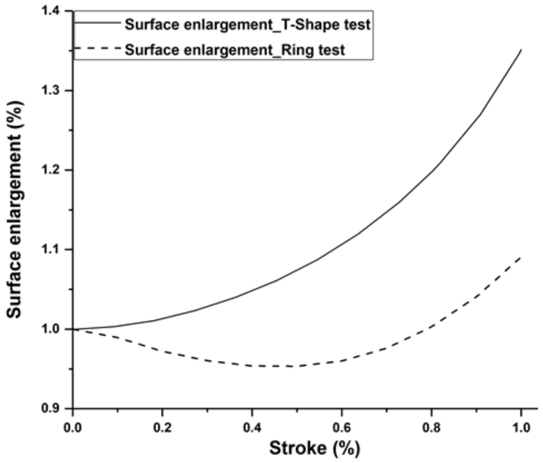

Fig. 3.10: Surface enlargement with m=0.8

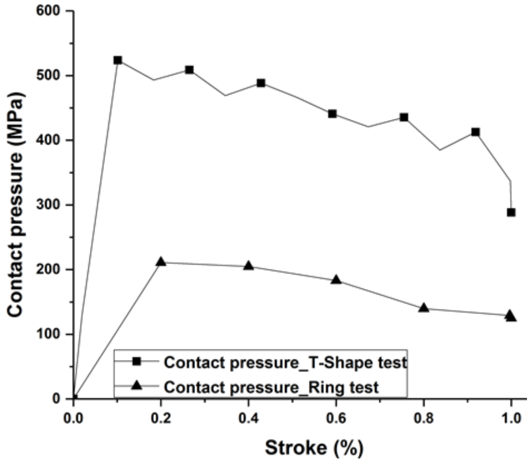

Fig. 3.11: Contact pressure with m=0.8

Fig. 3.11 shows the normalized contact pressure between die and workpiece gained by simulation at different strokes of both tests. The friction factor has been considered as 0.8. The contact pressure of T-Shape test is quite high and reaches values up to approximately 515 MPa. Similarly, the contact pressure of ring test is quite low and the value reaches up to 200 MPa.

3.3. Conclusions

A comprehensive numerical study on the ring and T-Shape friction test has been carried out. Based on the observations reported in this paper, the conclusions can be summarized as below:

3.3.1. Analysis of Ring test

- According to the results, it has been found that HTC, and press velocity are the most influencing factor affects the geometry of specimen and friction factor.

- The HTC is one of the critical influencing factors in this test. To control the errors from this input, the heat transfer tests must be performed using different contact pressures prior to ring test simulations.
- The press velocity is critical if a mechanical press is employed to conduct the ring tests. Precise experimental data must be used in the numerical simulations since an increase or decrease of the press strokes per minute can highly influence the numerically obtained calibration curves. This variation in calibration curves is not linear with the strokes per minute change, since the contact time during the forging is not linear with the speed, as the press ram obeys a sinusoidal shape during forging. In addition, mechanical press has higher speed and higher strain rate during deformation [ALT05]. During the test, the speed of the die varies with press ram displacement and therefore, there will be a variable strain rate during deformation.
- It has been demonstrated that the other studied parameters do not show relevant influence in the calibration curves and so are not critical inputs if the test is performed using standard procedures and deviations.
- Although the ring compression test is a well-known and simple test to perform, new guidelines are needed to standardize the test. Press rotation velocity should be measured precisely during the compression tests and the use of heat transfer coefficients in function of the contact pressure may be useful to numerically simulate the test and obtain representative calibration curves.

3.3.2. Analysis of T-Shape test

- It has been found that the HTC influences very small on force with very short forging time and the friction factor has the big influence.
- The influence of material on force measurement is very high.
- Inaccuracies in the material characterization could lead to inaccuracies in the COF calculation.
- Force depends greatly on the material model and the COF being the influence, of the HTC much smaller.
- It has been concluded that the geometrical shape of specimen can be an adequate technique to simplify the methodology.

3.3.3. Analysis of Tribology condition for both test

- It has been found from the analysis that the surface enlargement of the T-Shape test at about 35% whereas for the ring test the value at about 5%.

- The contact pressure of T-Shape test is quite high and reaches values up to approximately 515 MPa whereas, the contact pressure of ring test is quite low and the value reaches up to 200 MPa.
- It has been concluded that, T-shape compression test is suitable to evaluate the friction condition because this test induces a complex deformation path, large contact pressure and rather large surface expansion similar to what is occurred during a real forming operation.

CHAPTER 4

DETERMINATION OF THE HEAT TRANSFER COEFFICIENT BY COLUMNAR UPSETTING TEST

*“Knowing is not enough; we must apply
and willing is not enough; we must do.”*
-Johann Wolfgang von Goethe

4. DETERMINATION OF THE HEAT TRANSFER COEFFICIENT BY COLUMNAR UPSETTING TEST

4.1. Introduction

Hot forging of titanium takes place at high temperature and the flow properties and resulting microstructure of this alloy are very sensitive to temperature and its variation. The workpiece is usually glazed before forging to avoid oxidation and lubricant is applied while forging titanium alloys. The temperature at the interface depends on the thickness and the thermal properties of the layer formed by the glaze, the lubricant and the thermal properties of the workpiece and dies. There have been a number of investigations carried out to study the interface temperature and heat transfer coefficient (HTC) in hot forging processes because it is important to be able to predict and if possible, to control temperature fields arising during hot metal forming processes [JEO01].

This chapter describes the columnar upsetting test for the determination of HTC at the workpiece-die interface for two different contact pressures, based on the temperature history of the specimen. Then, an efficient numerical 3D model has been developed where; simulations have been carried out defining different values of the HTC for the determination of HTC at different contact conditions. That gives different temperature evolutions, which were used to estimate the HTC value which best fits the temperature read by the thermocouple in the real experiments. Additionally, HTC models at different temperature ranges have been analysed to analyse the variations in HTC but the final HTC has been considering at the stage of forging process. Variations in HTC have been obtained under different pressure with different surface condition during upsetting. Finally, the validation of final coefficients was determined by comparing the experimental results with the numerical simulation results using inverse analysis approach.

4.2. Experimental Procedure

4.2.1. Materials and Specimen Preparation

The material used in this work was a, 30 mm diameter bar, commercial grade Ti-6Al-4V alloy annealed at 800 °C for 1 h from Western titanium technologies co. ltd. The chemical composition of the used specimens of the Ti-6Al-4V alloy is presented in Table 4.1.

Table 4.1: Chemical composition in wt.% of Ti-6Al-4V

Element	Al	V	Fe	O	C	N	H	Ti
min	5.50	3.50	-	-	-	-	-	Bal.
max	6.75	4.50	0.4	0.20	0.08	0.05	0.015	Bal.

Cylindrical Ti-6Al-4V test pieces with diameter and height of 20 mm were machined for the test as shown in Fig. 4.1, with surface roughness (Ra) of 1.92 µm measured by Hommel tester T500 surface profilometer. Three types of surfaces were studied: billets without coating and billets with 40 and 80 µm of CONDAERO 228 glass coating as shown in Table 4.4. The specimens were glazed using CONDAERO 228 glass to prevent surface oxidation during heating of the specimen, a lubricating and insulating coating developed by CONDAT. Both the upper and lower dies were made of Uddeholm Alvar 14 tool steel (1.2714 / EN 56NiCrMoV7) hardened at 42 HRC. Surface roughness in both test-tooling systems is around Ra 2.70 µm.

The hole has been electric discharge machined (EDM) on the billets located in 2 mm from the die (contact surface), to place K type thermocouple having diameter of 1 mm and to a depth of 10 mm as shown in Fig. 4.1. The special high response K type thermocouple has been used to measure temperatures during the experiments in this test.

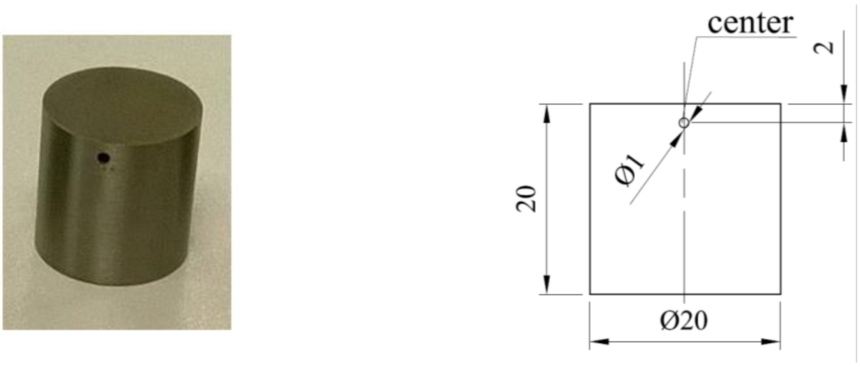

Fig. 4.1: Geometry of HTC specimen and thermocouple locations : (left) Test-Piece, (right) Engineering Drawing; all units are in mm

4.2.2. Surface topography measurements

A confocal imaging profiler (SENSOFAR S NEOX) was used to analyse the machined surface topography for both tool and specimen of this test as shown in Fig. 4.2. The analysed surface area was approximately 877x660 µm by acquiring the area using objectives of 20x magnifications. Three independent measurements were made on each sample and the mean value as well as standard deviation has been calculated as shown in Table 4.5. The acquisition conditions on 3D topographical measurements is shown in Table 4.2. All measurements were treated using the same data processing variables (see Table 4.3) through the metrological software SensoMap Premium 7.4.

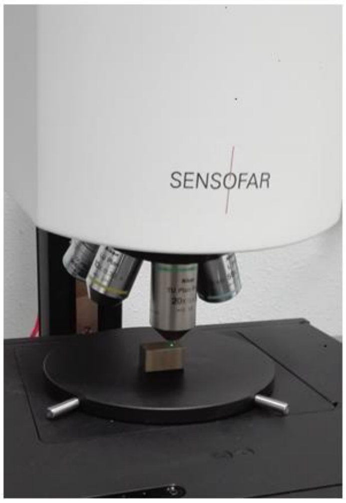

Fig. 4.2: Confocal profilometer SensoFar

Table 4.2: Acquisition conditions used in the study

Characteristics	Conditions
Microscopic objective	20x
Spatial sampling (µm)	0.65
Vertical Res (nm)	8
Viewing area (µm^2)	877x660
Measuring range (µm^2)	3250x3040

Table 4.3: Variables used for data processing in the study of data acquisition variables

S Filter	F Operator
Gaussian (λ_s = 1.3 µm)	First order polynomial fitting

Topographical parameters

A set of field parameters defined in ISO 25178 [ISO12] were selected for the study, belonging to height (S_q, S_{sk}, S_{ku}), spatial (S_{al}), hybrid (S_{dr}, S_{dq}) and functional (V_{mp}, V_{mc}, V_{vc}, V_{vv}) families. Where, S_q (Root mean square roughness), S_{dq} (Root mean square slope of the surface) and S_{dr} (Developed interfacial area ratio) considered more representative in this measurement which are highlighted in green are presented in Table 4.5 and Table 4.6. The formulation of these three parameters is shown in the equations (4.1), (4.2) and (4.3) respectively.

$$S_q = \sqrt{\frac{1}{MN} \sum_{j=1}^{N} \sum_{i=1}^{M} \eta^2(x_i, y_j)} \tag{4.1}$$

$$S_{dq} = \sqrt{\frac{1}{(M-1)(N-1)} \sum_{j=2}^{N} \sum_{i=2}^{M} \left[\left(\frac{\eta(x_i, y_i) - \eta(x_{i-1}, y_i)}{\Delta x} \right)^2 + \left(\frac{\eta(x_i, y_i) - \eta(x_i, y_{i-1})}{\Delta y} \right)^2 \right]} \tag{4.2}$$

$$S_{dr} = \frac{(Texture\ surface\ area) - (Cross\ sectional\ area)}{(Cross\ sectional\ area)} \tag{4.3}$$

4.2.3. Experimental set up

For this test, the complete tooling assembly was mounted on a high precision 40 kN SCHMIDT micro servo-press testing machine (shown in Fig. 4.3) which is able to perform closed loop controlled force application. The dies were maintained at a temperature of 200º C using a Hasco cartridge die heater. Two thermocouples were placed between the dies and this digital temperature control box in order to keep the dies at this required temperature. The lubricant based on CONDAFORGE 625 graphite diluted in water to 10% was sprayed to the dies using the pistol-spray before the deformation. The special high response K type thermocouple was embedded in the electro discharged machined holes in each specimen and connected to a National Instruments NI9215 module data logger to measure the temperature history from the furnace until the final cooling of the specimens. The information captured by the thermocouple placed at the specimen at a distance of 2 mm from the contact surface has been used in this work to calculate the HTC values by inverse analysis.

Experiments were carried out at contact pressure of 5 and 65 MPa and testing conditions are summarized in Table 4.4. A low pressure of 5 MPa is used to identify the HTC value at the beginning of the process and a contact pressure of 65 MPa is used as this value is right below the yield stress of Ti-6Al-4V at the working temperature. It was not possible to achieve higher contact pressures because the plastification of the specimen leads to the loss of the signal from the thermocouple.

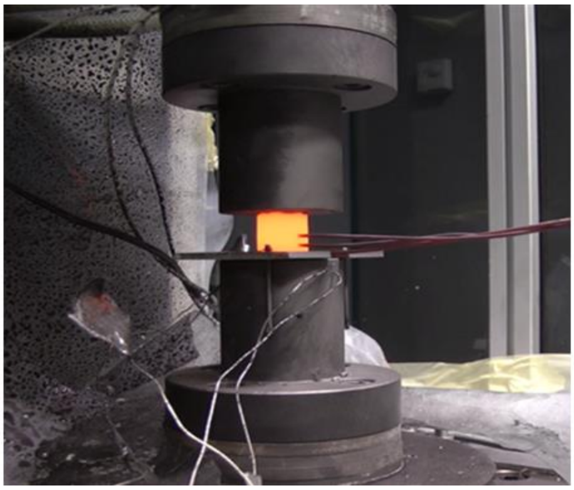

Fig. 4.3: Test set up

Table 4.4: Conditions on which the specimens tested for HTC

Tests	Lubricant	Specimens	Pressure (MPa)
Test 1	CONDAFORGE 625 diluted in water at 10%	without coating	5
Test 2		40 µm CONDAERO 228 coating	5
Test 3		80 µm CONDAERO 228 coating	5
Test 4		without coating	65
Test 5		40 µm CONDAERO 228 coating	65
Test 6		80 µm CONDAERO 228 coating	65

4.2.4. Test procedure

Specimens were heated to a temperature of 940° C in a Nabertherm 11 kW resistance furnace, with a soaking time of 10 minutes for the homogenization of the temperature. Once the specimen and dies reached their temperature equilibrium conditions, the specimen was transferred to the press and compressed between the dies to a predetermined pressure and outputs from the thermocouples were recorded on the computer. The nominal dwell period prior to deformation was taken to be 2 seconds and the time required to move the specimens from the furnace to the dies was about 4 seconds. These values were taken from video records of the experiments and recording started when the specimen left the furnace. The temperature history of the specimen was the input for the inverse HTC calculation.

4.3. Finite element simulation analysis

A finite element 3D model of Ti-6Al-4V alloy hot upsetting process was built using FORGE3® finite element software as shown in Fig. 4.4, in order to identify the HTC in the experiments explained before. Models uses rigid tools being the specimen deformable with the material properties of the Ti-6Al-4V. The temperatures of the specimens and dies were set to 940 ºC and 200 ºC respectively and the temperature of surroundings was 20 ºC for the simulation. Specimen was divided into 1102 tetrahedron elements with 4316 nodes and die was divided into a total of 4128 tetrahedron elements with 8252 nodes. The average mesh size was 0.8 mm. In this simulation, an air cooling was previously applied to the specimens in order to emulate the transfer time between the furnace and the tool. After this initial cooling step, with transfer duration of 4 seconds, a dwell time of 2 seconds was applied to simulate the test.

Finally, a targeted contact pressure was applied in the upper tool maintaining the specimen between the upper and the lower tool at that predefined pressure. During the entire simulation, the temperature history of the specimen was recorded by means of a virtual sensor in the area where the thermocouple was placed in the real experiments. The simulation was carried out defining different values of the HTC which gives as a result different temperature evolutions in the position where the virtual sensor is placed. After this, the correct HTC value was optimized for minimizing the differences between the numerical predictions and the results measured in the experiments.

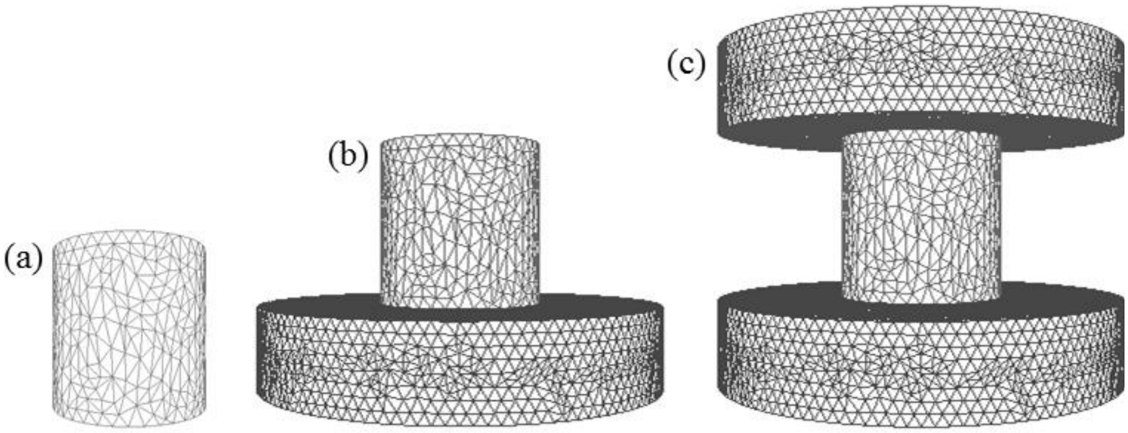

Fig. 4.4: FE model for hot upsetting process (a) transfer (b) pre-forming and (c) forming steps

4.4. Results and Discussion

4.4.1. Measurement of surface topography

An image of surface topography of the tool and specimen are presented in Fig. 4.5 and Fig.4.6 respectively. A wider surface with less number of peaks was observed in Fig. 4.5 whereas, in Fig. 4.6, the machined surfaces was observed with more number of peaks. considering height, which is more in sample surface compare to the tool as observed in Fig. 4.6 and Fig. 4.5.

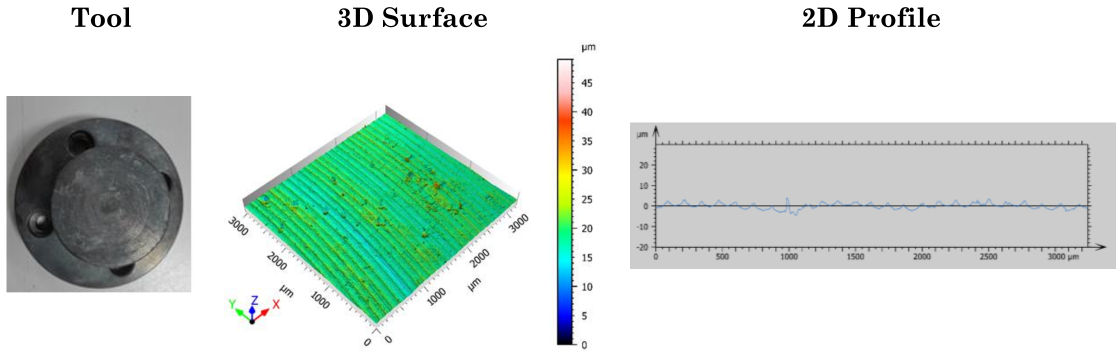

Fig. 4.5: Surface topography of HTC test tool

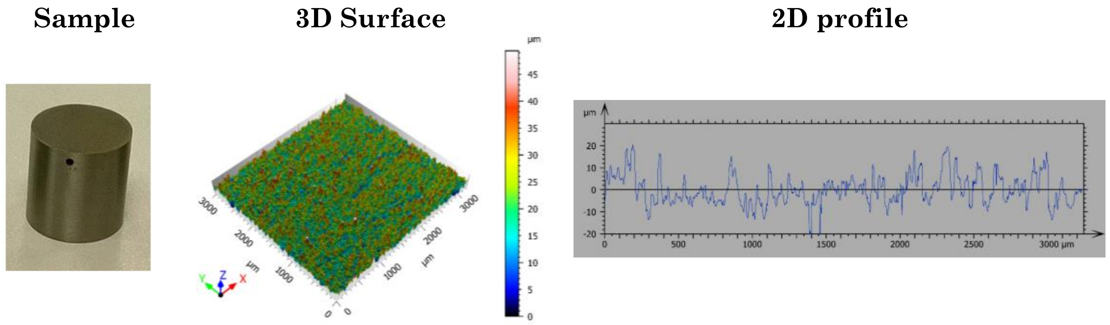

Fig. 4.6: Surface topography of HTC test sample

Also, list of all calculated parameters from the analysed surface of tool and specimen are presented in Table 4.5 and Table 4.6 respectively. It has been found from the Table 4.5, S_q value was 1.67 µm, S_{dq} value was approximately 0.20 µm and the S_{dr} value was about 1.74 µm for the tool of this test. Similarly, for the specimen, S_q value was 6.66 µm, S_{dq} value was approximately 1.70 µm and the S_{dr} value was about 50.62 µm.

Table 4.5: Calculated surface parameters of HTC tool

Parameters	Measurements			Summary		
	1.00	**2.00**	**3.00**	**MEAN**	**DEVIAT**	**COV (%)**
Sq	2.18	1.55	1.27	1.67	0.46	27.71
Ssk	-2.69	0.60	0.25	-0.62	1.81	-294.51
Sku	22.10	8.53	4.05	11.56	9.40	81.29
Sa	1.35	1.16	1.00	1.18	0.17	14.74
Sal (s = 0.2)	0.04	0.05	0.03	0.05	0.01	16.44
Str (s = 0.2)	0.05	0.03	0.02	0.04	0.01	38.28
Std	99.01	85.25	177.49	120.59	49.76	41.27
Sdq	0.24	0.19	0.15	0.20	0.04	21.26
Sdr	2.44	1.63	1.14	1.74	0.66	37.76
Vm (p = 100%)	0.02	0.02	0.01	0.02	0.01	33.85
Vmp (p = 10%)	9.87E-05	9.29E-05	6.82E-05	0.00	0.00	18.68
Vmc (p = 10%, q = 80%)	0.00	0.00	0.00	0.00	0.00	9.67
Vvc (p = 10%, q = 80%)	0.00	0.00	0.00	0.00	0.00	6.91
Vvv (p = 80%)	0.00	0.00	0.00	0.00	0.00	47.31
Spd (poda = 5%)	91.89	29.75	52.09	57.91	31.48	54.35
Spc (poda = 5%)	946.22	927.39	573.67	815.77	209.87	25.73
Sds	23846.74	23628.31	26011.59	24495.55	1317.46	5.38
Ssc	195.09	158.63	152.21	168.65	23.13	13.71

Table 4.6: Calculated surface parameters of HTC sample

Parameters	Measurements			Summary		
	1.00	**2.00**	**3.00**	**MEAN**	**DEVIAT**	**COV (%)**
Sq	6.94	6.61	6.43	6.66	0.26	3.88
Ssk	0.37	0.35	0.33	0.35	0.01	4.18
Sku	4.59	3.61	3.60	3.94	0.57	14.50
Sa	5.37	5.21	5.05	5.21	0.16	3.09
Sal (s = 0.2)	0.03	0.04	0.03	0.03	0.00	5.89
Str (s = 0.2)	0.79	0.76	0.76	0.77	0.01	1.92
Std	103.50	4.76	177.48	95.25	86.66	90.98
Sdq	1.90	1.61	1.59	1.70	0.17	10.03
Sdr	55.27	47.69	48.91	50.62	4.07	8.03
Vm (p = 100%)	0.07	0.05	0.05	0.06	0.01	18.50
Vmp (p = 10%)	0.00	0.00	3.77E-04	0.00	0.00	7.10
Vmc (p = 10%, q = 80%)	0.01	0.01	0.00	0.01	0.00	1.87
Vvc (p = 10%, q = 80%)	0.01	0.01	0.00	0.01	0.00	4.54
Vvv (p = 80%)	0.00	0.00	0.00	0.00	0.00	2.30
Spd (poda = 5%)	275.90	275.09	320.07	290.35	25.74	8.87
Spc (poda = 5%)	3075.85	2283.83	1922.02	2427.24	590.13	24.31
Sds	17542.39	17159.06	17125.54	17275.67	231.60	1.34
Ssc	938.39	844.22	846.87	876.50	53.62	6.12

4.4.2. Temperature changes measured at specimen

A typical example of the temperature variations measured in the specimen is shown in Fig. 4.7 (a). For doing so, the temperature history of the specimen was recorded for the different experiments covering the uncoated specimens and the specimens of 40 μm, 80 μm coated at 5 and 65 MPa. It can be considered that the temperature change occurs during four stages, summarized as follows:

(a) transfer of the workpiece from the furnace to the lower die (transfer stage)
(b) contact between heated workpiece and lower die sprayed by fine graphite lubricant (pre-forming)
(c) forming stage
(d) removal of the applied load (post-forming)

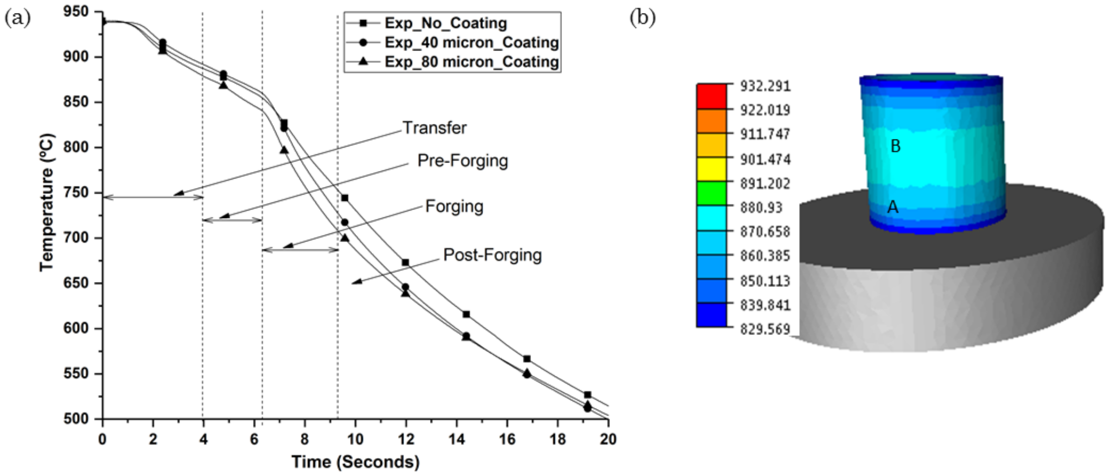

Fig. 4.7: Temperature changes in different workpiece: (a) Experimental and (b) FE model of temperature distribution

Considering the four stages in detail, it can be seen that the specimen temperature dropped by about 40 to 50 °C while the specimen was transferred from the furnace to the die. When the specimen was placed on the bottom die, the later temperature dropped due to heat losses from radiation, convection and conduction. As the pressure was very low before the top die moved down to forge the specimen, the heat transfer coefficient was quite low and the heat transferred from the specimen to the die was relatively small. During upsetting, the pressure built up on the interface and the dies and the specimen came into firm contact. This enabled heat transfer to occur more easily and it was continuing when specimen temperatures when forging began, due to the sharp increase of the heat transfer coefficient corresponding to the increase in pressure on the interface. Similarly, all the tests showed that the specimen temperature decrease, which is related to the heat transferred across the interface, was strongly dependent upon the interface pressure. It was also observed that the temperature decreased very quickly only after the interface pressure built up, which is better described in Fig. 4.7 (b).

4.4.3. Determination of interface HTCs

Fig. 4.8 and Fig. 4.9 shows the comparison of experimental results and specimen temperature profiles calculated from the FE simulation for 5 and 65 MPa. From the Fig. 4.7a, it has been found that the minimum temperature of Ti-6Al-4V alloy at the forging stage is 720 °C. Also, from the industrial survey and during the simulation of compression tests the minimum forging temperature was found around 720 °C. For this reason, the HTC value was fitted to the experimental data, starting at the initial forging temperature of around 940 °C and ending at this minimum temperature of 720 °C. The tests have been simulated using the different HTC values in FE simulation to find best HTC value.

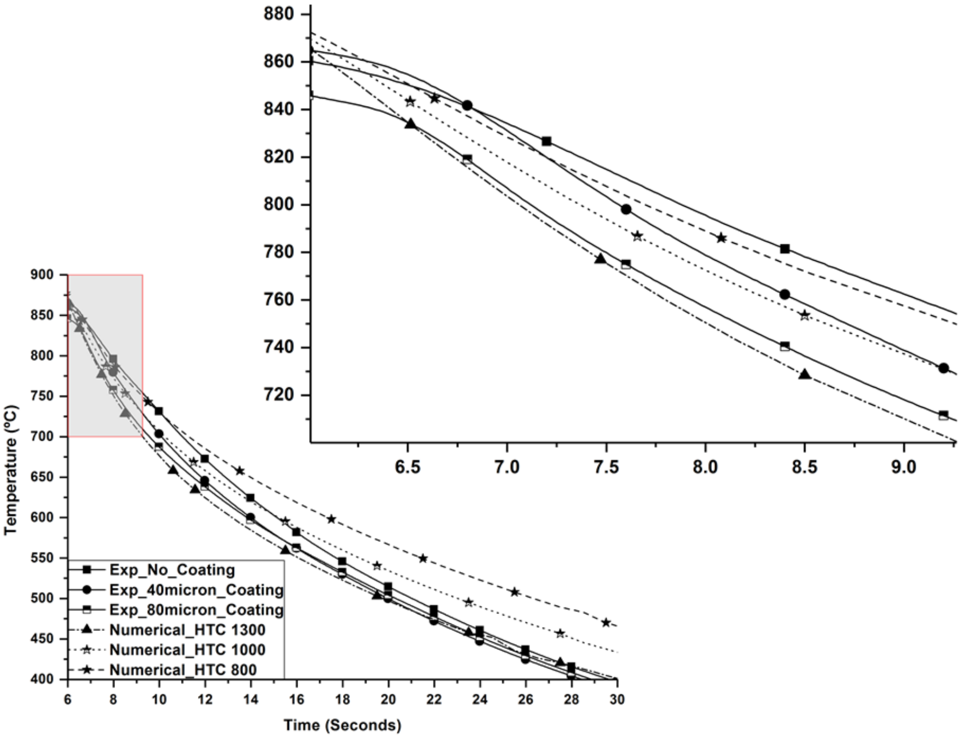

Fig. 4.8: The comparison of FE prediction and experimental results of different specimen temperature at the forging stage for 5 MPa contact pressure

It has been found that, at low pressures of 5MPa the estimated HTC remains at a value of about 1 kW/m^{2}K for all surfaces. However, the HTC value for the uncoated specimen is around 0.8 kW/m^{2}K, for the specimen coated with 40 μm is around 1 kW/m^{2}K and for the specimen coated with 80 μm is around 1.3 kW/m^{2}K as shown in zoomed part of Fig. 4.8. These differences are not significant. For the higher contact pressure of 65 MPa, the estimated HTC remains at a value of about 3 kW/m^{2}K for all surfaces. Although, the HTC value is around 5 kW/m^{2}K for uncoated specimens meanwhile for both, 40 μm and 80 μm coated specimens, the

HTC value is around 3 kW/m²K as shown in zoomed part of Fig. 4.9. So, the influence of the coating in the HTC value at high pressures is clearly noticeable.

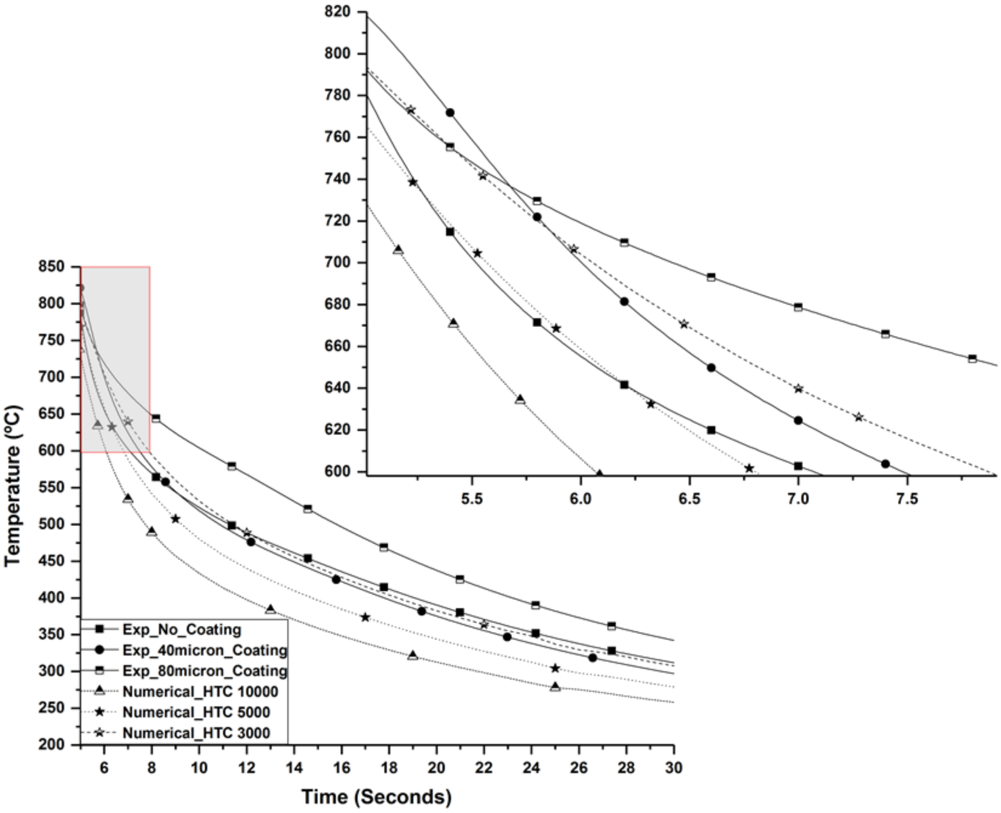

Fig. 4.9: The comparison of FE prediction and experimental results of different specimen temperature at the forging stage for 65 MPa contact pressure

Effect of glaze thickness on HTC

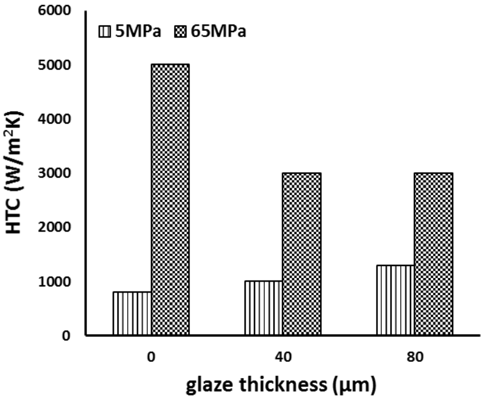

Fig. 4.10: Effect of glaze thickness

The effect of the glass on heat transfer was studied using test pieces having different thickness glass coatings under different pressures as shown in Fig. 4.10. The coating thickness (i.e, 40 and 80 µm) does not seem to affect the HTC value for both contact pressures, since at low contact pressure the HTC value does only change slightly. Similarly, for high contact pressure both 40 µm and 80 µm coated specimens resulted in the same HTC value of

3 kW/m2K. For 65 MPa, heat conductivity decreases with increasing coating thickness, showing the heat insulating property of the glaze. Heat conductivity is higher for the work-piece under pressure, due to the greater contact surface area. A difference in coating thickness from zero to 40 µm causes HTC to reduce to about half, for high pressure conditions.

4.5. Conclusions

Based on the observations reported in this paper, the conclusions can be summarized as below:

- The columnar test together with a closed loop force control has been proven to be an accurate method to predict HTC values.
- A minimum HTC value of 1 kW/m^{2}K was measured at low contact pressure for all surfaces and for higher contact pressure of 65 MPa, the HTC value is approximately 3 kW/m^{2}K for all surfaces.
- The contact pressure clearly influences the heat transfer from the specimen through the dies and HTC value increases with the contact pressure.
- The coating thickness does not seem to affect the HTC value for both contact pressures, since at low contact pressure the HTC value does only change slightly. Similarly, for high contact pressure both 40 µm and 80 µm coated specimens resulted in the same HTC value of 3 kW/m^{2}K.
- HTC value does depend on the contact pressure so the use of pressure dependent HTC is highly recommended.
- It has been found that, the value of S_q, S_{dq} and S_{dr} was about 1.67 µm, 0.20 µm and 1.74 µm respectively for the tool and for the specimen, the value of S_q, S_{dq} and the S_{dr} was approximately 6.66 µm, 1.70 µm and 50.62 µm respectively.

CHAPTER 5

INVESTIGATING FRICTION FACTOR THROUGH RING COMPRESSION TEST

"You've got to experiment to figure out what works."
-Andrew Weil

5. INVESTIGATING FRICTION FACTOR THROUGH RING COMPRESSION TEST

5.1. Introduction

Ring compression test has proven to be one of the most prevalent friction tests for measuring the friction factor. This test includes small surface expansion within the contact surfaces and simpler deformation path [PEZ11]. In addition, finite element simulation of forming processes requires precise value of friction factor. The friction factor is usually measured using ring compression test's calibration curves and these curves could be plotted using analytical/finite element approach.

In the present research, the friction factor of Ti-6Al-4V alloy hot forging were evaluating using combined approach of ring-compression test and FE simulations where, the deformed geometry of the sample was utilized for obtaining friction coefficient. It is noticed in particular that the HTC has significant effects on the metal flow and calibration curves, thereby affects the measurement of interfacial friction factor (from chapter 2 and 3). In this test, HTC as a function of pressure was employed to generate the calibration curves using finite element simulations for determining the interfacial friction coefficients. Finally, friction factor was determined by comparing the experimental results with the numerical simulation results of compression test using inverse analysis approach.

5.2. Experimental Procedure

5.2.1. Materials and Specimen Preparation

For the ring test, the specimens were machined from Ti-6Al-4V bar with the ratio of outer diameter: inner diameter: height equal to 6:3:2 and turned to 30 mm outer diameter, 15 mm inner diameter and 10 mm height with surface roughness (Ra) of 1.92 μm respectively is shown in Fig. 5.1. This used ratio is the most prevalent geometry for ring test [RAO93]. Machining tolerances were verified to be ±0.1 mm, a sufficiently narrow tolerance not affecting the numerical predictions.

Three types of surfaces were studied: billets without coating and billets of 40 and 80 μm of CONDAERO 228 glass coating as shown in Table 5.1. The specimens were glazed using CONDAERO 228 glass (a lubricating and insulating coating developed by CONDAT) to prevent surface oxidation during heating of the specimen and to improve the material flow lowering the friction coefficient between the billet and tooling.

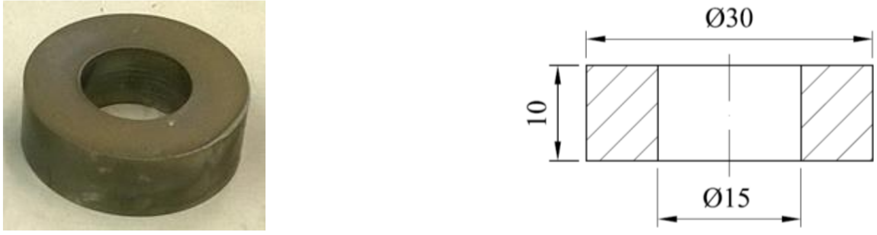

Fig. 5.1: geometry of ring specimen: (left) Test-Piece (right) Engineering Drawing; all units are in mm

Both the upper and lower dies were made of Uddeholm Alvar 14 tool steel (1.2714 / EN 56NiCrMoV7) hardened at 42 HRC. Surface roughness in test-tooling systems is around Ra 2.70 µm. Results of surface topography measurements are discussed in section 5.4.1, whose procedure is similar to those described in chapter 4, section 4.2.2.

5.2.2. Experimental set up

The complete tooling assembly was mounted on a 1250 kN GAMEI mechanical press (shown in Fig. 5.2). The dies were heated up to 200° C and maintained at a temperature of 200° C using a Hasco cartridge die heater. Two thermocouples were placed between the dies and this digital temperature control box in order to keep the dies at this required temperature. The lubricant based on CONDAFORGE 625 graphite diluted in water to 10% was sprayed to the dies using the pistol-spray before the deformation and stroke was set to obtain a 50% of height reduction for the tests. The rotation speed of the press was 30 strokes per minute and the ram stroke was 100 mm for this test.

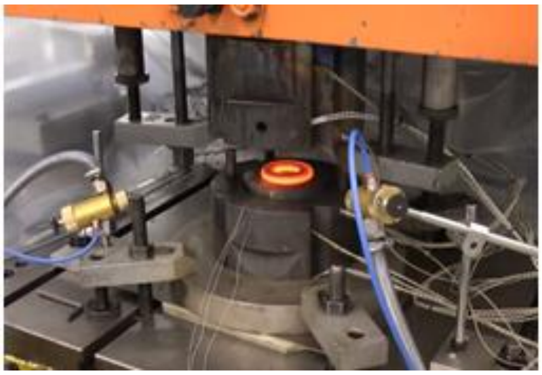

Fig. 5.2: Experimental set up with the water-graphite lubricant spraying system

5.2.3. Test procedure

Specimens were heated up to a temperature of 940° C in a Nabertherm 11 kW resistance furnace, with a soaking time of 10 minutes for the homogenization of the temperature. Once the specimen reached its temperature conditions, the specimen was transferred to the press and compressed between the dies to a predetermined stroke. The nominal dwell period prior to deformation was taken to be 3 seconds and the time required to move the specimens from the furnace to the dies was about 5 seconds. These values were taken from video records of the experiments.

In this test, specimens were compressed to a height reduction of 50% and three replicates were produced for each testing condition in order to provide statistical meaning. Nine samples were upset in this test to a deformation of 50% in height, so the heights of the samples were reduced from 10 mm down to 5 mm. Conditions on which the specimens were tested is shown in Table 5.1. After the compression, each sample was air cooled, cleaned and measured by a micrometer. The inner diameter and the final height were measured in both directions at right angles, on the specimens ends and at the middle in order to avoid the effect of the barrelling on the accuracy of the friction factors. Since the inner diameter is the most important variable for the COF calculation, a mean value of this dimension was used to calculate the percentage change of inner diameter.

In the present study, the law of constant friction is used to model the friction interface for the hot forging of Ti-6Al-4V alloy. The *m* value that governs the friction will be calculated by means of an inverse analysis approach.

Table 5.1: Testing Conditions of ring test

Tests	Lubricant	Samples	Measurement
Test 1-3	CONDAFORGE 625 diluted in water at 10%	without coating	Inner diameter variation after 50% height reduction
Test 4-6		with 40 µm CONDAERO 228 coating	
Test 7-9		with 80 µm CONDAERO 228 coating	Mean value of 3 repetitions

The percentage reduction in height and percentage reduction in internal diameter were calculated using the (5.1) and (5.2) relations, respectively:

$$\Delta h\% = \frac{h_0 - h}{h_0} \times 100 \tag{5.1}$$

$$\Delta d\% = \frac{d_i - d_i'}{h_0} \times 100 \tag{5.2}$$

where h_0 and *di* are initial height and internal diameter, respectively. The *h* and d_i*'* are denoting to the abovementioned values after deformation.

5.3. Numerical Modelling

In order to identify the COF in the experiments explained before, numerical 3D model was created using FORGE3® finite element software. This model emulates the experiments carried out before and the targeted variables (the COF) were optimized for minimizing the differences between the numerical predictions and the results measured in the experiments. Fig. 5.3 illustrates the stages of deformation during the ring compression test simulation. Models use rigid tools being the specimen deformable with the material properties of the Ti-6Al-4V. The temperatures of the specimens and dies were set to 940 ºC and 200 ºC respectively and the temperature of surroundings was 20 ºC in the simulation.

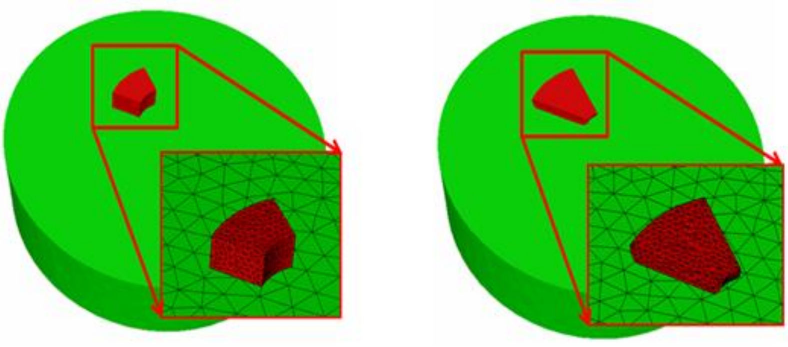

Fig. 5.3: Initial and final view of ring test simulation

In the simulation, symmetry was applied to the specimens in order to reduce the computational time in the simulations. This way, only one eighth of the specimen was simulated. In the finite element discretization, the specimen was divided into 894 tetrahedron elements with 3598 nodes and the die was divided into 2352 tetrahedron elements with 1178 nodes. The average mesh size was 0.6 mm.

Air cooling was previously applied to the specimens in order to emulate the transfer time between the furnace and the tool. After this initial cooling step, with a duration of 5 seconds, a dwell time of 3 seconds was applied (waiting time) and finally the upper tool applied the mechanical press movement using the characteristic eccentricity and ram arm dimensions of the press. The HTC applied between the specimen and the die was defined as a function of pressure in FEM to simulate the ring test (as concluded in chapter 4). After this, the ring was deformed until a deformation of 50% in height and several simulations were carried out covering the whole range of friction coefficient from *m*= 0.0 to 1.0 i.e. from frictionless to sticking condition and the variation of the aforementioned relation was plotted.

During the entire simulation, one sensor follows the evolution in height and another sensor follows the evolution of the internal diameter of the ring. This way the relation between the internal diameter and the height was continuously plotted. As shown in the results, the comparison of the real dimensions of the ring and the predictions carried out by the simulation defines the correct COF between the specimen and the tool.

5.4. Results and Discussion

5.4.1. Surface topography measurements

An image of surface topography of the tool and specimen are presented in Fig. 5.4 and Fig.5.5 respectively. Both machined surface of tool and sample have more number of peaks and height but considering height, which is more in sample surface compare to the tool as observed in Fig. 5.4 and Fig. 5.5.

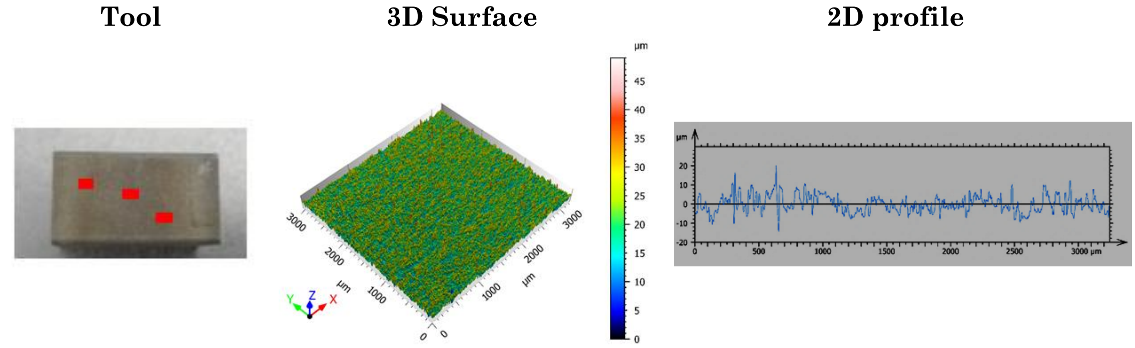

Fig. 5.4: Surface topography of ring test tool

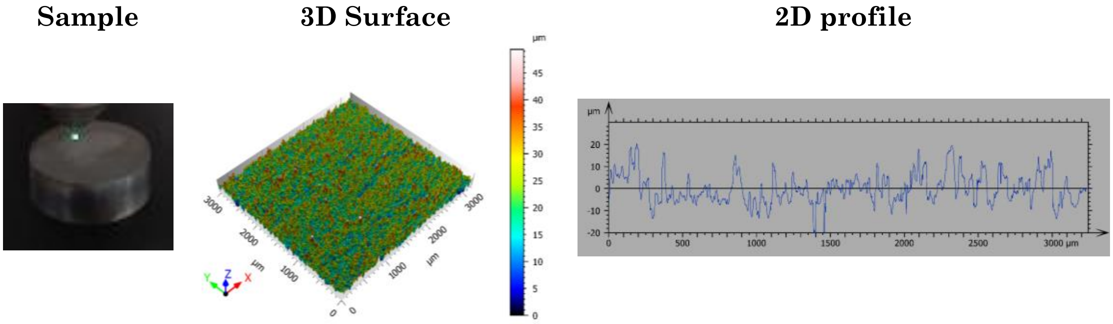

Fig. 5.5: Surface topography of ring test sample

In addition, a list of all calculated parameters from the analysed surface of tool and specimen are presented in Table 5.2 and Table 5.3 respectively. It has been found from the Table 5.2, Sq value was 4.46 µm, Sdq value was approximately 1.59 µm and the Sdr value was about 43.27 µm for the tool of this test. Similarly, for the specimen, Sq value was 6.66 µm, Sdq value was approximately 1.70 µm and the Sdr value was about 50.62 µm.

Table 5.2: Calculated surface parameters of ring test tool

Parameters	Measurements			Summary		
	1.00	**2.00**	**3.00**	**MEAN**	**DEVIAT**	**COV (%)**
Sq	4.56	4.39	4.43	4.46	0.09	2.03
Ssk	0.06	0.32	0.22	0.20	0.13	64.57
Sku	7.61	4.47	3.71	5.27	2.07	39.24
Sa	3.50	3.46	3.52	3.50	0.03	0.87
Sal (s = 0.2)	0.02	0.02	0.03	0.02	0.00	10.39
Str (s = 0.2)	0.65	0.60	0.58	0.61	0.03	5.61
Std	3.25	3.50	161.25	56.00	91.15	162.77
Sdq	1.81	1.54	1.40	1.59	0.21	13.28
Sdr	48.11	42.65	39.05	43.27	4.56	10.55
Vm (p = 100%)	0.07	0.04	0.04	0.05	0.02	35.81
Vmp (p = 10%)	0.00	0.00	0.00	0.00	0.00	5.09
Vmc (p = 10%, q = 80%)	0.00	0.00	0.00	0.00	0.00	1.70
Vvc (p = 10%, q = 80%)	0.01	0.01	0.01	0.01	0.00	0.71
Vvv (p = 80%)	0.00	0.00	0.00	0.00	0.00	4.92
Spd (poda = 5%)	355.66	442.35	461.33	419.78	56.33	13.42
Spc (poda = 5%)	4380.96	3357.46	2916.07	3551.50	751.47	21.16
Sds	21304.94	21395.58	21318.95	21339.82	48.79	0.23
Ssc	982.10	919.34	889.39	930.28	47.31	5.09

Table 5.3: Calculated surface parameters of ring test sample

Parameters	Measurements			Summary		
	1.00	**2.00**	**3.00**	**MEAN**	**DEVIAT**	**COV (%)**
Sq	6.94	6.61	6.43	6.66	0.26	3.88
Ssk	0.37	0.35	0.33	0.35	0.01	4.18
Sku	4.59	3.61	3.60	3.94	0.57	14.50
Sa	5.37	5.21	5.05	5.21	0.16	3.09
Sal (s = 0.2)	0.03	0.04	0.03	0.03	0.00	5.89
Str (s = 0.2)	0.79	0.76	0.76	0.77	0.01	1.92
Std	103.50	4.76	177.48	95.25	86.66	90.98
Sdq	1.90	1.61	1.59	1.70	0.17	10.03
Sdr	55.27	47.69	48.91	50.62	4.07	8.03
Vm (p = 100%)	0.07	0.05	0.05	0.06	0.01	18.50
Vmp (p = 10%)	0.00	0.00	3.77E-04	0.00	0.00	7.10
Vmc (p = 10%, q = 80%)	0.01	0.01	0.00	0.01	0.00	1.87
Vvc (p = 10%, q = 80%)	0.01	0.01	0.00	0.01	0.00	4.54
Vvv (p = 80%)	0.00	0.00	0.00	0.00	0.00	2.30
Spd (poda = 5%)	275.90	275.09	320.07	290.35	25.74	8.87
Spc (poda = 5%)	3075.85	2283.83	1922.02	2427.24	590.13	24.31
Sds	17542.39	17159.06	17125.54	17275.67	231.60	1.34
Ssc	938.39	844.22	846.87	876.50	53.62	6.12

5.4.2. Determination of COF

After the realization of the experiments, the ring specimens were measured to identify the COF value that best fits to the behavior of the material within the tool when being deformed. The rings before and after the realization of the experiments are shown in Fig. 5.6. It is clear that the application of coating produces different deformed profiles of the rings. The inner diameter of specimens with coating is greater than that with non-coating condition. This is in a good agreement with the basic principle of ring- compression test.

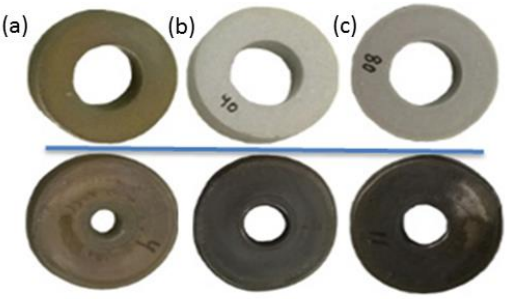

Fig. 5.6: Samples before deformation (top) and at 50% height reduction deformation (bottom) using lubricant: (a) Uncoated, (b) 40 µm Coated and (c) 80 µm Coated

Based on these experimental results, the height, the inner diameter and the outer diameter variation for all the specimens were calculated which is shown in Fig. 5.7. It has been concluded that, specimens without coating having less inner diameter as compared to 40 and 80 µm coated specimen. Hence, it proves that the non-coated specimen has high friction as they have small dimension compared to coated specimens.

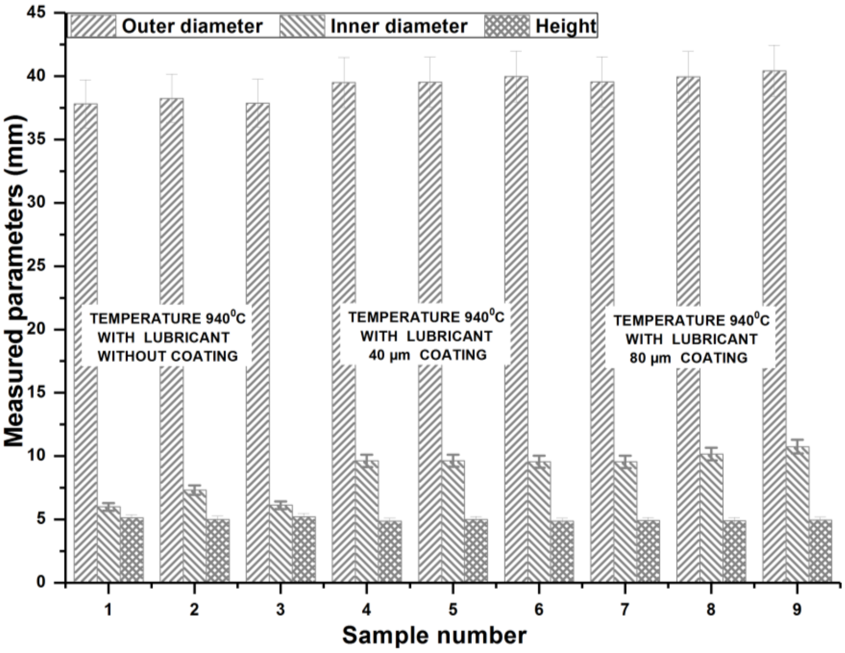

Fig. 5.7: Internal diameter, external diameter and height of the ring samples after the experiments

Fig. 5.8 shows the relation between the variation of the inner diameter and the variation of the height. In this figure, the curves represent the numerical relation for the different COF and the dots represents the relation of the inner diameter compared to the height for the specimens deformed in the experimental work. Based on the results plotted in Fig. 5.8, it can be observed that the glass coating clearly benefits the forging of the Ti-6Al-4V alloy since a lower COF value is achieved. The COF value for the coated specimens is about *m*= 0.3 meanwhile for the non-coated specimens the *m*= 0.8-1. It can also be observed that the thickness of the coating is not really affecting the value of COF since the specimens coated with a 40 µm and 80 µm layers offer the same COF value.

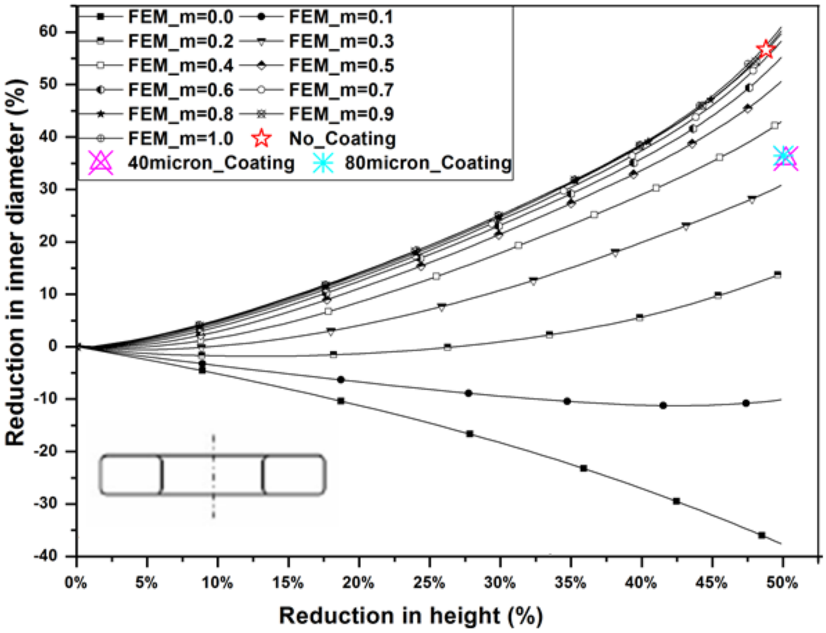

Fig. 5.8: Calibration curves obtained from the FEM and experimental results at height reduction of 50% with different friction factors

5.5. Conclusions

- The COF obtained from calibration curves for non-coated specimens varies from 0.8 to 1 meanwhile the COF is approximately 0.3 for 40 µm and 80 µm coated specimens. Therefore, the glass coating clearly improves the forgeability of titanium alloys reducing the COF value.
- The coating thickness does not seem to affect the COF since both 40 µm and 80 µm coated specimens resulted in the same friction value.
- The friction factor applicable to forging conditions cannot be estimated in the ring test without regard to heat transfer effects.
- It has been found that, the value of Sq, Sdq and Sdr was about 4.46 µm, 1.59 µm and 43.27 µm respectively for the tool. Similarly, for the specimen, value of Sq Sdq and Sdr was approximately 6.66 µm, 1.70 µm and 50.62 µm respectively.

CHAPTER 6

INVESTIGATING FRICTION FACTOR THROUGH T-SHAPE COMPRESSION TEST

> *"To raise new questions, new possibilities,*
> *to regard old problems from a new angle,*
> *requires creative imagination and*
> *marks real advance in science."*
> -**Albert Einstein**

6. INVESTIGATING FRICTION FACTOR THROUGH T-SHAPE COMPRESSION TEST

6.1. Introduction

A suitable friction experiment should provide conditions as similar as possible to those usually noticeable in most the practical forming operations. Recently a T-Shape test has been developed by Zhang et al. in the year of 2008 to avoid the difference of friction conditions [ZHA09]. The T-shape compression test is a test to determine friction coefficient by combined compression and extrusion in metal forming processes. Only cylindrical surface of billet is in contact with punch and die where the sectional shape of formed part looks likes 'T' [FER11]. This test includes large surface expansion ratio up to 50% and the contact pressure can reach four times the flow stress of the material within the contact surfaces, similar to what is occurred during a real forming operation [ZHA09]. Therefore, the resulted friction factors are reliable and applicable.

In the present research, the frictional conditions of hot Ti-6Al-4V forging has been studied using the T-shape compression tests. A comprehensive numerical and experimental study has been carried out to calculate the COF where, geometrical shape of specimen has been chosen to simplify this methodology. Three surface conditions were analyzed in the present study: billets without coating, 45 µm and 90 µm of CONDAERO 228 glass coating. The objective of this chapter was to study the influence of the contact pressure and surface enlargement in the performance of glass coatings used in this test. The calibration curves were generated using finite element simulations for various values of friction factor and according to simulation results, the total width (w) and flange height (h) were inspected to determine the friction behavior from the finished workpiece. After the realization of the experiments, the shape of specimens (i.e. total height, total width, flange height, etc.) have been measured and compared with the simulation results to estimate the friction factor under all surface conditions. These measurements with the use of inverse modelling techniques enabled a precise characterization of the forging friction coefficient.

6.2. Experimental Procedure

6.2.1. Materials and Tooling Preparation

Ti-6Al-4V alloy was selected for preparation of the test samples. The geometry of specimens was cylindrical having diameter of 20 mm and a height of 50 mm with surface roughness (Ra) of 0.4 µm respectively. Machining tolerances were verified to be ±0.1 mm. The turning operation was performed on the billets where, the turning parameters were; cutting speed (V_c) is 180 m/min, cutting insert corner radius: 0.4 mm, feed rate (f): 0.1 mm/rev. The insert used for this turning operation was: SANDVIK VBMT 16 04 04-MF 1025 (ISO Nomenclature).

The forging tools were manufactured using the Uddeholm Alvar 14 tool steel (1.2714/ EN 56NiCrMoV7) hardened at 42 HRc. Surface roughness of test-tooling systems is around Ra 2.70 µm. To get the formed part like 'T' for the test, the lower die was machined with a V-shape groove by wire-cut Electrical Discharge machining (EDM) where Groove angle (β) is 15°, entry radius is 2.5 mm and total depth is 25 mm with a final radius of 1 mm. The groove dimensions and T-Shape tooling are shown in Fig. 6.1.

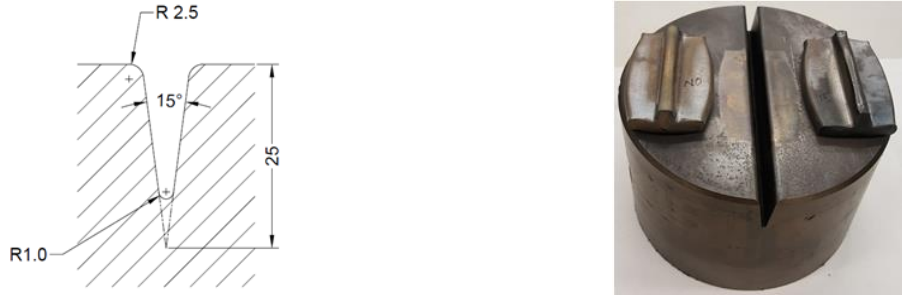

Fig. 6.1: (left) The sectional shape of die, (right) experimental grooved die together with deformed specimen

The results of surface topography measurements are discussed in section 6.4.1, whose procedure is similar as described in chapter 4, section 4.2.2.

6.2.2. Experimental set up

The complete tooling assembly was mounted in a 1250 kN GAMEI mechanical press. The tool system was maintained at a temperature of 200° C by means of a cartridge die heater (Hasco). A cartridge dies heater (Hasco) is a digital temperature control box that was used to control the tool temperature during the test. Two thermocouples were placed between the dies and this digital temperature control box in order to keep the dies at a required temperature. Before doing all the tests, the lubricant based on CONDAFORGE 625 graphite diluted in water to 10% using a pistol-spray was sprayed to the upper and lower dies. For the tests, the rotation speed of the mechanical press has been adapted to be 30 strokes/min and the press was programed to obtain a flange height (press gap) of 6 mm.

6.2.3. Test procedure

Specimens were conducted at the deformation temperature of 940° C and every specimen was heated to the testing temperature in a Nabertherm 11 kW resistance furnace for 10 minutes.

Once the test-piece reached its temperature conditions, the test-piece was transferred to the press and compressed between the dies to a predetermined stroke. The testing conditions are summarized in Table 6.1.

Table 6.1: Testing Conditions of T-Shape test

Tests	Lubricant	Samples	Measurement
Test 1-3	CONDAFORGE 625 diluted in water at 10%	without coating	Flange width of compression part
Test 4-6		with 40 µm CONDAERO 228 coating	
Test 7-9		with 80 µm CONDAERO 228 coating	Mean value of 3 repetitions

All the specimen with lubricated conditions were upset in which the specimens were undergoes extrusion in the V-groove and compresses radially resulting in a T-Shaped formed product (Fig. 6.1 (right)). Three replicates were produced for each testing condition in order to provide statistical meaning. After hot compressions, each sample was air cooled, cleaned and measured by digital Vernier caliper. The final width the samples present in the flat area of the forgings was used as the characteristic measure to calculate the coefficient of friction in this test.

6.3. Numerical Modelling

Using FORGE3® commercial software, a 3D FE model was developed. The constant friction law was used in order to identify the COF in the experiments explained before related to test conditions. Fig. 6.2. Illustrates the stages of deformation during the T-Shape simulation. The model used rigid tools being the specimen deformable with the material properties of the Ti-6Al-4V alloy.

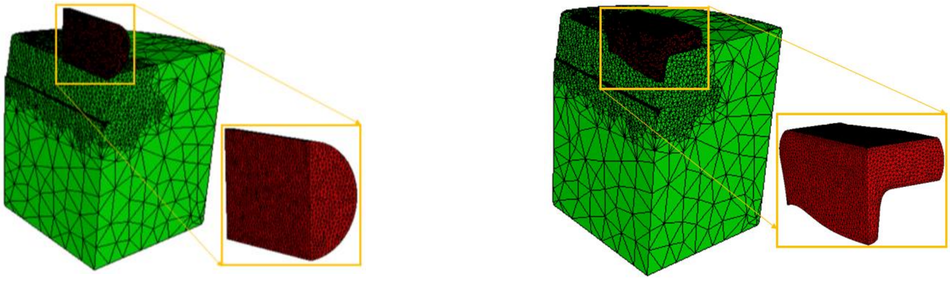

(a) Before deformation *(b) After deformation*

Fig. 6.2: Specimen deformation process in FEM simulation

In the simulation, two symmetry planes were applied to the specimens in order to reduce the computational time. This way, only one quarter of specimen was simulated and the press gap was set to 6-7 mm (final web height). In the finite element discretization, the specimen has been divided into 16108 tetrahedron elements with 3808 nodes. Lower die has been divided into 25071 tetrahedron elements with 5391 nodes. In order to investigate the friction factor, simulations have been done using the inputs indicated below. Finer mesh was employed of the specimen and the average mesh size was 0.5 mm. The temperatures of the specimens and dies were set to 940 °C and 200 °C respectively, and the temperature of surroundings was 20 °C in the simulation.

Air cooling was previously applied to the specimens in order to emulate the transfer time between the furnace and the tool. After this initial cooling step, with a duration of 10 seconds, a dwell time of 2 seconds was applied (waiting time) and finally the upper tool applied the mechanical press movement using the characteristic eccentricity and ram arm dimensions of the press. The HTC applied between the specimen and the die was taken from HTC results (chapter 4), which was defined as a function of pressure in FEM to simulate the ring test. The simulation was conducted over friction coefficient from 0.2, 0.4, 0.6, 0.8, 0.9 and 1.0. This way the evolution of the web height and the web width were continuously monitored using two nodes and compared with experimental results to calculate the real friction value.

6.4. Results and conclusions

6.4.1. Surface topography measurements

An image of surface topography of the tool and specimen are presented in Fig. 6.3 and Fig.6.4 respectively. Both machined surface of tool and sample have with more number of peaks height but considering height, which is more in tool surface compare to the specimen as observed in Fig. 6.3 and Fig. 6.4.

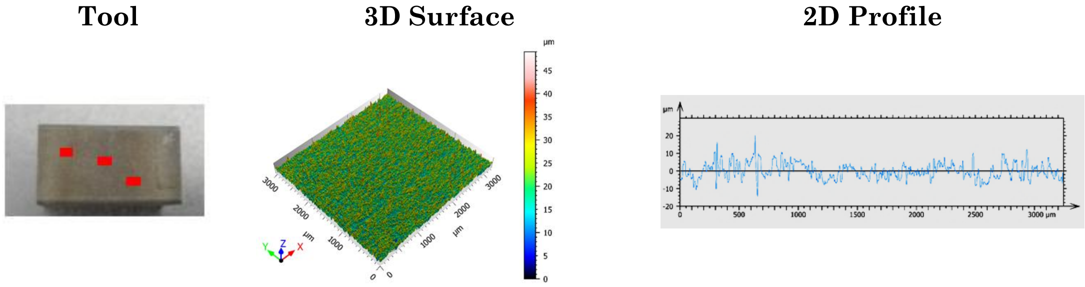

Fig. 6.3: Surface topography of T-Shape test tool

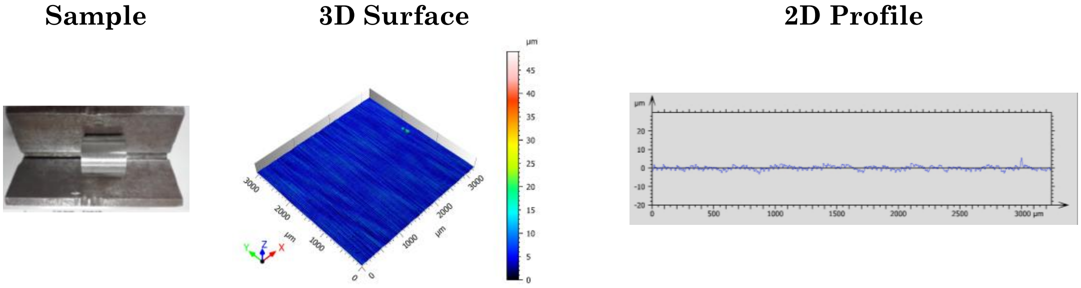

Fig. 6.4: Surface topography of T-Shape test sample

In addition, a list of all calculated parameters from the analysed surface of tool and specimen are presented in Table 6.2 and Table 6.3 respectively. It has been found from the Table 6.2, Sq value was 4.46 µm, Sdq value was approximately 1.59 µm and the Sdr value was about 43.27 µm for the tool of this test. Similarly, for the specimen, Sq value was 1.17 µm, Sdq value was approximately 0.27 µm and the Sdr value was about 3.25 µm.

Table 6.2: Calculated surface parameters of T-Shape tool

Parameters	Measurements			Summary		
	1.00	**2.00**	**3.00**	**MEAN**	**SD**	**COV (%)**
Sq	4.56	4.39	4.43	4.46	0.09	2.03
Ssk	0.06	0.32	0.22	0.20	0.13	64.57
Sku	7.61	4.47	3.71	5.27	2.07	39.24
Sa	3.50	3.46	3.52	3.50	0.03	0.87
Sal (s = 0.2)	0.02	0.02	0.03	0.02	0.00	10.39
Str (s = 0.2)	0.65	0.60	0.58	0.61	0.03	5.61
Std	3.25	3.50	161.25	56.00	91.15	162.77
Sdq	1.81	1.54	1.40	1.59	0.21	13.28
Sdr	48.11	42.65	39.05	43.27	4.56	10.55
Vm (p = 100%)	0.07	0.04	0.04	0.05	0.02	35.81
Vmp (p = 10%)	0.00	0.00	0.00	0.00	0.00	5.09
Vmc (p = 10%, q = 80%)	0.00	0.00	0.00	0.00	0.00	1.70
Vvc (p = 10%, q = 80%)	0.01	0.01	0.01	0.01	0.00	0.71
Vvv (p = 80%)	0.00	0.00	0.00	0.00	0.00	4.92
Spd (poda = 5%)	355.66	442.35	461.33	419.78	56.33	13.42
Spc (poda = 5%)	4380.96	3357.46	2916.07	3551.50	751.47	21.16
Sds	21304.94	21395.58	21318.95	21339.82	48.79	0.23
Ssc	982.10	919.34	889.39	930.28	47.31	5.09

Table 6.3: Calculated surface parameters of T-Shape sample

Parameters	Measurements			Summary		
	1.00	**2.00**	**3.00**	**MEAN**	**SD**	**COV (%)**
Sq	1.16	1.11	1.23	1.17	0.06	5.04
Ssk	0.02	0.40	0.01	0.15	0.22	148.24
Sku	3.67	6.60	3.38	4.56	1.78	39.02
Sa	0.92	0.87	0.98	0.93	0.06	6.07
Sal (s = 0.2)	0.02	0.04	0.04	0.04	0.01	28.88
Str (s = 0.2)	0.06	0.09	0.12	0.10	0.03	32.95
Std	89.23	89.23	89.22	89.23	0.00	0.00
Sdq	0.29	0.26	0.26	0.27	0.02	5.86
Sdr	3.61	3.07	3.05	3.25	0.32	9.86
Vm (p = 100%)	0.01	0.00	0.00	0.01	0.00	25.56
Vmp (p = 10%)	5.31E-05	5.39E-05	####	0.00	0.00	0.96
Vmc (p = 10%, q = 80%)	0.00	0.00	0.00	0.00	0.00	6.86
Vvc (p = 10%, q = 80%)	0.00	0.00	0.00	0.00	0.00	6.20
Vvv (p = 80%)	0.00	0.00	0.00	0.00	0.00	5.38
Spd (poda = 5%)	44.27	77.58	78.901	66.92	19.62	29.32
Spc (poda = 5%)	804.31	668.50	673.51	715.45	77.01	10.76
Sds	20116.06	20521.43	20507	#####	230.07	1.13
Ssc	177.91	170.29	176.01	174.74	3.97	2.27

6.4.2. Determination of COF

Fig. 6.5 shows the effect of geometrical parameter i.e; total height (H), delta height (ΔH), total width (w) and delta width (Δw) with friction factor based on the simulation results of this test. These parameters have been measured numerically to identify the most representative one to measure the friction coefficient by inverse simulation. Based on this figure, it has been found that total width is friction sensitive parameter for this test.

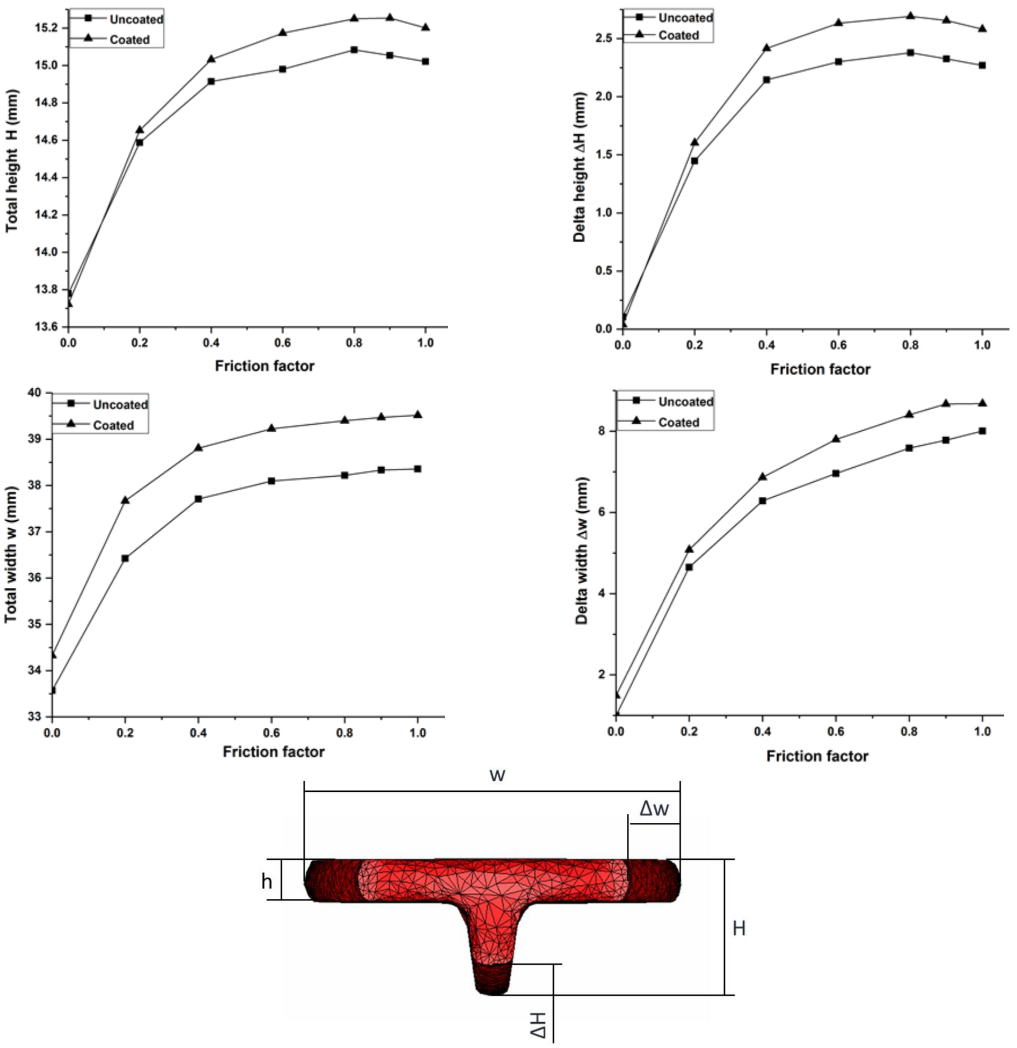

Fig. 6.5: Effect of geometrical parameters with friction factor

According to 3D simulation results, the two aspect which can be inspected from the finished workpiece to determine the friction behavior during the test were the total width (*w*) and flange height (*h*) which shown in Fig. 6.6.

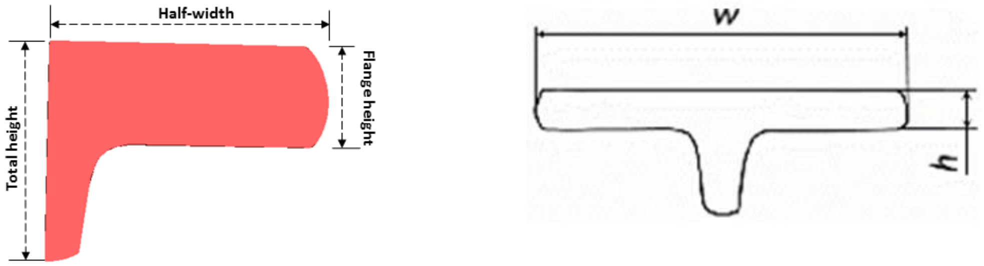

Fig. 6.6: Deformed T-Shape specimen; (left) view from simulation, (right) schematic view

Fig. 6.7 presents the measurement of the total width (*w*) evolution against flange height (*h*) for different friction factors obtained by numerical simulation and experimental results. The experiment used 9 workpieces to provide different flange heights with different width in order to produce a data scatter from which a conclusion can therefore be made. For the calculation of the T-Shape friction factor inverse modelling was also used. Based on the results plotted in Fig. 6.7, it can be observed that the glass coating clearly benefits the forging of the Ti-6Al-4V alloy since a lower COF value is achieved. The COF value for the 90 μm glass coated specimens is about 0.4 where the billets having 45 μm glass coating result in a friction factor of 0.6 meanwhile for the non-coated specimens the *m* = 0.8-1.0. It can also be observed that the thickness of the coating is really affecting the value of COF since the specimens coated with a 45 μm and 90 μm layers offers slightly different COF values.

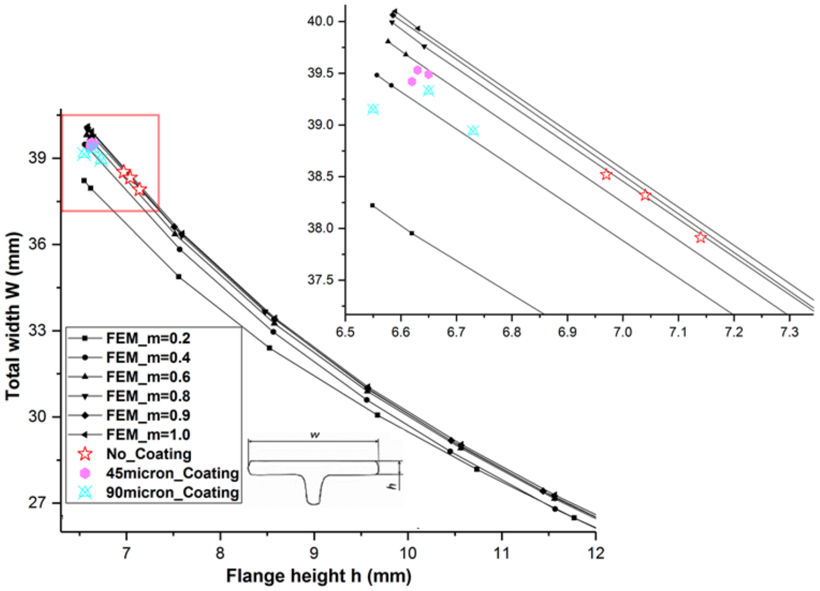

Fig. 6.7:: Calibration curves and experimental data of T-Shape tests

From the experimental results, it has been clearly observed that the contact pressure and specially the surface enlargement suffered by the material have a big influence on the friction factor. High contact pressure and larger surface enlargement resulted in higher friction among contact surfaces and therefore led to higher friction factors in this test. As the surface in contact with the tools are expanded, the coating effect is lost in the new contact areas that are created since the glass coating is brittle and is not following the materials surface enlargement. This effect would explain the increase of friction factor since the new fresh material is uncoated being the friction higher in these areas. Also, the reason of bigger friction factors of these tests as compared to the ring test was the complex deformation path in the T-shape test. The material had to flow through the punch and the die while in the ring test the material flowed freely without any limitation. On the other hand, the ring test is simpler to perform and it is a valid method to compare different coating solutions and make a scattering evaluation of them. In this case, it is clearly observed that coated rings avoid the friction factor to increase dramatically.

6.5. Conclusion

A comprehensive numerical and experimental study on the T-Shape friction test has been carried out. Based on the observations reported in this paper, the conclusions can be summarized as below:

- T-Shape has been proven to be a more sensitive test, regarding the coatings thickness influence. Ring test predicts same friction factor for both coating thicknesses (aprox. 0.35) while the T-Shape predicts a higher value for the low thickness coating (aprox. 0.6) in comparison to 0.4 obtained with the thicker coating).
- The COF obtained from calibration curves for uncoated specimens varies from 0.8 to 1.0 meanwhile, the COF is approximately 0.4 and 0.6 for 45 µm and 90 µm respectively in this test.
- It has been found that, the value of Sq, Sdq and Sdr was about 4.46 µm, 1.59 µm and 43.27 µm respectively for the tool of this test and for the specimen, the value of Sq, Sdq and Sdr was Sq value was approximately 1.17 µm, 0.27 µm and 3.25 µm respectively.
- It has been concluded that this test in comparison to ring test, is able to obtain high surface enlargement and thus makes differences when using different coating thickness.
- Upon comparing the surface qualities of this test with ring and HTC test, it was found that the surface qualities varies in all the tests. Comparison of the influences of different surface qualities has not being performed in this work. However, this can be analyzed in the future.

CHAPTER 7

ANALYSIS OF THE EFFECT OF GLASS COATING ON ALPHA-CASE FORMATION AND DEFECTS

"What we measure affects what we do."
-Joseph Stiglitz

7. ANALYSIS OF THE EFFECT OF GLASS COATING ON ALPHA-CASE FORMATION AND DEFECTS

7.1. Introduction

One of the major drawbacks of titanium alloys is their low oxidation resistance when they are exposed for long-term at elevated temperatures in an oxygen containing environments. In such conditions, titanium reacts readily with oxygen, thereby forming an oxide scale on the surface and a hard and brittle oxygen enriched layer beneath the scale, known as “alpha-case” [LUT07, DON00]. It is well known that, alpha-case significantly reduces the mechanical properties of titanium, such as ductility, fracture toughness and fatigue life. Titanium’s high strength to density ratio makes it ideal for aerospace, automotive, chemical and biomedical industry but formation of alpha-case compromises this strength. Even a small fracture in the alpha-case may cause a part to fail. Therefore, any alpha-case formed on titanium alloys during various manufacturing processes must be removed before the final part is mounted in an engine. Additionally, long time exposure at elevated temperatures during operation of an engine could possibly also lead to formation of alpha-case on actual parts, therefore knowledge and understanding of the alpha-case formation and its effect is important. However, no publications have been found where the coating layer brakeage and its influences in the metal flow of the material have been analyzed especially in the T-Shape friction test of Ti-6Al-4V hot forging.

The objective of this study was to understand, and to obtain, an accurate rate of alpha-case layer formation and to investigate coatings in an attempt to reduce alpha-case formation in a Ti-6Al-4V alloy forging at elevated temperatures. The forged Ti-6Al-4V alloy T-Shape specimens were selected for this study because of high pressure and high surface enlargement occurs in this test and since the glass coating is brittle, which can promote cracking much more than ring test specimen. An open crack was found in specimen since the alpha-casing also caused premature crack initiation in affected samples. Microstructural and microhardness analysis were performed to study the alpha-case layer and crack. Measurements of the depth of alpha-casing, as determined by optical microscopy, and Vickers hardness testing whereas optical microscopy was used to the find the crack and observe microstructure near the crack.

7.2. Methodology

The forged Ti-6Al-4V alloy T-Shape specimens (the specimens are the ones that have forged in chapter 6) were selected for experimentation and experimentation was performed under three types of surfaces: Ti-6Al-4V with no coating, 45 and 90 µm of glass coating. This initial material has a microstructure with equiaxed primary alpha grains and elongated alpha needles in transformed beta matrix (see Fig. 7.1).

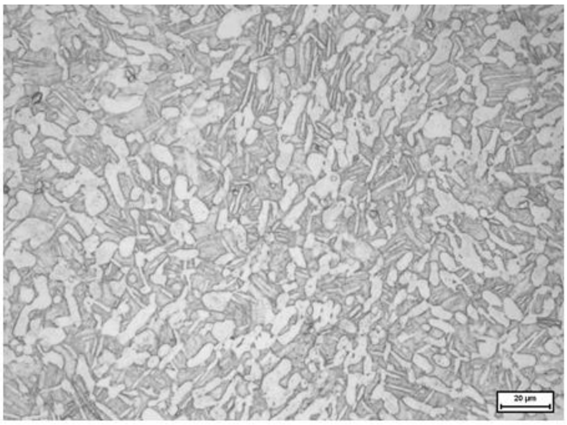

Fig. 7.1: Optical micrographs showing the microstructure of forged Ti-6Al-4V. In micrographs light or grey areas is a phase and dark areas is β

7.2.1. Sample preparation

Cutting samples of titanium alloy with alpha-case can be a lengthy task since the alpha-case is much harder than the titanium itself. Thus, after each sample had been forged, T-Shape specimens were sectioned (shown in Fig. 7.2) using 20A25 *Struers* cut-off wheel by using the manual cut off machine (Brand-Struers, Model-labotom 3) before being mounted. Each sample was cut in order to expose a cross section at which the depth of alpha-case and crack could be examined.

The cut pieces were mounted using phenolic resin by hot mounting press (Brand-Neurtek instruments, Model- OPAL 410), and then metallographically prepared, which involves grinding and polishing. Here, the samples were initially ground with 240, 360, 800, 1200 grit silicon carbide papers using water as lubricant for 10 minutes using Grinding and polishing machine (Brand- Buehler, Model-beta grinder polisher). The sample was rotated opposite the direction the polishing wheel was spinning to polish in more than one direction along the sample. After grinding, samples were polished using the diamond paste (3 µm) to get the adequate mirror quality surface. After the polishing, the samples were chemically etched using Kroll´s reagent (100 ml water, 1-3 ml hydrofluoric acid, 2-6 ml nitric acid) to reveal the hardness and microstructure (see Fig. 7.2). The acid was applied for 10-15 seconds and then rinsed in water to stop the etching from continuing. Optical observation and Vickers hardness test were performed for this study.

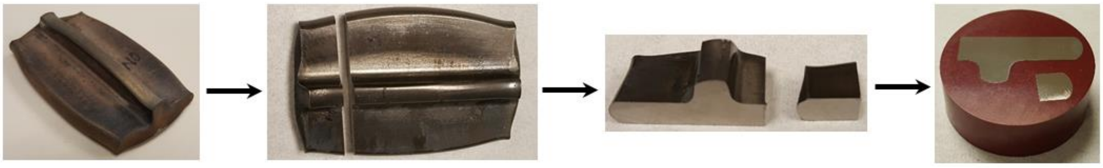

Fig. 7.2: Sample sectioning and mounting for metallographic analysis

7.3. Experimental techniques

7.3.1. Light Optical Microscopy (OM) Study

The depth of alpha-case layer was evidenced into each sample after the etching procedure using a Leica optical microscope at 50 and 1000x magnification. The alpha-case was easily recognizable as a brighter, white layer that occurred along the surface. It was necessary to analyse each side of the samples to determine alpha-case. Similarly, the crack was found using the optical micrographs of all samples (see Fig. 7.3).

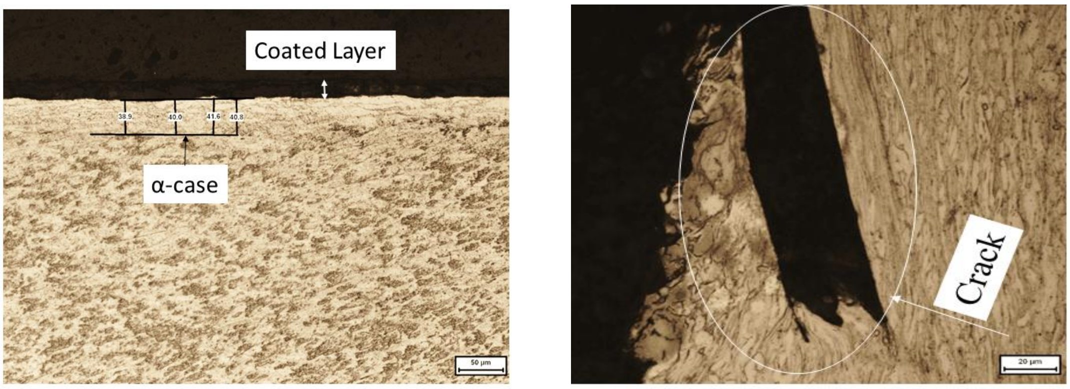

Fig. 7.3: Optical micrographs of (left) alpha-case layer (right) crack along entire periphery of cross- sectioned samples

7.3.2. Micro Hardness Evolution

The true depth of the alpha-case cannot be seen completely when taking images with the microscope. The oxygen diffuses further into the sample than is visible as described by the α+β phase [CHR10]. Thus, to obtain a more accurate measurement of the alpha-case and to estimate the error in the visual readings, microhardness testing was performed. Micro hardness profiles were obtained using the Zwick Vickers Microhardness Tester at 400x magnification, based on pressing a diamond indenter (square based pyramid with an angle of 136 ° into the work-piece under test with 200 g and loading time was 10 s). Samples were placed in the microscope, and measurements were made using the Vickers Microhardness scale. The first imprint was made on the edge with alpha-case of each sample and subsequent imprints were made toward the center of sample until the hardness readings were consistent is presented in Fig. 7.4.

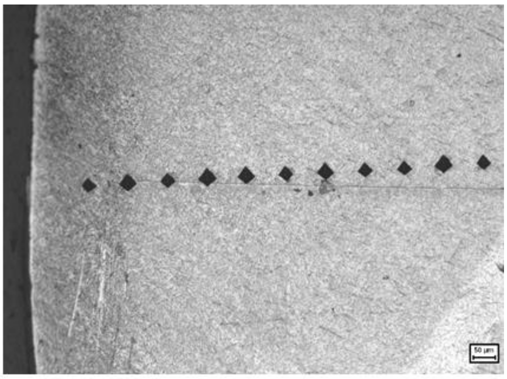

Fig. 7.4: Microhardness test marks at various places for Ti6Al4V T-Shape specimen

7.4. Results and discussion

7.4.1. Microstructure Observation

Fig. 7.5 shows the microstructures observed at the cross section of the Ti-6Al-4V alloy T-Shape specimen manufactured by forging process after etching. It can be found that, forged Ti-6Al-4V alloy T-Shape is formed with alpha-case layer and with surface defects.

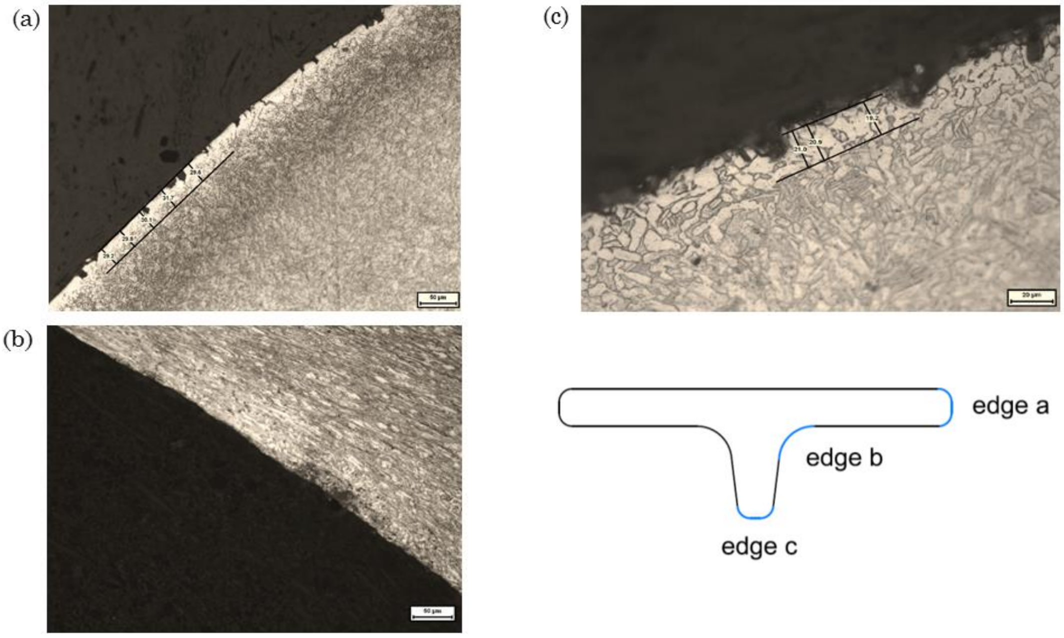

Fig. 7.5: Microstructures observed at different locations for Ti-6Al-4V T-Shape specimen

Observed microstructure indicatea an equiaxed structure composed of primary α grains and transformed β, where the transformed β consists of elongated α needles. It is obvious that the friction force changed the grain boundary pattern near the die surface. In the vicinity of the edge radius of V-groove section of the die, are located the more elongated grains (i.e; Fig.7.5b). However, the grains located far from the die surface were less influenced by friction (i.e; Fig.7.5a and Fig.7.5c). It seems that the edge of compression has high alpha-case; hence, alpha-case was studied on that part for all three-surface specimen.

7.4.2. Alpha-case investigation

7.4.2.1. Light Optical Microscopy (OM) analysis

Fig. 7.6 shows the optical micrographs of alpha-case in Ti-6Al-4V T-Shape specimen. Since, the alpha-case region was a lighter shade in contrast than the α+β region, it was able to be optically measured. That the alpha-case has a different phase structure than matrix region can be observed. The alpha-case can be noted by a smooth and homogeneous appearance whereas the α+β region has both regions of alpha and beta case dispersed within one another.

In order to obtain an average value of the alpha-case, separate readings were taken within the microscope view, and averaged to determine the alpha-case depth along the side (see Fig. 7.6). As expected, measurements performed in the optical microscope for the three different experimental conditions (shown in Table 7.1) revealed that the alpha-case thickness was larger for the uncoated samples. This is due to the different diffusivities of oxygen and different oxidation behaviours when using different coatings. It is observed that the maximum depth of alpha-case formed is approximately 29 μm for uncoated and for 45 and 90 μm coated is 17 and 15 μm respectively.

Table 7.1: Measurements performed on Ti-6Al-4V with different experimental conditions

Tests	Samples	Alpha scale in Maximum thickness
1	with lubricant, without coating	29 μm
2	with lubricant, with 45 μm CONDAERO 228 coating	17 μm
3	with lubricant, with 90 μm CONDAERO 228coating	15 μm

7.4.2.2. Micro Hardness analysis

In addition to microscopy, microhardness profiles were carried out to determine the actual depth of the alpha layer diffused into the titanium. Since the alpha-case surface is much harder than the titanium itself, it is necessary to determine the depth at which the surface hardness stabilizes. Figure. 7.7 shows the microhardness profiles of Ti-6Al-4V T-Shape specimen from the surface to the bulk for three different surfaces. It was found that the highest microhardness values were observed at the alpha-case layers in the sample surface and gradually decreasing until reaching the bulk hardness of the alloy. The decrease in hardness was therefore due to the interstitial diffusion of oxygen in the titanium metal matrix. The mean hardness of Ti-6Al-4V titanium was approximately 300-350 HV0.2 depending on the grain orientation and phase present at the microhardness test location. The micro-hardness testing shows an alpha-case region all the way to 150 µm for the uncoated specimen and 140 µm for 45 µm coated specimen and 120 µm for 90 µm coated specimen.

By using the estimated hardness values where microhardness testing stabilizes of this alloy, the real depth of the oxygen-affected zone was calculated. The difference in depth of alpha-case measured in optical microscope, indicated by the plateau in the hardness measurements, suggests that there are uncertainties in identifying the border between the alpha-case layer and the bulk material in optical microscope after etching.

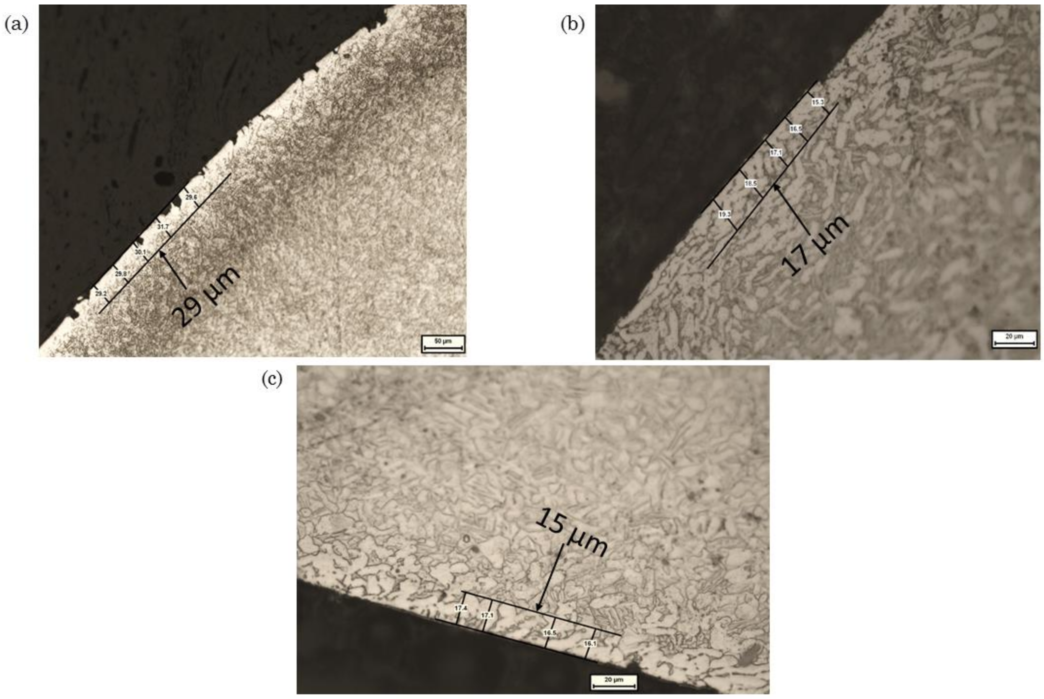

Fig. 7.6: Typical Optical micrographs of alpha-case measurements of Ti-6Al-4V T-Shape specimen (a) without coating, x200 (b) 45 µm coating, x500 (c) 90 µm coating, x500

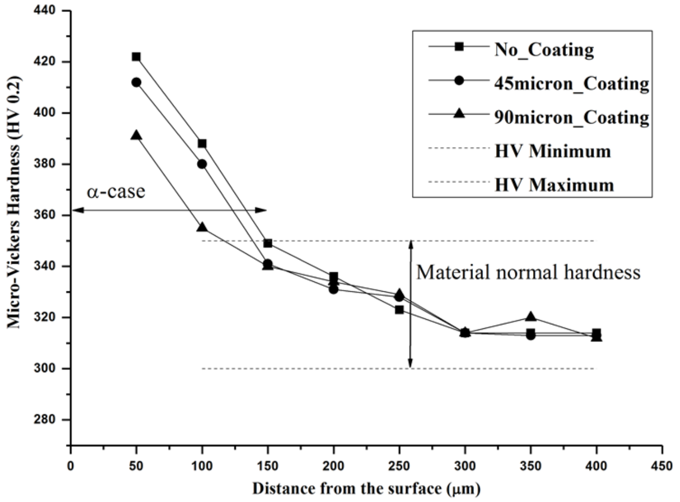

Fig. 7.7: Micro hardness profile for Ti-6Al-4V T-Shape specimen

7.4.3. Cracks or defect analysis

Fig. 7.8 and Fig. 7.9 show an optical photograph of the crack area. It can be seen, that the microstructures of these areas strongly difference from the matrix (Fig. 7.1). In Fig. 7.8a and Fig. 7.9a, more α-phase existed with different appearances. On the both sides of the crack, α-phase was basically twisted in incompletely deformed rough banding. The nearer to the crack, the rougher the α-phase was.

On the left side of the crack, there was an obvious transition zone from the edge of the crack to the matrix, where the shape changed from big blocky to elongated banding (shown in Fig. 7.8b, 7.9b). However, the matrix was composed of highly deformed uniform equiaxed structure and transformed β. No cracks were found on the 90 µm coating samples. It has been observed that the maximum depth of crack formed is approximately 262 µm for uncoated and for 45 µm coated is 160 µm (shown in Fig. 7.8a, 7.9a). Many small cracks also were observed as shown in Fig 7.8 c and 7.9 c. It can be seen that, the alpha-case is completely fractured at very early stages of deformation due to its brittle nature.

In view of these results, it can be concluded that the crack propagation started from the alpha-case zone toward the inside of the bulk sample and crack depth was more severe in uncoated specimen as compared to the 45 µm coated specimen.

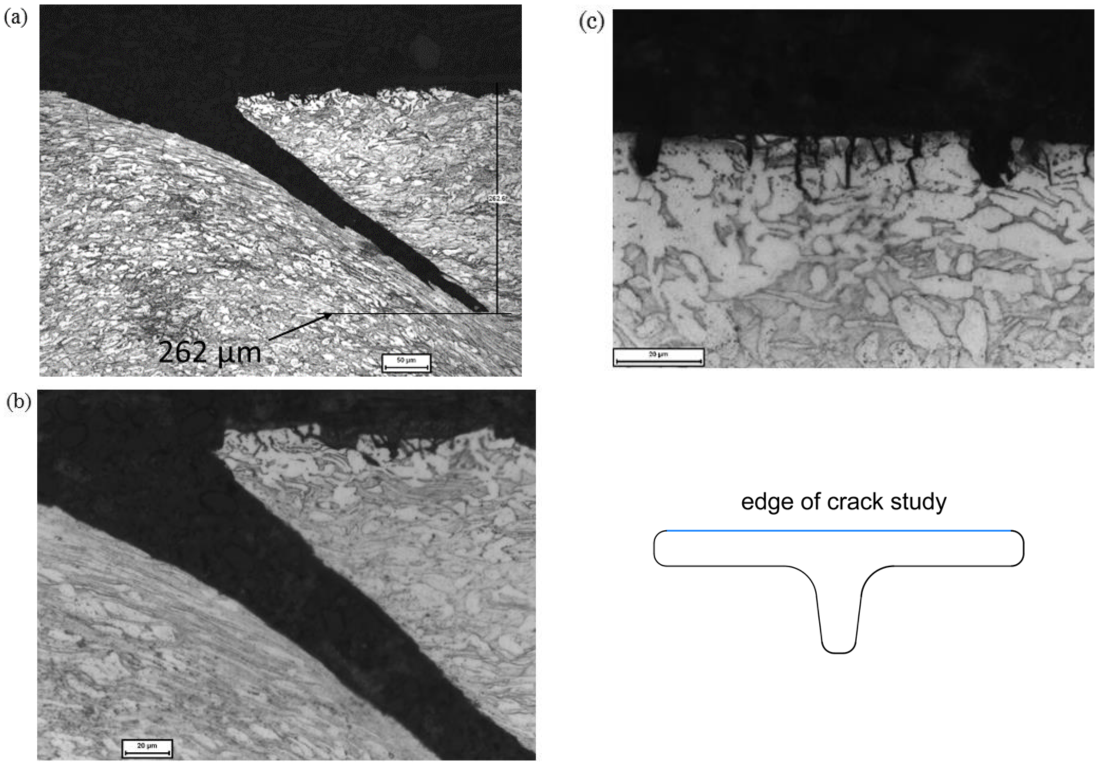

Fig. 7.8: Optical photographs of the crack area of uncoated T-Shape specimen

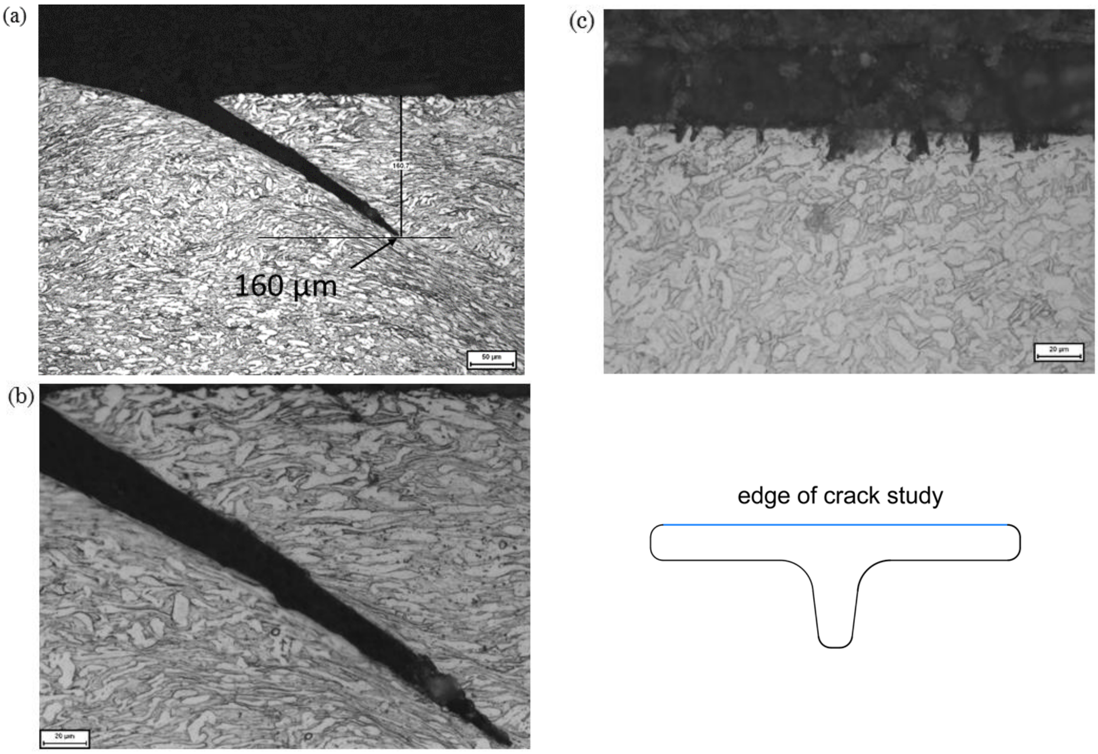

Fig. 7.9: Optical photographs of the crack area of 45 µm coated T-Shape specimen

7.5. Conclusion

In the present work, forged Ti-6Al-4V alloy T-Shape specimens were investigated in order to study the alpha-case formation and crack defects. The obtained conclusions can be summarized as:

- Alpha thickness is thicker in uncoated specimen than the coated specimen due to different diffusivities of oxygen resulting in different oxidation behavior.
- Alpha-case measurements for uncoated is 29 µm and for 45 and 90 µm coated are 17 and 15 µm respectively in optical microscope whereas micro-hardness testing shows an alpha-case region all the way to 150 µm for uncoated specimen and 140, 120 µm for 45 and 90 µm coated specimen.
- The hardness values in the alpha-case are higher in magnitude than in the bulk.
- There was an obvious transition zone from the edge of the crack to the matrix on one side of the crack, where the shape and size of the microstructure changed from big block to elongated wattle.
- Crack depth was more in uncoated specimen as compared to the 45 µm coated.

CHAPTER 8

FINAL CONCLUSIONS AND FUTURE WORK

"Determine that the thing can and shall be done,
and then we shall find the way."
-Abraham Lincoln

8. FINAL CONCLUSIONS AND FUTURE WORK

8.1. Conclusions

The main goal of present dissertation has been to study the effects of glass coating on Ti-6Al-4V hot forging. Three types of surfaces have been analyzed for this study which are, Ti–6Al–4V specimens with no coating and two others with different layer thickness of glass coating. For that, this work has been analysed by the contact condition between Ti-6Al-4V specimens and heated tool steel with the purpose of calculating the heat transfer coefficient (HTC) and coefficient of friction (COF) at the interface of the specimens and the tools. Finally, the alpha-case formation and cracks during hot forging was investigated by microstructural analysis. In order to meet this main goal, the study comprise the following specific objectives:

I. The ring and T-Shape test of Ti-6Al-4V alloy has been numerically analyzed using three-dimensional (3D) finite element modelling (FEM) simulation in order to identify important influencing parameters considering different variables, which affects the frictional behaviour, force and deformed specimen geometry in the Ti-6Al-4V hot forging process.

II. Columnar upsetting thermal tests have been conducted at two contact pressures to characterize HTC precisely that best fits in the contact between the Ti-6Al-4V specimens and the steel tools in forging process. The validation of final coefficients has been determined by the inverse algorithm has made by comparison between the upsetting process and the FE analysis results.

III. Ring and T-Shape tests have been conducted to estimate the friction factor taking into account the influence of the HTC in both tests. Numerical simulations of both Ring and T-Shape tests have been carried out for various values of friction factor using the found HTC value. Later, all the simulation results have been compared with experimental results to estimate the accurate friction factor by inverse modelling.

IV. Finally, all the 3-surface specimen after forging, have been looked at the effects of exposure to the atmosphere at elevated temperatures to study the alpha-case and the defects.

The main conclusions concerning objective (I), dealt with in Chapter 3, are:

Analysis of ring test

- It has been found from this analysis that HTC, and press velocity are the most influencing factors affecting the final geometry of specimen and friction factor.
- Although the ring compression test is a well-known and simple test to perform, new guidelines are needed to standardize the test. Press rotation velocity should be measured precisely during the compression tests and the use of heat transfer coefficients in function of the contact pressure may be useful to numerically simulate the test and obtain representative calibration curves.

Analysis of T-Shape test

- It has been found that the HTC influences very small on force with very short forging time and the friction factor has the big influence.
- The influence of material on force measurement is very high.
- Inaccuracies in the material characterization could lead to inaccuracies in the COF calculation.
- It has been concluded the geometrical shape of specimen was a good way to simplify the methodology.

Analysis of Tribology condition for both test

- It has been found from the analysis that the surface enlargement of the T-Shape test at about 35% whereas for the ring test the value at about 5%.
- The contact pressure of T-Shape test is quite high and reaches values up to approximately 515 MPa whereas, the contact pressure of ring test is quite low and the value reaches up to 200 MPa.
- It has been concluded that, T-shape compression test is suitable to evaluate the friction condition because this test induces a complex deformation path, large contact pressure and rather large surface expansion similar to what is occurred during a real forming operation.

The main conclusions concerning objective (II), dealt with in Chapter 4, are:

- The columnar test together with a closed loop force control has been proven to be an accurate method to predict HTC values.

- A minimum HTC value of 1 kW/m^{2}K was measured at low contact pressure for all surfaces and for higher contact pressure of 65 MPa, the HTC value is 3 kW/m^{2}K for all surfaces.

- The coating thickness does not seem to affect the HTC value for both contact pressures, since at low contact pressure the HTC value does only change slightly. Similarly, for high contact pressure both 40 µm and 80 µm coated specimens resulted in the same HTC value of 3 kW/m2K.

- The contact pressure clearly influences the heat transfer from the specimen through the dies and HTC value increases with the contact pressure.

The main conclusions concerning objective (III), dealt with in Chapter 5, are:

- The COF obtained from calibration curves for non-coated specimens varies from 0.8 to 1 meanwhile the COF is approximately 0.3 for 40 µm and 80 µm coated specimens. Therefore, the glass coating clearly improves the forgeability of titanium alloys reducing the COF value.
- The coating thickness does not seem to affect the COF since both 40 µm and 80 µm coated specimens resulted in the same friction value.

The main conclusions concerning objective (III), dealt with in Chapter 6, are:

- It is observed that T-Shape is a more sensitive test for testing glass coatings and could represent the real industrial applications more precisely.
- Comparing the results obtained from the experimental with the simulations calibration curves were found that the best m varies between 0.8-1 for uncoated samples and m is 0.4 and 0.6 for 45 µm and 90 µm respectively in this test.
- It has been concluded that this test in comparison to ring test, is able to obtain high surface enlargement and thus makes differences when using different coating thickness.
- Upon comparing the surface qualities of this test with ring and HTC test, it was found that the surface qualities varies in all the tests. Comparison of the influences of different surface qualities has not being performed in this work. However, this can be analyzed in the future.

The main conclusions concerning objective (IV), dealt with in Chapter 7, are:

- Alpha thickness is thicker in uncoated specimen than the coated specimen due to different diffusivities of oxygen resulting in different oxidation behavior.
- Alpha-case measurements for uncoated is 29 μm and for 45 and 90 μm coated are 17 and 15 μm respectively in optical microscope whereas micro-hardness testing shows an alpha-case region all the way to 150 μm for uncoated specimen and 140, 120 μm for 45 and 90 μm coated specimen.
- The hardness values in the alpha-case are higher in magnitude than in the bulk.
- Crack depth was more in uncoated specimen as compared to the 45 μm coated.

8.2. Future work

The following future studies can be suggested:

- This work can be applied for other metal forming process like warm forging or cold forging to obtain new values of coefficients.

- Simulations could also be conducted by using different simulation software packages to compare the results.

- To experimental, theoretical and analytical determination of friction factor by employing the ring and T-Shape compression test under different lubricants.

- Water based graphite is most widely used lubricant in the hot forging process which is applied to dies by spraying millions of atomized lubricant droplets through nozzles. The mode of spray not only influences lubricant wetting on the die, but also determines the thermal effects on the die surface. Since the number of available lubricant systems and spraying method rises along with new ecological demands, a qualified selection and optimization process becomes vital.

- The friction is dependent on the surface roughness. The surface roughness of the tools influences the friction conditions in forging. With a high surface roughness, there is high friction present, because of the need to lift one surface over the asperities on the other. However, for very smooth surfaces the real area of contact increases and so does the friction. Using tool surface topography as a variable, someone can study friction influencing in the forging process.

- The ring compression study can be extended for forgings with different geometries.

- Study and analysis the effect of load condition applied to the specimen under described friction test and effect of loading in interface friction.

- Experimenting with different coatings to completely prevent alpha-case formation.

- In hot forging processes, die life has an important role on the productivity and the quality of the finished products and the factors that affecting die life are thermal fatigue, plastic deformation and wear. Among these, wear is the main failure cause in hot forging dies. According to an investigation, more than 70% of tool replacements are due to premature die wear [CSE93]. Therefore, the die wear is the dominating tool failure factor for the forging tool replacement. Under high process temperature conditions, work piece and tool material may stick together causing adhesive wear. Additionally, the oxidation of the work piece surface creates hard particles like scale which cause extensive abrasive wear. As a consequence, these conditions lead to reduced tool life. So, Prediction of the die wear is an essential task during the hot forming process, since the wear process depends on many parameters that make it so complicated for investigation.

- Tool steels which are readily workable in the soft state possess favourable mechanical properties such as relatively high hardness and toughness after hardening and so are suitable for the manufacture of hot forging dies. However, there is a need to improve the performance of these tools, and this can be achieved by the use of coatings or surface treatments by reducing wear and friction by adding hardness to the surface or decreasing interaction forces [HEI12]. Die surface treatments such as nitriding, weld overlays and chemical and physical vapor deposition of heat resistant ceramic materials have been observed to substantially increase the life of the hot work dies. Coatings have not been so commonly used in forging yet because the complexity and size of these tools make it complicated and expensive to apply coatings. This disadvantage has considered a serious enough to further consideration.

Bibliography

[ALT83] T. Altan, S. Oh, H. L. Gegel, “Metal forming: Fundamentals and Applications” *American Society for Metal*, 1983.

[ALT97] T. Altan and V. Vasquez, “Status of process simulation using 2D and 3D finite element method ‘What is practical today? What can we expect in the future?”, *Journal of Materials Processing Technology*, vol. 71, page.49-63, 1997.

[ALT05] T. Altan, G. Ngaile, G. Shen, “Cold & Hot Forging: Fundamentals and Applications”, *ASM International*, 2005.

[AER07] Aerospace Series-Test Methods-Titanium and titanium alloys-Part 009-Determination of surface contamination (SS–EN 2003–009:2007), *Swedish Standards Institute*, 2007.

[ASM90] ASM handbook, *ASM International*, Materials Park, Ohio, 1990.

[AVI64] B. Avitzur, “Forging of Hollow discs”, *Israel J. Technol.*, vol. 2, page.295-304, 1964.

[BAR02] P. F. Bariani, G. Berti, T. Dal Negro, and S. Masiero, “Experimental evaluation and FE simulation of thermal conditions at tool surface during cooling and deformation phases in hot forging operations”, *CIRP Annals-Manufacturing Technology*, vol. 51, page.219-222, 2002.

[BAI12] Q. Bai, J. Lin, L. Zhan, T. A. Dean, D. S. Balint and Z. Zhang, “An efficient closed-form method for determining interfacial heat transfer coefficient in metal forming”, *International Journal of Machine Tools and Manufacture*, vol. 56, page.102-110, 2012.

[BAL02] V. V. Balasubrahmanyam and Y. V. R. K. Prasad, “Deformation behavior of beta titanium alloy Ti-10V-4.5Fe-1.5Al in hot upset forging”, *Materials Science & Engineering: A*, vol. 336, page.150-158, 2002.

[BEA06] J. D. Beal, R. Boyer and D. Sanders, “Metalworking: Sheet Forming”, *ASM Handbook*, The Boeing Company, Vol.14B, page.656-669, 2006.

[BEC58] G. Beck, “Thermal conditions in tool steels in hot upsetting and forging between dies”, *Stahl and Eisen*, vol. 78, page.1556-1563, 1958.

[BIE05] T. R. Bieler, R. M. Trevino, L. Zeng, B. Franco, L. L. Gerald and W. Peter, "Alloys: Titanium", *Encyclopedia of Condensed Matter Physics*, Elsevier, Oxford, page.65-76, 2005.

[BON15] B. Barooghi Bonab, M. H. Sadeghi, H. Halimi Khosrowshahi and A. Amiri, "A Study on Hot Working and Frictional Behaviour of 6082 Aluminium Alloy during Hot Forming Using Pressure Tests and Finite Element Simulation", *Transactions of FAMENA*, vol. 39, page.43-52, 2015.

[BOY92] H. E. Boyer and T. Gall, "Metals Handbook: Desk Edition", *ASM*, 1992.

[BOY94] R. Boyer, G. Welsch and E. W. Collings, "Materials Properties Handbook: Titanium Alloys", *Metals Park, OH,* ASM, 1994.

[BRU04] S. Bruschi, S. Poggio, F. Quadrini and M. E. Tata, "Workability of Ti-6Al-4V alloy at high temperatures and strain rates", *Materials Letters*, vol. 58, page.3622-3629, 2004.

[BUR90] P. R. Burte, Y. T. Im, T. Altan and S. L. Semiatin, "Measurement and analysis of heat transfer and friction during hot forging", *Trans. ASME, J. Engg. for Industry*, vol. 112, page. 332-339, 1990.

[BUS92] A. Buschhausen, J. Y. Lee, K. Weinmann and T. Altan, "Evaluation of lubrication and friction in cold forging using a double backward extrusion process", *J. Mater. Process. Technol.*, vol. 33, page.95–108, 1992.

[COC96] B. Cockeram and R. A. Rapp, "Isothermal and cyclic oxidation resistance of boron-modified and germanium-doped silicide coatings for titanium alloys", *Oxidation of Metals*, vol. 45, page. 427-467, 1996.

[CHR10] J. Chretien, "Titanium Alpha Case Prevention", Diss. Worcester polytechnic institute, 2010.

[CHA02] C. C. Chang and A. N. Bramley, "Determination of the heat transfer coefficient at the workpiece-die interface for the forging process", *Proceedings of the Institution of Mechanical Engineers, Part B: Journal of Engineering Manufacture*, vol. 216, page.1179-1186, 2002.

[CHO15] T. Choda, H. Oyama, and S. Murakami, “Technologies for Process Design of Titanium Alloy Forging for Aircraft Parts”, KOBELCO TECHNOLOGY REVIEW, vol. 33, page. 44-49, 2015.

[CSE93] L. Cser, M. Geiger, K. Lange, “Tool life and tool quality in bulk metal forming” Proc. Inst. Mech. Eng., vol. 39, page.207-223, 1993.

[DAE92] M. A. Daeubler and D. Helm, “Surfaces and Elevated Temperature Effects. in Titanium´92, Science and Technology” *The Minerals, Metals and Materials Society*, USA, 1992.

[DEA04] P. A. Dearnley, K. L. Dahm and H. Çimenoglu, “The corrosion-wear behaviour of thermally oxidised CP-Ti and Ti-6Al-4V”, *Wear*, vol. 256, page.469-479, 2004.

[DIE88] G. E. Dieter, “Mechanical Metallurgy”, *Mc Graw Hill*, SI Metric ed., 1988.

[DON00] M. J. Donachie, “Titanium: A Technical Guide, 2nd ed. Edn”*, ASM International,* Materials Park, OH, 2000.

[DOB09] R. G. Dobeson, “Alpha case formation and prevention in titanium alloys” 2009.

[DOB11] R. Dobeson, N. Petrazoller, M. Dargusch, and S. McDonald, “Effect of thermal exposure on the room temperature tensile properties of Grade 2 titanium”, Materials Science and Engineering: A, vol. 528, page.3925-3929, 2011.

[DU94] H. L. Du, P. K. Datta, D. B. Lewis and J.S. Burnel-Gray, “Air oxidation behaviour of Ti-6Al-4V alloy between 650 and 850 °C”, *Corrosion Science*, vol. 63, 631-642, page.1994.

[DU96] H. L. Du, P. K. Datta, D. B. Lewis and J. S. Burnel–Gray, “High temperature corrosion of Ti and Ti–6Al–4V alloy”, *Oxidation of Metals*, vol. 45, page.507–527, 1996.

[DUT99] R. Dutton, V. Seetharaman, R. Goetz and S. Semiatin, “Effect of flow softening on ring test calibration curves,” *Mater. Sci. Eng. A*, vol. 270, page. 249–253, 1999.

[FRA94] S. Frangini and A. Mignone, “Various aspects of the air oxidation behaviour of Ti6Al4V alloy at temperatures in the range 600–700 °C”, *Journal of Materials Science*, vol. 29, page.714–720, 1994.

[FUJ80] S. Fujishiro and D. Eylon, “Improved mechanical properties of α+β Ti alloys by Pt ion plating”, *in Titanium*, 1980.

[FUJ80] S. Fujishiro and D. Eylon, “Improvement of Ti alloy fatigue properties by Pt ion plating”, *Metallurgical Transactions A*, Vol. 11: page.1259-1263, 1980.

[FER11] F. Fereshteh-Saniee, H. Badnava and S.M. Pezeshki-Najafabadi, “Application of T-shape friction test for AZ31 and AZ80 magnesium alloys at elevated temperatures”, Materials and Design., vol. 32 page.3221–3230, 2011.

[FED80] E. Felder and J. L. Montagu, “Friction and wear during the hot forging of steels”, *Tribology International*, vol. 13, page.61-68, 1980.

[GAD13] R. Gaddam, B. Sefer, R. Pederson and M. L. Antti, “Study of alpha-case depth in Ti-6Al-2Sn-4Zr-2Mo and Ti-6Al-4V” *Materials Science and Engineering*, IOP Publishing, Vol. 48, page. 012002, 2013.

[GEI76] R. Geiger, “Metal flow in combined can extrusion”, *Verlag Giradet*, Essen, Germany, 1976.

[GHA15] E. Ghassemali, X. Song, M. Zarinejad, A. Danno and M. J. Tan, “Bulk Metal Forming Processes in Manufacturing”, *Handbook of Manufacturing Engineering and Technology*, page.171-230, 2015.

[GUR01] I. Gurrappa and A. K. Gogia, “Development of oxidation resistant coatings for titanium alloys”, *Materials Science and Technology*, vol. 17, page.581–587, 2001.

[GUR03] I. Gurappa, “Prediction of titanium alloy component life by developing an oxidation model”, Journal of Materials Science Letters, vol. 22, page.771-774, 2003.

[GUL09] H. Guleryuz and H. Cimenoglu, “Oxidation of Ti–6Al–4V alloy”, *Journal of Alloys and Compounds*, vol. 472, page.241-246, 2009.

[GRO13] P. Groche, C. Müller, J. Stahlmann and S. Zang, “Mechanical conditions in bulk metal forming tribometers-Part one”, *Tribology International*, vol. 62, page.223-231, 2013.

[HEI12] J. Heinrichs, “On Transfer of Work Material to Tools”, *Uppsala University*, 2012.

[HU98] Z. M. Hu, J. W. Brooks and T. A. Dean, “The interfacial heat transfer coefficient in hot die forging of titanium alloy”, *Proc. Instn Mech. Engg. Part C, Journal of Mechanical Science*, vol. 212, page.485-496, 1998.

[IMA96] M. A. Imam, and A. C. Fraker, “Titanium alloys as implant materials”, *Medical applications of titanium and its alloys: The material and biological issues*. ASTM International, 1996.

[IM03] Y. T. Im, S. H. Kang, J. S. Cheon, “Finite element investigation of friction condition in a backward extrusion of aluminum alloy” *J. Manuf Sci Eng.*, vol. 125, page.378-383, 2003.

[IMM97] Institute of Metals and Materials Australasia, IMMA handbook of engineering materials, 5th ed., Institute of Metals and Materials Australasia, Parkville, Vic, 1997.

[ISO92] S. Isogawa, A. Kimura and Y. Tozawa, “Proposal of an evaluating method on lubrication”, *CIRP Annals – Manufacturing Technology*, vol. 41, page.263–266, 1992.

[JAM03] C. W. James and G. Lutjering, “Titanium”, *Springer–Verlag*, 2003.

[JAI67] S. C. Jain and A. N. Bramley, “Speed and frictional effects in hot forging”, Proceedings of the Institution of Mechanical Engineers, vol. 182, page.783-798, 1967.

[JAI90] V. Jain, “Determination of heat transfer coefficient for forging applications”, J. Mater. Shaping Technol, vol. 8, page.193-202, 1990.

[JOS52] W. Jost “Diffusion in Solids, Liquids, Gases”, *Ed. Academic Press*, New York, 1952.

[JOU09] M. S. Joun, H. G. Moon, I. S. Choi, M. C. Lee, B. Y. Jun, “Effects of friction laws on metal forming processes”, *Tribol Int.*, vol. 42, page.311-319, 2009.

[JEO01] D.J. Jeong, D. J. Kim, J. H. Kim, B. M. Kim, T. A. Dean, “Effects of surface treatments and lubricants for warm forging die life”, *Journal of Materials Processing Technology*, vol. 113, page.544-550, 2001.

[KAR95] K. F. Karhausen, “Integrierte Prozeß-und Gefügesimulation bei der Warmumformung” Stahleisen, 1995.

[KEA07] R. G. Keanini, G. K. Watkins, T. Okabe and M. Koike, “Theoretical study of alpha case formation during titanium casting”, *Metallurgical and Materials Transactions B*, vol.38, page.729-732, 2007.

[KEL69] M. A. Kellow, A. N. Bramley, and F. K. Bannister, “The Measurement of Temperatures in Forging Dies”, *Inter.* J. *Mach. Tool Des. Res.,* vol. 9, page. 239-260, 1969.

[KOF58] P. Kofstad, K. Hauffe and H, Kjöllesdal, “Investigation on the oxidation mechanism of titanium”, *Acta Chemica Scandinavica*, vol. 12, page.239-266, 1958.

[KOF66] P. Kofstad, “High Temperature Oxidation of Metals”, *Wiley*, New York, 1966.

[KOB89] S. Kobayashi and T. Altan, “Metal Forming and the Finite Element Method”, *Oxford University Press*, New York, chap. 1-9, 1989.

[KOF88] P. Kofstad, “High Temperature Corrosion”, *Elsevier Applied Science Publishers,* Crown House, Linton Road, Barking, Essex IG 11 8 JU, UK, 1988.

[KUN56] M. Kunogi, “A new method of cold extrusion”, *J. Sci. Res. Inst*, vol. 50, page. 215–246, 1956.

[KUB98] K. Kubiak, and J. Sieniawski, “Development of the microstructure and fatigue strength of two phase titanium alloys in the process of forging and heat treatment”, *Journal of Materials Processing Technology*, vol. 78, page.117-121. 1998.

[LAZ98] L. Lazzarotto, A. Dubois, L. Dubar, A. Verleene and J. Oudin, "Testing of a zinc phosphate stearate coating according to true conditions of contact in wire drawing. *Surf. Eng.*, vol. 14, page.335–338, 1998.

[LEY00] C. Leyens, M. Peters and A. Kaysser, "Oxidation-Resistant Coatings for Application on High-Temperature Titanium Alloys", *Aeroengines. Advanced Engineering Materials,* vol. 2, page. 265-269, 2000.

[LEY02] C. Leyens, M. Peters, P. E. Hovsepian, D. B. Lewis, Q. Luo and W. D. Münz, "Advanced nitride coatings for oxidation protection of titanium alloys" *Materials for Advanced Power Engineering*, 2002.

[LEY03] C. Leynes and M. Peters, "Titanium and Titanium alloys: Fundamentals and Applications", *Wiley-VCH*, 2003.

[LIN95] S. Y. Lin, "An investigation of die-workpiece interface friction during the upsetting process", *J Mater Process Technol*, vol.54, page.239-248, 1995.

[LI01] L. X. Li, D. S. Peng, J. A. Liu and Z. Q. Liu, "An experiment study of the lubrication behavior of graphite in hot compression tests of Ti–6Al–4V alloy", *J Mater Process Tech*, vol. 112, page.1-5, 2001.

[LUT07] G. Lutjering, J. Williams, Engineering material and process: Titanium, *Springer*, second edition, 2007.

[LUO86] Z. J. Luo, H. Z. Guo "Determining rules of specimen size when ring-compression method was used for testing the friction coefficient" Equip Environ Eng., vol. 1, page.13-17, 1986.

[MAJ02] A. Majorell, S. Srivatsa and R.C., Picu, "Mechanical behavior of Ti-6Al-4V at high and moderate temperatures-Pat I: Experimental results", *Materials Science & Engineering: A*, vol. 326, page.297-305, 2002.

[MAN11] T. B. Mang, K. Bobzin, T. Bartels, "Industrial tribology; tribosystems, friction, wear and surface engineering, lubrication", Wiley-VCH, Weinheim, 2011.

[MAL64] A. T. Male, M. G. Cockcroft, "A method for the determination of the coefficient of friction of metals under condition of bulk plastic deformation", *J. Inst. Met*, vol. 93, page.38-46, 1964.

[MAL94] Z. Malinowski, J. G. Lenard and M. E. Davies, “A study of the heat-transfer coefficient as a function of temperature and pressure”. *J. Mater. Processing Technol.*, vol. 41, page. 125-142, 1994.

[MAO09] Y. Mao, “Forging process design for risk reduction”, *Doctoral dissertation*, The Ohio State University, 2009.

[MEN09] P. L. Menezes, K. K. Kishore and S. V. Kailas, “Influence of friction during forming process-a study using a numerical simulation technique”, *Int. J Adv. Manuf. Tech.*, vol. 40, page.1067-1076, 2009.

[MEN16] J. Mendiguren, R. Ortubay, E. S. de Argandoña, and L. Galdos, “Experimental characterization of the heat transfer coefficient under different close loop controlled pressures and die temperatures”, *Applied Thermal Engineering*, vol. 99, page.813-824, 2016.

[MOD05] Moderncasting.com, Available at, http://www.moderncasting.com/MoreInfo/1104/MoreInfo1104.pdf, 2005.

[NIE01] L. Niewolak, V. Shemet, A. Gil, L. Singheiser and W. J. Quadakkers, “Alumina-forming coatings for titanium and titanium aluminides”, *Advanced Engineering Materials*, vol. 3, p. 496-500, 2001.

[NSH94] W. Nshama, J. Jeswiet and P. H. Oosthuizen, “Evaluation of temperature and heat transfer conditions at the metal forming interface”, *J. Mater. Processing Technol.*, vol. 45, page.637-742, 1994.

[OKA11] H. Okamoto, “O–Ti (Oxygen–Titanium)”, *Journal of Phase Equilibria and Diffusion*, vol. 32, page.473–474, 2011.

[OBE09] B. Oberwinkler, M. Riedler and W. Eichlseder, “Light weight design of Ti-6Al-4V forgings”, 25th Annual Conf. Proc., International Titanium Association, 2009.

[OH82] S. I. Oh, “Finite element analysis of metal forming processes with arbitrarily shaped dies”, *International Journal of Mechanical Sciences*, vol. 24, page.479-493, 1982.

[PAT01] S. N. Patankar, Y. T. Kwang, and T. M. Jen, “Alpha casing and superplasitic behavior of Ti-6-4”, *Journal of Materials Processing Technology*, vol. 24, page. 112, 2001.

[PED01] R. Pederson, O. Babushkin, F. Skystedt, R. Warren, “The use of high temperature X-ray diffractometry to study phase transitions in Ti-6Al-4V”, *Titanium alloys at elevated temperature: structural development and service behaviour*, Institute of Materials, page.1533-1538, 2001.

[PEZ11] S. M. Pezeshki, H. Badnava, and F. Fereshteh-Saniee, “Frictional Condition Evaluation in Hot Magnesium Forming Using T-Shape and Ring Compression Tests”, 2011.

[PIT04] F. Pitt and M. Ramulu, “Influence of grain size and microstructure on oxidation rates in titanium alloy Ti–6Al–4V under superplastic forming conditions”, *Journal of Materials Engineering and performance*, vol. 13, page.727-734, 2004.

[POQ13] D. Poquillon, C. Armand and J. Huez, “Oxidation and oxygen diffusion in Ti–6Al–4V alloy: Improving measurements during Sims analysis by rotating the sample”, *Oxidation of metals*, vol. 79, page.249-259, 2013.

[PRA98] Y. V. R. K. Prasad, T. Seshacharyulu, “Processing maps for hot working of titanium alloys”, *Materials Science & Engineering: A*, vol. 243, page.82-88, 1998.

[RAO93] K. P. Rao, K. Sivaram, “A review of ring-compression testing and applicability of the calibration curve”, *J. Mater. Process. Tech.*, Vol. 37, page. 295-318, 1993.

[RMI00] RMI Titanium Company, “Titanium Alloy Guide”, *An RTI International Metals*, 2000.

[ROB04] T. Robinson, H. Ou and C.G. Armstrong, “Study on Ring Compression Test Using Physical Modelling and FE Simulation”, *Journal of Materials Processing Technology*, vol.154, page.54-59, 2004.

[RUD96] N. T. Rudkins, P. Hartley, I. Pillinger and D. Petty, “Friction modelling and experimental observations in hot ring compression tests”, *Journal of Materials Processing Technology*, vol. 60, page.349-353, 1996.

[SAD90] M. H. Sadeghi and T. A. Dean, “Analysis of ejection in precision forging”, *International Journal of Machine Tools and Manufacture*, vol. 30, page.509-519, 1990.

[SCH06] C. Schuman, E. Lenarduzzi, S. Weber, M. J. Philippe, D. Petelot and P. Bounie, “Modelling the oxygen diffusion profile in TA3V and T40 during heat-treatment under air between 620 and 850 °C”, *Surface and Coatings Technology*, vol. 200, page.4572-4578, 2006.

[SCH98] SCHULER GmbH, “Metal Forming Handbook” *Springer*, Berlin, page. 441-449,1998.

[SCH07] T. Schrader, M. Shirgaokar and T. Altan, “A critical evaluation of the double cup extrusion test for selection of cold forging lubricants”, *J. Mater. Process Tech.*, vol. 189, page.36-44, 2007.

[SCH83] J. A. Schey, “Tribology in Metal Working Friction Lubrication and Wear”, *ASM International*, Metals Park, OH, Chap. 1-5, 1983.

[SES00] T. Seshacharyulu, S. C. Medeiros, W. Frazier, Y. Prasad, “Hot working of commercial Ti-6Al-4V with an equiaxed α-β microstructure: materials modelling considerations”, *Material Science and Engineering A*, vol. 284, page.184-194, 2000.

[SEM87] S. L. Semiatin, E. W. Collings, V. E. Wood and T. Altan, “Determination of the interface heat transfer coefficient for non-isothermal bulk-forming processes”, *Trans. ASME, J. Engg. for Industry*, vol. 109, page.49-57, 1987.

[STR60] J. Stringer, “The oxidation of titanium in oxygen at high temperatures”, *Acta Metallugica*, vol. 8, page.758-766, 1960.

[SOF02] H. Sofuoglu, H. Gedikli, “Determination of friction coefficient encountered in large deformation processes”, *Tribol Int.*, vol. 35, page.27-34, 2002.

[TAN02] X. Tan, “Comparisons of friction models in bulk metal forming”, *Tribology International,* vol.35, page.385-393, 2002.

[TZO00] G. Y. Tzou, H. H. Hsu, Y. H. Hsiao, “Investigation of a slab method analysis and FEM simulation on rotating compression forming of ring,” *J Mater Process Technol*, vol. 3, 2000.

[THO69] E. G. Thomsen, “Friction in forming processes”, *Annals of the International Institute for Production Engineering Research*, vol. 17, page.187-193, 1969.

[UNN86] J. Unnam, R. N. Shenoy and R. K. Clark, “Oxidation of commercial purity titanium”, *Oxidation of Metals*, vol. 26, page.249–261, 1986.

[VEN09] B. D. Venkatesh, D. L. Chen, and S. D. Bhole, “Effect of heat treatment on mechanical properties of Ti- 6Al-4V ELI alloy”, *Materials Science and Engineering: A*, vol. 506, page.117-124, 2009.

[VIG63] C. W. Vigor and J. W. Hornaday, “A Thermocouple for Measurement of Temperature Transients in Forging Dies”, *Temperature, Its Measurement and Control in Science and Industry*, New York, vol. 3, page. 625-630, 1963.

[WAN01] J. P. Wang, “A new evaluation to friction analysis for the ring test”, *Int J Mach Tools Manuf.*, vol. 41, 311-324, 2001.

[WAL05] I. Walker, “Considerations on the selection of alloys for use in pressure cells at low temperatures”, *Cryogenics*, vol. 45, page.87-108, 2005.

[WEI99] I. Weiss and S. Semiatin, “Thermomechanical processing of alpha titanium alloys- an overview”, *Materials Science and Engineering A,* vol. 263, page.243-256, 1999.

[WIL04] W. R. D. Wilson, S. R. Schmid and J. Liu, “Advanced simulations for hot forging: heat transfer model for use with the finite element method”, *Journal of Materials Processing Technology*, vol. 155, page. 1912-1917, 2004.

[YEO11] J. T. Yeom, N. K. Park, T. J. Shin, S. M. Hwang, S. S. Hong, I. O. Shim and C. S. Lee, “Characterization of the interface heat transfer coefficient during non-isothermal bulk forming of Ti–6Al–4 V alloy”, *Proceedings of the Institution of Mechanical Engineers, Part B: Journal of Engineering Manufacture*, vol. 225, page.1703-1712, 2011.

[ZEN00] W. Zeng and Y. Zhou, “The influence of microstructure on dwell sensitive fatigue in Ti–6.5Al–3.5Mo–1.5Zr–0.3Si alloy,” *Mater. Sci. Eng. A*, vol. 290, page. 33–38, 2000.

[ZEN14] S. Zeng, A. Zhao, H. Jiang, X. Fan, X. Duan and X. Yan, “Cyclic oxidation behaviour of the in Ti–6Al–4V alloy”, *Oxidation of metals*, vol. 81, 467-476, 2014.

[ZHA09] Q. Zhang, E. Felder and S. Bruschi, “Evaluation of friction condition in cold forging by using T- shape compression test”, *J. Mater. Process. Technol.*, vol. 209, page.5720-5729, 2009.

[ZHO98] M. Zhou, “Constitutive modelling of the viscoplastic deformation in high temperature forging of titanium alloy IMI834”, *Materials Science & Engineering*: *A*, vol. 245, page.29-38, 1998.

[ZHA08] Q. Zhang, M. Arentoft, S. Bruschi, L. Dubar and E. Felder, “Measurement of friction in a cold extrusion operation: study by numerical simulation of four friction tests”, *Inter. J. Mater. Form.*, vol. 1, page.1270-1274, 2008.

[ZHU11] Y. Zhu, W. Zeng, X. Ma, Q, Tai, Z. Li and X. Li, “Determination of the friction factor of Ti-6Al-4V titanium alloy in hot forging by means of ring-compression test using FEM”, *Tribol Int.*, vol. 44, page.2074-2080, 2011.

Publications

Conferences:

International

1) R. Sethy, L. Galdos, J. Mendiguren and E. S. Argandoña (2015, December). Friction and Heat Transfer Coefficient Determination of Titanium Alloys during Hot Forging Conditions. *International conference on Advances in Materials and Processing Technologies (AMPT)*, Madrid, Spain.
2) R. Sethy, L. Galdos, J. Mendiguren and E. S. Argandoña (2016, April). Investigation of influencing factors on friction during ring test in hot forging using FEM simulation. *19th ESAFORM international Conference*, Nantes, France.
3) R. Sethy, L. Galdos, J. Mendiguren and E. S. Argandoña (2016, September). Identification of Friction Coefficient in Forging Processes by Means T-Shape Tests in High Temperature. *Metal forming, 16th International Conference*, Krakow, Poland.
4) L. Galdos, J. Mendiguren, E. S. Argandoña, R. Sethy and J. Agirre (2017, September). Characterization of Ti64 forging friction factor using ceramic coatings and different contact conditions. *International Conference on the Technology of Plasticity (ICTP)*, Cambridge, United Kingdom.

National:

1) R. Sethy, L. Galdos, J. Mendiguren and E. S. Argandoña (2016, June). Effect of Influencing Factors on Friction modelling during hot forging by means of ring-compression test using FEM of AISI 304L. XIV Congreso Nacional de Materiales, Gijón, Spain.

Journals:

1) R. Sethy, L. Galdos, J. Mendiguren and E. Sáenz de Argandoña (2016). Friction and Heat Transfer Coefficient Determination of Titanium Alloys during Hot Forging Conditions. *Advanced Engineering Materials*, Wiley Online Library Publication.

2) R. Sethy, L. Galdos, J. Mendiguren and E. Sáenz de Argandoña (2016). Identification of Friction Coefficient in Forging Processes by Means T-Shape Tests in High Temperature, *Key Engineering Materials*, Vol. 716, pp. 165-175, Trans Tech Publications.

3) R. Sethy, L. Galdos, J. Mendiguren and E. Sáenz de Argandoña (2016). Investigation of influencing factors on friction during ring test in hot forging using FEM simulation, *AIP Conference Proceedings*, Vol. 1769, No. 1, pp. 130009, American Institute of Physics Publishing.

4) L. Galdos, J. Mendiguren, E. S. Argandoña, R. Sethy and J. Agirre (2017). Characterization of Ti64 forging friction factor using ceramic coatings and different contact conditions, *Procedia Engineering*, Elsevier Publication. (Communicated)